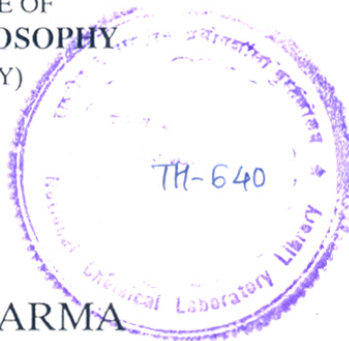# MODELLING BIOLOGICAL SYSTEMS:

A FRACTAL APPROACH

A THESIS
SUBMITTED TO THE
UNIVERSITY OF POONA
FOR THE DEGREE OF
DOCTOR OF PHILOSOPHY
(IN CHEMISTRY)

BY

ARCHANA SHARMA

M.Sc (Biochemistry)

515.17 : 577 (043)
SHA

DIVISION OF CHEMICAL ENGINEERING
NATIONAL CHEMICAL LABORATORY
PUNE-411 008, INDIA

JUNE 1991

to
mummy and papa

DECLARATION

Certified that the work incorporated in the thesis **MODELLING BIOLOGICAL SYSTEMS: A FRACTAL APPROACH** submitted by **Archana Sharma** was carried out by the candidate under my supervision. Such materials as has been obtained from other sources has been duly acknowledged in the thesis.

DATE : 24 July 1991

(B.D. KULKARNI)
Research Guide

ACKNOWLEDGEMENTS

I express a deep sense of gratitude to my research advisor Dr. B.D. Kulkarni whose valuable guidance, understanding and encouragement at all stages of this work has culminated in the form of a thesis. Without his critical evaluation and deep rooted knowledge, this compilation would not have been possible. His quest for knowledge and strive for excellence will always remain as a source of inspiration with me.

I am extremely grateful to Dr. V. Ravi Kumar, Dr. S.S. Tambe, Dr. N.K. Yadav and Dr. V.K. Jayaraman for their critical comments and timely suggestions. My special thanks are due to Dr. S. Krishnan for his invaluable assistance and help offered during the course of this work. I thank Pushkaraj Apte for adding color to this thesis. I am very thankful to him for sparing time to take all the photographs presented here.

Mere words are not enough to acknowledge the help and suggestions offered by my colleagues, Satish Inamdar, Ujwal Shinde, Rajani Prasad, Parkash Badola, Jayant Bandyopadhyay, Satish Jagtap, Ajay Chhatre and Murli Nair. I appreciate the substantial help rendered by my friends Medha Shrikhande, Devyani Dey, Suhita Shendye and Abhay Shendye who have contributed immensely in their own ways towards the success of this thesis.
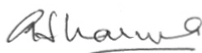
Special thanks are due to Mr. B.G. Poman and Mr. T.S Kamble. Support and help of the library and administrative staff of the National Chemical Laboratory is duly acknowledged.

It is with a deep sense of gratitude that I appreciate the encouragement and help rendered to me by Dr. V.M. Nadkarni, Head, Chemical Engineering Division and Dr. R.A. Mashelkar, Director, National Chemical Laboratory.

The financial assistance in the form of a research fellowship from the Council of Scientific and Industrial Research (CSIR), New Delhi, is gratefully acknowledged.

Last but not the least, I am very thankful to my parents, brother and sister who have stood by me throughout and encouraged and guided me at every step. Without their undying patience, this thesis would never have come through.

DATE: 24 July 1991

(ARCHANA SHARMA)

clouds are not spheres, mountains are not cones, coastlines are not circles, and bark is not smooth, nor does lightning travel in a straight line....

Benoit B. Mandelbrot

CONTENTS

SYNOPSIS OF THESIS

A fractal is an object with a sprawling and tenuous pattern. As the pattern is magnified it reveals repetitive levels of detail so that similar structures exist on all scales. A fractal might therefore look the same whether viewed on the scale of a meter, a millimeter or a micrometer. In other words, fractal structures are shapes that cannot be defined by Euclidean geometry. Mandelbrot pointed out that many disorderly objects in nature have this property. They are often remnants of chaotic nonlinear dynamics and possess the property of scale invariance.

Biological molecules, though made of simple recurring units, exhibit immense complexity when viewed globally. Proteins, carbohydrates, nucleic acids, etc. are all polymeric macromolecules with a very large molecular mass. Their spatial arrangements are also enigmatic and have virtually defied understanding until the advent of techniques such as X-ray crystallography and NMR along with genetic engineering. These have not only been able to elaborate the intricacy of their organization, but have also provided clues to tailor them to our requirements. Biological molecules and membrane bilayers have been defined as fractals earlier.

The complexities of biological reactions are usually explained by considering complex reaction kinetics and interactions between the reacting species. These can now be explained in a simple way by considering the biological macromolecules as fractals. Application of the concept of fractals to biological systems in order to analyze structure-function relationships, understand and explain the complexity of biological organization and reactions has been attempted in the present thesis.

Chapter one introduces the subject matter of the thesis and surveys the literature on fractals. Relevant analysis of biological systems has also been discussed critically.

The effects of fractal nature of enzymes on the reactions they catalyze have been analyzed in chapter two. The results indicate that non-idealities in their performance, such as multi-stationarity and substrate inhibition can arise due to their fractal nature.

Protein conformation is not static in nature. The active site and certain regions in proteins are mobile. Similarly, the proteins and lipids in a membrane bilayer are always in a state of constant random motion. The shape of membranes have earlier been described as fractals. With the consideration of the constant motion of regions which constitute the fractal, the concept of mobile shapes of fractals or *fractiles* emerges. The effect of mobility on reactions has been considered in chapter three. Reactions on *fractile* surfaces when the overall dimension of the system may or may not undergo a change have been critically analyzed. Selectivity behavior on *fractile* surfaces has also been discussed.

The morphology of bacterial colonies is also fractal in nature. The time based change in fractal shape and dimension of bacterial colonies has been discussed. Reasons why bacterial colonies take diverse shapes under different environmental conditions have been evaluated and subsequently simulated in chapter four. Critical effects of concentration of nutrients, their rates of diffusion, thickness of the gel and yield coefficients of cells per unit substrate has been studied. The results clearly show that environmental conditions can drastically affect the shapes of colonies.

The shape of biological molecules modelled as fractals and *fractiles* can be represented by a fractal dimension. Fractal dimension of an object only indicates how the it fills the space it is embedded in. It gives a probability that a point in space is occupied by an object and is therefore a global parameter associated with the object or shape. This therefore can result in different objects or shapes possessing the same fractal dimension. The same fractal dimension, however, does not mean that the objects or shapes possess similar topology or textures. In chapter five an algorithm for evaluating the topology of

protein surfaces has developed. An index which describes the roughness of the surface has been defined. The topology of various proteins has been described in terms of the roughness index and the correlation between roughness and fractal dimension has been attempted.

In chapter six, a method for the two-dimensional representation of protein surfaces has been developed. The algorithm enables one to visualize the entire surface of the protein at the same time. This facilitates one in comparing the surface of different proteins in order to understand the effect of surface topologies on protein-substrate, protein-protein and protein-ligand interactions. Studies on subtilisin, a serine protease, have been undertaken in an attempt to understand differential stability and activity of the protein from different sources.

Chapter seven concludes the thesis giving a concise summary of the results obtained and brings out the importance and implications of the above work and discusses scope of further applications.

CHAPTER 1

LITERATURE REVIEW

CHAPTER 1

1.1 INTRODUCTION

The geometry of objects, ranging in size from the atomic scale to the size of the universe, is central to the models we make to understand nature. It has now been accepted that randomness is an essential ingredient of most natural phenomena. The Euclidean lines, circles, spheres, tetrahedra that have served as a basis for the intuitive understanding of the geometry of natural objects are now being altered to account for randomness. Therefore mathematicians have developed geometrical concepts that transcend traditional geometry. The application of these concepts to natural sciences, in the past, was considered as abstract and pedantic. However, Benoit B. Mandelbrot, with his creative and monumental work, has generated a wide spread interest in *fractal geometry* (Mandelbrot, 1977), a concept he introduced to account for randomness in order. He derived the word from the Latin *fractus*, the adjectival form of *frangere*, or *to break*.

1.2 THE CONCEPT OF FRACTAL STRUCTURES

Investigators who study bulk matter face a problem of bewildering complexity. Each macroscopic bit of the world contains gigantic numbers of atoms and molecules that are often arranged in complicated, and apparently disorderly patterns. In case of a perfect crystal or a smoothly flowing liquid, the pattern is uniform on large scales. Even though a great deal can be understood about such systems, the vast majority of complicated natural phenomena such as turbulent flows of liquids or air, the accretion of metal particles in an electrolytic bath and the formation of mountain ranges etc. have virtually defied

understanding (Sander, 1987).

In the past 10 years both scientists and mathematicians have made much progress towards gaining such comprehension. Central to many of the new insights is the revolutionary concept of a *fractal* (Mandelbrot, 1977). A fractal is an object with a sprawling, tenuous pattern (Figure 1.1). As the pattern is magnified it reveals repetitive levels of detail, so that similar structure exists on all scales. A fractal might, for example, look the same whether viewed on the scale of a meter, a millimeter or a micrometer (Figure 1.2). In other words, fractals possess the property of *self-similarity* and are *scale-invariant*. Mandelbrot (1983, 1984) pointed out that many disorderly objects in nature have this property. Therefore, fractal structures are shapes that cannot be defined by Euclidean geometry. They are often remnants of chaotic nonlinear dynamics (Goldberger *et al*, 1990). The key problem in the physics of fractals (Pietronero and Tosatti, 1986) is to understand the essential elements for the generation of these structures (Pietronero, 1990).

1.2.1   What a Fractal is Not

Take a geometric shape and examine it in increasing detail. That is, take smaller and smaller portions near a point P, and allow every one to be dilated, that is, enlarged to some prescribed overall size. If the shape belongs to standard geometry, it is well known that the enlargements become increasingly smooth. Ultimately, nearly every connected shape is locally linear. More generally, one can say that nearly every standard shape's local structure converges under dilations to one of the small number of *universal attractors*. Mathematical and natural fractals are shapes whose roughness and fragmentation *neither* tend to vanish, *nor* fluctuate up and down, but remain *essentially unchanged* as one zooms in continually and examination is refined (figure 1.2). Hence, the structure of every piece

FIGURE 1.1

A fractal is a sprawling and tenuous structure. Shown here are some variants of the Mandelbrot set that have been generated on the computer.
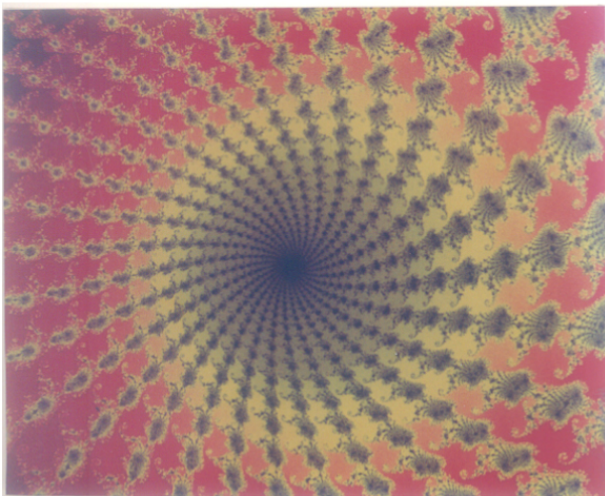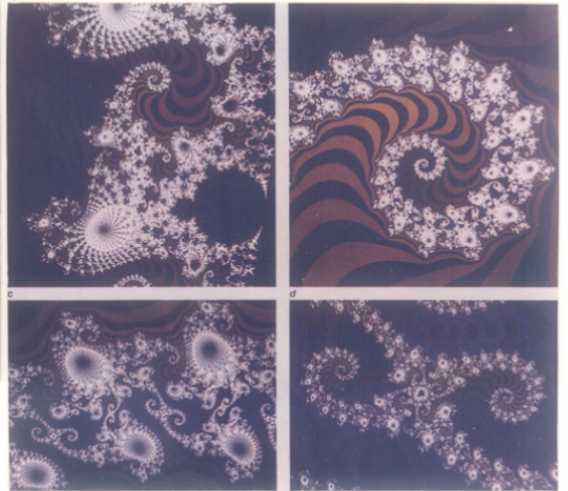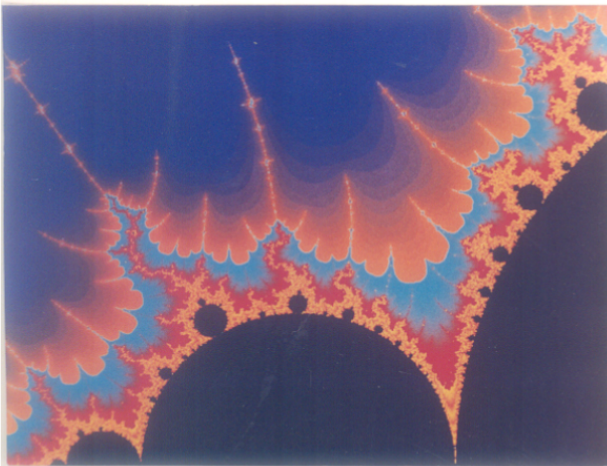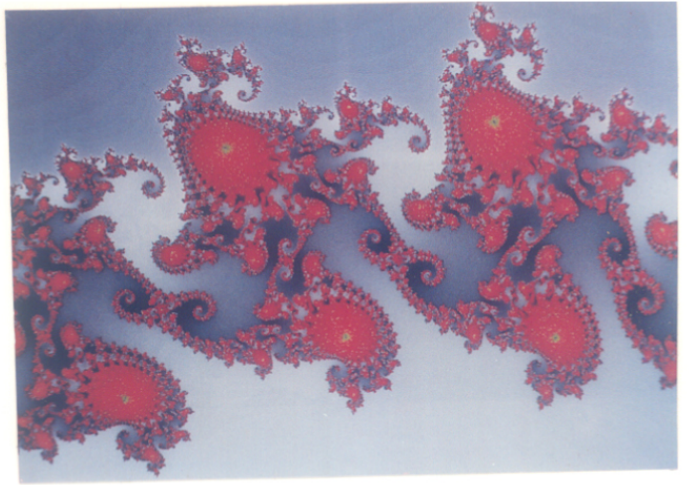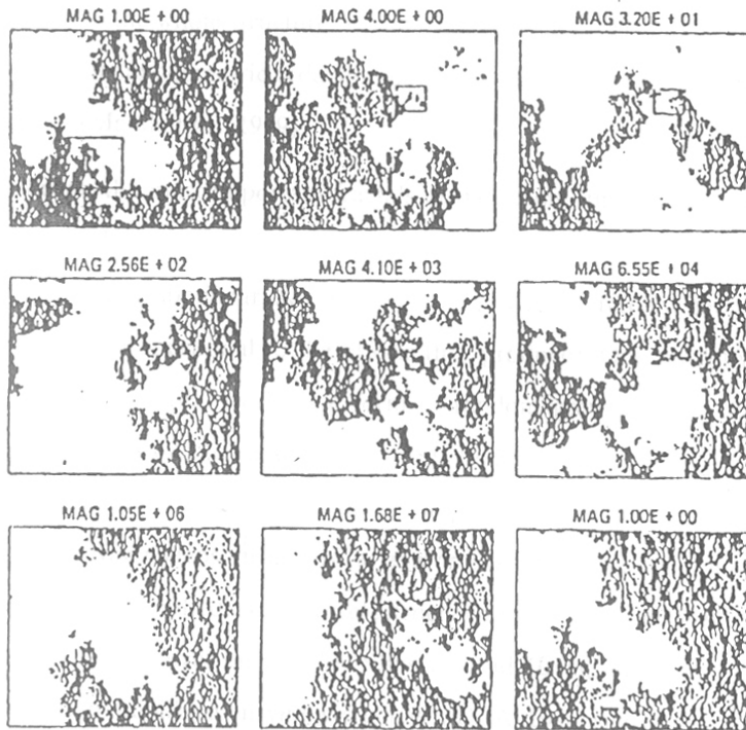
FIGURE 1.2

Zoom sequence of the coastline of a statistically self-similar fractal landscape D = 2.2. Each succeeding picture shows a blowup of the framed portion of the previous image. As the surface is magnified, a small portion looks similar to (but not exactly the same) a larger portion. The total magnification corresponds to 16 million.

holds the key to the whole structure. An alternative term is *self-similar*. It expresses that each part is a linear geometric reduction of the whole, with the same reduction ratios in all directions (Mandelbrot, 1989).

However, the most important fractals deviate from linear *self-similarity*. Some of these are fractals that describe general randomness, while others are fractals that can describe chaotic, or nonlinear, systems (where the factors affecting the way the system behaves are not proportional to the effects they produce). One model where random fractals describe the real world is a form of random growth called *diffusion limited aggregation*, or DLA (Witten and Sander, 1981, 1983). A typical DLA is shown in figure 1.3. This yields tree-like shapes of baffling complexity. DLA can be used to model how ash forms, how water seeps through rock, how cracks spread in a solid, how the lightning discharges, effect of applied voltage on electrochemical deposition (Usami and Nagatani, 1990) and to show corrosion of alloy films by acid (Ding and Liu, 1990). We have considered an immobilized enzyme system as a DLA. Extensive simulations have been carried out on this fractal (chapter 2).

The importance of a DLA model is that it shows a relation between fractals and growth. There are many ways that objects in nature can grow. A perfect crystal, for instance, grows near equilibrium: it *tries* many configurations until it finds the state with the most stable structure. When a molecule is added to the growing crystal, it must in general search over many possible sites before it finally sticks in a favorable place. An equilibrium crystal forms slowly and is subject to constant rearrangement. Most real processes of growth, however, do not have the luxury of time. All biological life, for example, is out of equilibrium (Meakin and Stanley, 1983; Sander, 1986, 1987; Alstrom, 1990; Stanley *et al*, 1990; Ben-Jacob and Garik, 1990).

FIGURE 1.3

Fractal pattern produced by computer simulation of a process called *diffusion limited aggregation.* Particles are released one at a time from an area outside the illustration and allowed to wander toward the origin. The color code indicates when the particles arrived: pink represents the early-arriving particles and white the late-arriving ones (Voss, 1988).
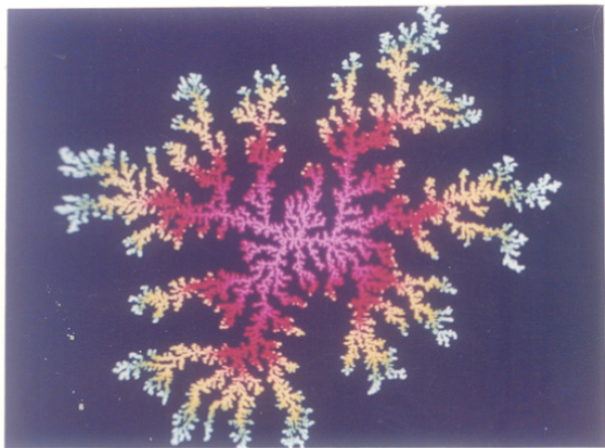
Scale-invariance has a noteworthy parallel in contemporary chaos theory, which reveals that many phenomena, even though they follow strict deterministic rules, are in principle unpredictable. Chaotic events, such as turbulence in atmosphere or the beating of a human heart, show similar patterns of variation on different time-scales, much as scale-invariant objects show similar structural patterns on different spatial scales. The correspondence between fractals and chaos is no accident. Rather it is a symptom of deep-rooted relation: fractal geometry is the geometry of chaos (Jurgens *et al*, 1990).

1.2.2 Examples of Fractals in Nature

An increasing amount of evidence suggests that nature's love of fractal shapes is a deep one (Morse *et al*, 1985; Barnsley, 1988) (Figure 1.4). Fractals known as percolation clusters (Figure 1.5) have been identified with pattern of a fluid flowing through a solid matrix, such as water seeping through a soil or coffee through ground coffee beans. We have modelled a fractal enzyme molecule as a percolation cluster. Simulations were carried out on these fractals, the details of which can be seen in chapter 2. Soot, colloids and some polymers seem to be fractals. Fractals also occur in the motion of air bubbles in oil, the growth of some crystals and the behavior of electrical discharges resembling lightning bolts. The random patterns of clouds and coast lines are almost certainly fractals as well (Stauffer, 1985). The growth of bacterial colonies also results in fractal shapes (Sharma *et al*, 1990b). This has been studied in chapter 4.

In biological systems, one can expect the formation of fractal structures at interfaces between two or more phases (Smirnov, 1990). Several biological patterns contain many components, which are found in a physical solution in states of different phases. It can lead to particle formation at the interface and further to their sticking into a fractal cluster. An example of such a type concerns the behavior of some phospholipids in a watery

FIGURE 1.4

Some examples of fractals in nature, natural and computer generated.
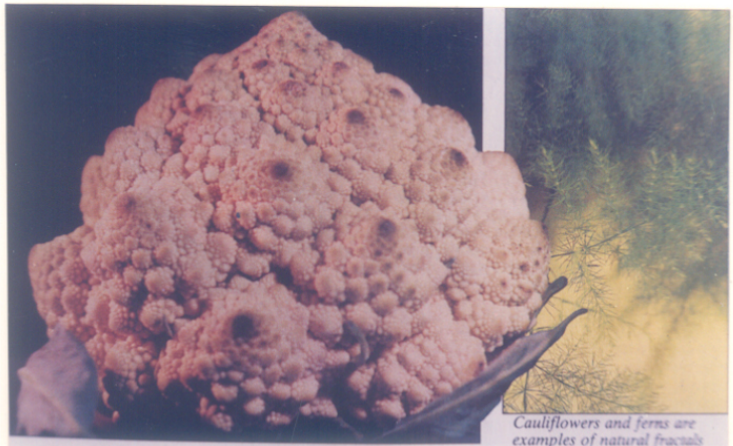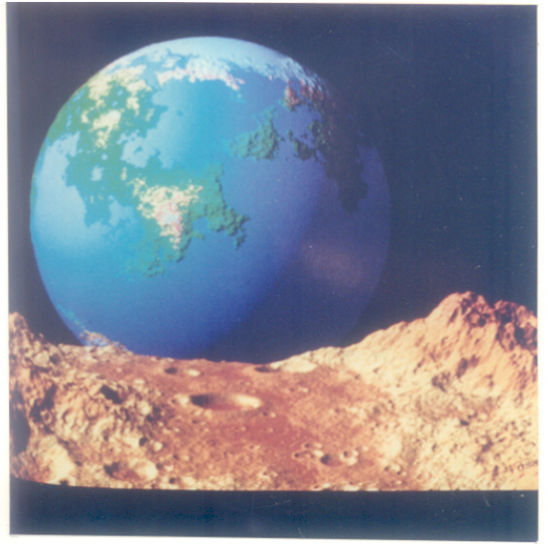
Cauliflowers and ferns are examples of natural fractals

FIGURE 1.5

(top left)-A percolation network, for sites at concentration p = 59.00%, occupied at random on a square grid of 3000 sites on a side, derived from periodic boundary conditions. Sites are considered connected if they are adjacent along a vertical or horizontal direction, not along the diagonals. The arrays of connected sites are clusters. The critical concentration for the largest cluster to span the grid from one side to another is 59.28%, in d = 2, so that this network is below the critical concentration; (top right)-The same construction, but at p = 59.30%, just above the critical concentration for site percolation, p_c = 59.28%, in d = 2. The white cluster is now an infinite cluster; (bottom left)-The expansion to full size of the small square in the previous picture, showing that the average geomerical of the infinite cluster (in white) is the same as in that picture. This is an illustration of self-similar geometry; (bottom right)-The same construction as in the first picture, but at p = 59.60%, above the critical concentration for site percolation in d = 2 (Orbach, 1986).
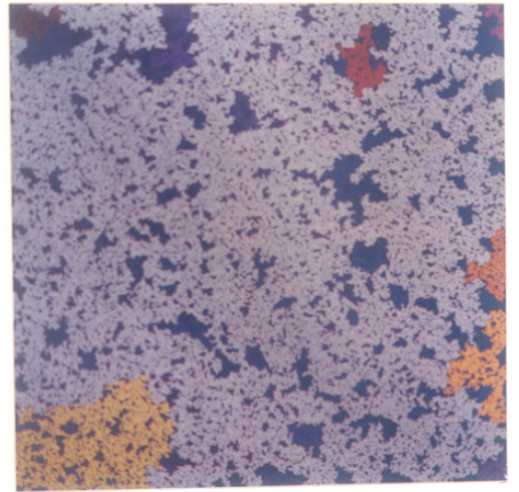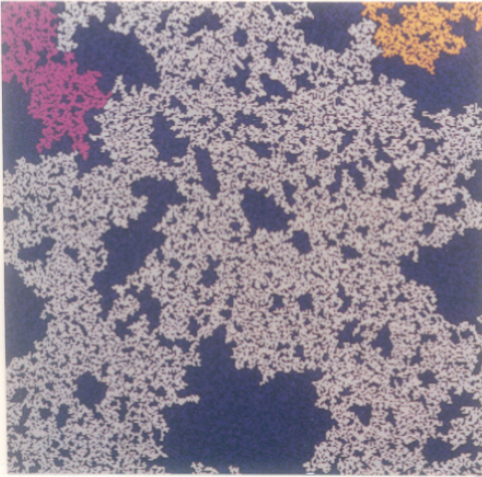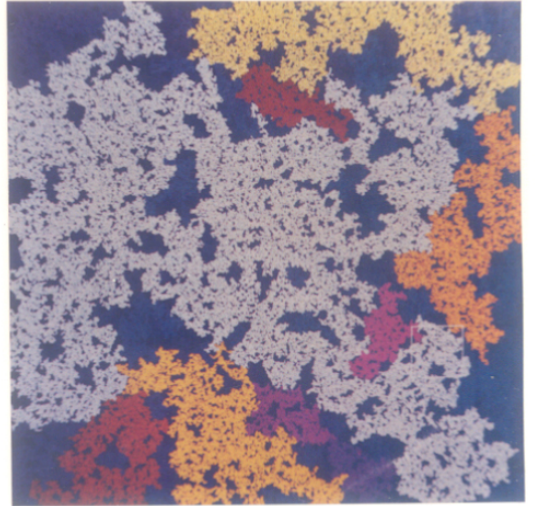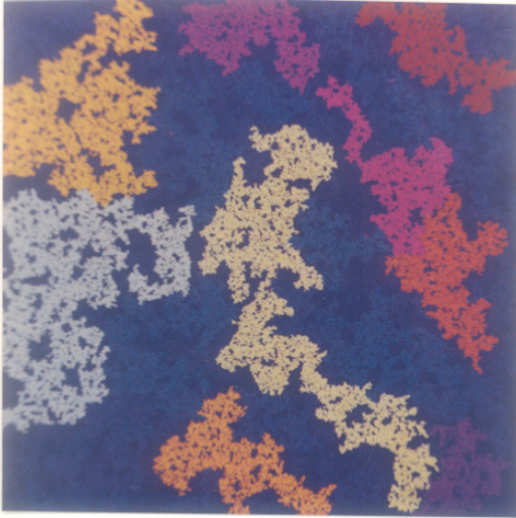
solution at the air-water interface (Miller *et al*, 1986). The phospholipid is collected in some domains which form a fractal structure by sticking to each other. The domains aggregate due to interactions and a change in the surface tension of the water through the action of these domains. The fractal dimension of such self-similar structures of crystalline domains is equal to 1.5 +/- 0.1.

In the human body fractal like structures abound in networks of blood vessels, nerves and ducts. The most carefully studied fractal in the body is *the systems of tubes that transport gas* to and from the lungs (Goldberger and West, 1987) (figure 1.6). Many other organs also appear to be fractal in nature, though their dimension has not been quantified. Such structures have tremendous advantages; they can increase the surface area available for absorption and distribution of nutrients or substrates. Fractal structures by virtue of their redundancy and irregularity are robust and resistant to injury. Fractal like structures play a very important role in healthy, mechanical and electrical dynamics of the heart (Goldberger *et al*, 1988)

Other examples of fractals in biological systems include proteins and nucleic acids (figure 1.7). Much work has been done in applying the concept of fractals to such systems (Stapleton *et al*, 1980; Isogai and Itoh, 1984; Lewis and Rees, 1985; Pfeifer *et al*, 1985; Chen and Teixeira, 1986; Wako, 1989; Sharma *et al*, 1990a, 1990b). The property that objects can look statistically similar while at the same time different in detail at different length scales, is the central feature of fractals in nature (Voss, 1988).

1.2.3   *Quantification in Terms of the Fractal Dimension*

As fractals are composed of similar structures of ever fine detail, their length is not well defined. As a result of this mathematicians calculate the *dimension* of a fractal structure to quantify how it fills space (Sander, 1986). The familiar concept of dimension

FIGURE 1.6

Airways of the lung (top) shaped by evolution and embryonic development resemble fractals generated by computer (bottom). The bronchi and bronchioles of the lung form a *tree* that has multiple generations of branchings. The small-scale branching of the airways looks like branching at larger scales. When physiologists quantified observations of the branching pattern, they discovered that the lung tree has fractal geometry (Goldberger *et al*, 1990).
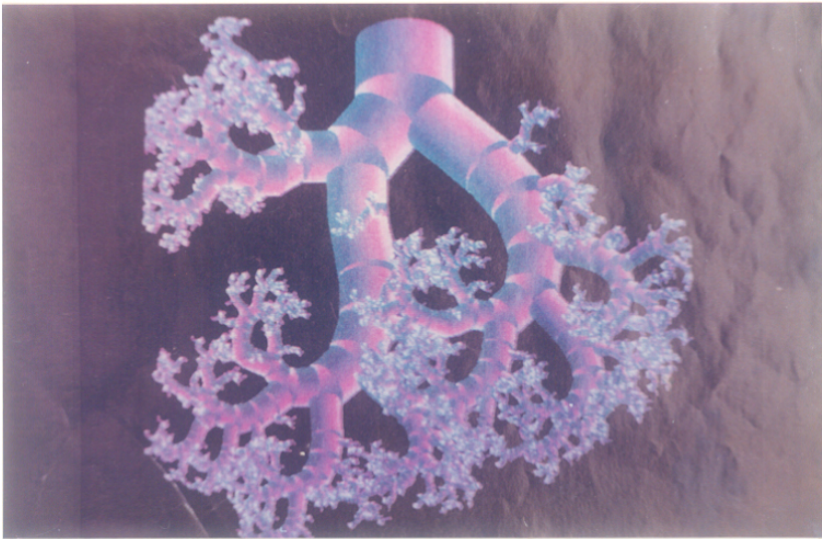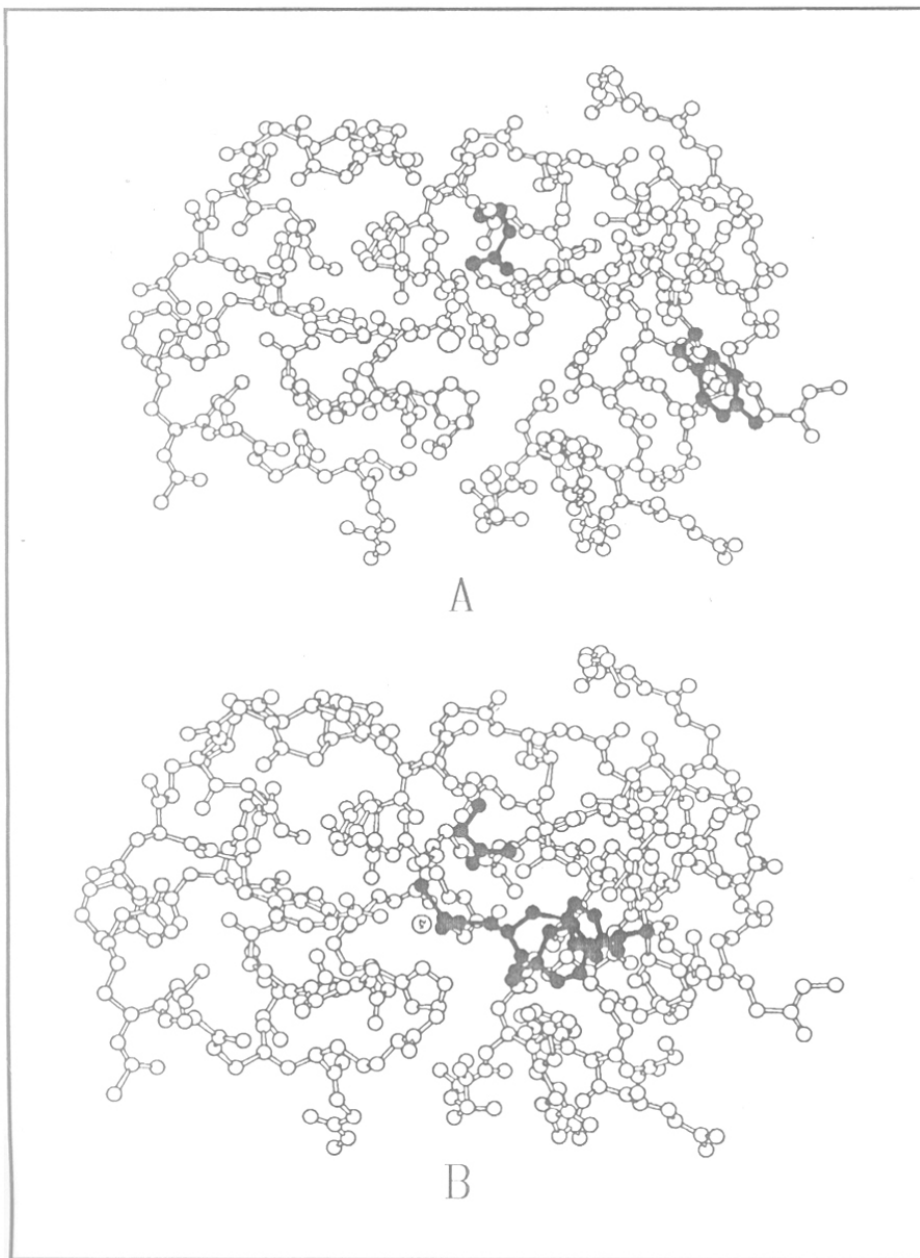
FIGURE 1.7

The structure of Carboxypeptidase A.

a) enzyme alone.

b) enzyme-substrate complex.

TH-640

applies to Euclidean geometry (Falconer, 1989). Lines have one dimension, circles have two and spheres have three dimensions. Fractal dimensions, however, can sample between one to three and it need not have an integral value. The greater the dimension of a fractal, the greater the chance that a given region of space contains a piece of that fractal. The fractal dimension of an object is an *universal property* of the system and is independent of how the object was formed. The fractal dimension and the other universal properties are related to the behavior at larger scales, where the particular details average out. As a consequence, a simple model that neglects most of the complexity of the real system, but nonetheless, describes the scaling properties of the system correctly, is obtained. Abstract discussions of objects now called as fractals were given long before Mandelbrot by other mathematicians (Mandelbrot, 1974). Just as round objects are symmetric under conditions of rotations, fractals are symmetric under conditions of dilations, or changes of scale.

The property of self-similarity or *scaling* is one of the central concepts of fractal geometry. It is closely connected with our intuitive notion of *dimension* as illustrated in figure 1.8.

An object normally considered as one-dimensional, a line segment, for example, also possesses a similar scaling property. It can be divided into N identical parts each of which is scaled down by the ratio $r = \frac{1}{N}$ from the whole. Similarly, a two-dimensional object, such as a square area in the plane, can be divided into N self-similar parts each of which is scaled down by a factor $r = \frac{1}{\sqrt{N}}$. A three-dimensional object like a solid cube may be divided into N little cubes each of which is scaled down by a ratio $r = \frac{1}{\sqrt[3]{N}}$. With self-similarity the generalization of fractal dimension is straightforward. A D-dimensional self-similar object can be divided into N smaller copies of itself each of which is scaled down by a factor r where $r = \frac{1}{\sqrt[D]{N}}$ or
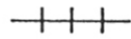
1-D N parts, scaled by ratio $r = 1 / N$

$$N r^1 = 1$$
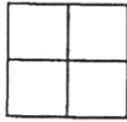
2-D N parts, scaled by ratio $r = 1 / N^{\frac{1}{2}}$

$$N r^2 = 1$$
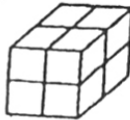
3-D N parts, scaled by ratio $r = 1 / N^{\frac{1}{3}}$

$$N r^3 = 1$$

GENERALIZE

for an object of N parts, each scaled down by a ratio r from the whole

$$N r^d = 1$$

defines the fractal (similarity) dimension **D**

$$D = \frac{\log N}{\log 1 / r}$$

FIGURE 1.8

Interpretation of standard integer dimension figures in terms of exact self-similarity and extension to non-integer dimensioned fractals.

$$N = \frac{1}{r^D}$$

Conversely, given a self-similar object of N parts scaled by a ratio r from the whole, its *fractal* or *similarity dimension* is given by

$$D = \frac{\log(N)}{\log\left(\frac{1}{r}\right)}$$

1.2.4 Methods For Calculating Fractal Dimension

There are many definitions of the fractal dimensions of an object, including box dimension, Bouligand-Minkowski dimension, and intersection dimension. Although they are all equivalent in the continuous domain, they differ substantially when discretized and applied to digitized data. The fractal dimension can be used to compare the complexity of two curves or two surfaces (Dubuc *et al*, 1989a), and therein lies its importance for applications.

The fractal dimension of a one-dimensional object can be evaluated by a technique known as the *structured walk* (Kaye, 1981). The technique is the simplest method employed to measure the fractal dimensions of irregular profiles. In the structured walk technique, the perimeter of an irregular structure is approximated by using a measuring stick to mark off units of a defined length. The perimeter of the resulting polygon is then obtained by multiplying the length of the measuring stick by the number of integral units required to cover the object (figure 1.9a). The perimeter of the original irregular object is then estimated from the perimeter of the polygon. Changing the length of the measuring stick will result in different estimates of the perimeter of the irregular object. The measured perimeter of the object is not constant, but is a function of the size of the measuring unit.
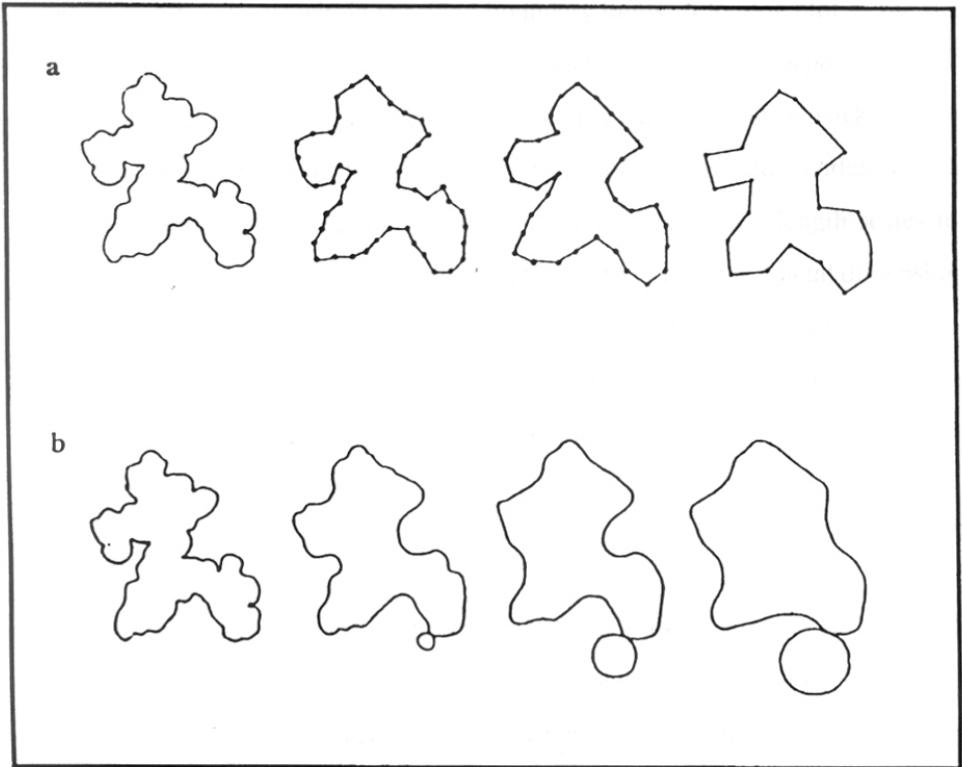
FIGURE 1.9

a) The structured walk technique used to calculate fractal dimension. The perimeter of an object is approximated by a polygon marked off using a measuring stick of a defined length. The estimated perimeter is a function of the measuring stick.

b) An alternative method for calculating the perimeter of an object is to roll a probe circle of a specified radius around the perimeter. The fractal dimension is calculated from a log-log plot of the perimeter versus the probe radii.

Natural fractals have slightly different properties than ideal fractals; ie., their fractal nature is defined only within specified boundary limits. A log-log plot of the perimeter of an object versus the size of the measuring stick used to define its perimeter will result in a sigmoidal curve. For both very large and very small measuring sticks, the slopes of the plots is close to zero while the length of the perimeter is independent of the size of the measuring unit. These limits define the boundaries of the length scales to use in describing natural fractals. Once the boundary is described, the fractal dimension can be calculated from the slope of the log-log plot. Ideally, a straight line relationship between log (length of perimeter) and log (length of measuring stick) will be observed (Mandelbrot, 1983). The fractal dimension D may be obtained from the slope, m, of the plot by the relationship

$$D = 1 + |m|$$

An alternative approach to the structured walk technique, for calculating the perimeter of an object, is to role a circle of a given radius around the perimeter, as illustrated in figure 1.9b. Previously, the perimeter was defined by enclosing a object with a boundary polygon whose sides are the length of the measuring stick. The perimeter can also be defined using a circular probe of specified radius. By rolling a circular probe around the object, the length of the perimeter can be estimated from the path traced by the boundary of the circle. As the radius of the circular probe is decreased, the perimeter of the object is increased. Again, the fractal dimension of an object is calculated by plotting the log of the perimeter versus the log of the probe radius.

The definition of box dimension (Dubuc *et al*, 1989b; Block *et al*, 1990; Grassberger, 1990) is based upon a quantization of the space in which the curve is embedded. Define a decreasing sequence ϵ_k tending to 0 slowly, such as a geometric sequence (a sufficient

condition is that the ratio $\ln \epsilon_k / \ln \epsilon_{k-1}$ tends towards 1). The set E can then be covered by a grid with pixel (i.e., picture element) length ϵ_k, and the number of pixels $\Omega(E, \epsilon_k)$ that intersect E can be counted. More formally, the *box dimension* is given by

$$\Delta_B(E) = \lim_{k \to \infty} \frac{\ln \Omega(E, \epsilon_K)}{\ln \left(\frac{1}{\epsilon_k}\right)}$$

An estimate of $\Delta_B(E)$ is given by the slope of the line passing through the points

$$(\ln(1/\epsilon_k), \ln \Omega(E, \epsilon_k))$$

In computing the fractal dimension of a biopolymer chain, the number of monomers N(R) is counted as a function of the radial distance R from an arbitrary origin, and fit N(R) to R^d. Such fits need to be done about several origins within the structure. For proteins one uses the X-ray crystallographic coordinates (Bernstein *et al*, 1977) of the α-carbons (those carbon atoms along the polypeptide backbone at which the amino acid residues attach) to denote the monomer position. Viewing the protein first as a polypeptide chain, the chain fractal dimension d_c can be defined as the scaling exponent of the contour length (length along the chain, proportional to N) with respect to the end-to-end length.

The protein chain is divided into twenty equal segments and the resulting nineteen equally spaced, interior α-carbons are used as origins. The following procedure is carried out for each value of R_{inc}, a parameter that is varied. For the calculation of d_c, the number of α-carbons connected contiguously within a distance of R of the origin is counted for values of R equal to integral multiples of R_{inc}. The number counted N is thus a measure of the contour length of the two chain segments of end-to-end length R, which start at the specified origin. When R reaches a value large enough that either end of the protein

is encountered, the process is terminated. After the algorithm has been performed using all nineteen origins, a value for the average fractal dimension is obtained as the best fit of $N(R) \propto R^d$, by a least squares linear fit of log (N) to log (R).

By contrast the path of the protein's polypeptide backbone can be ignored and the total mass (either contiguous or noncontiguous) is scaled with respect to the distance in the embedding space. An average residue mass is assigned to each α-carbon and simply count all α-carbons within spheres of radius R. All other aspects of computation remain the same. The above procedure is called as the reentrant scaling exponent (Colvin and Stapleton, 1985; Wagner *et al*, 1985).

1.3   APPLICATION OF FRACTAL CONCEPTS TO REAL SYSTEMS

1.3.1   *Fractal Reaction Kinetics*

Among the most important chemical reactions are those called as *heterogeneous*. These reactions take place at the interfaces of different phases, for example, gas-solid or liquid-solid boundaries, and include industrial surface-catalysis and electrode reactions, as well as many bioenzymatic reactions and membrane reactions and some geochemical and atmospheric reactions (Kopelman, 1988). In addition there are many heterogeneous *non-chemical* reactions: in solid-state physics there are electron-hole, soliton-antisoliton, exciton-exciton *recombinations* as well as aggregations of excitations, defects and so forth (Klymko *et al*, 1982, 1983; Kopelman, 1986; Kopelman *et al*, 1986). Charge and excitation recombination, as well as excitation quenching, are also found in biological systems, such as photosynthetic units (Kopelman, 1988).

Heterogeneous catalysis is perhaps the most prominent example in chemistry of the important role that geometry plays in determining reaction efficiencies. The majority of

industrial and laboratory-made catalysts are structurally very complex: the surfaces are irregular, the pore size has a typical distribution as does the particle size, and the surface is not homogeneously reactive at all its sites. The recognition that a variety of randomly irregular structures in Nature is describable in terms of fractal geometry has boosted intensive interest in the chemical reactivity of fractal systems including catalytic processes (Pfeifer and Avnir, 1983; Avnir *et al*, 1983; Farin and Avnir, 1987, 1988a, 1988b; Avnir *et al*, 1989; Sheintuch and Brandon, 1989; Avnir and Farin, 1990).

Experiments on exciton-fusion reaction where two triplet (T) excitons fuse and form a singlet (S) exciton clearly reveal the anomalous dependence of K on time. The sample consists of a solid solution of $(C_{10}H_8/C_{10}D_8)$ where the molecules of one of the species are randomly distributed among the lattice sites. Beyond a certain critical concentration, $C_{10}H_8$ molecules form a macroscopic cluster which resembles a loosely connected network called a *percolation cluster*. Theoretical simulations on such clusters verify the experimentally observed anomalous behavior which is generally referred to as fractal kinetics. It is now known that reactants which are spatially constrained on the microscopic levels obey rate laws of fractal kinetics. The past decade has witnessed very vigorous activities in this area with a spate of experimental details and theoretical simulations bringing forth the fundamental issues involved in areas such as chemistry, biology, geology, solid state physics, astrophysics and atmospheric sciences.

The universally found instruction in chemical synthesis is to *stir well*. However, convective stirring cannot be achieved for reactions in or on media that are solid, viscous, porous, or otherwise unstructured. In absence of convective stirring, there is still diffusive stirring, which is called as *self stirring*. However, under dimensional constraints (surface reactions) or topological constraints (surface reactions), self stirring may be highly

inefficient. Fractal spaces such as percolation clusters are ideal testing grounds for *understirred* reaction kinetics and such studies are called as *fractal-like reaction kinetics* (Kopelman, 1988).

Effect of diffusion on fractal surfaces on the reaction rates have shown that the anomalous diffusion on such surfaces can drastically affect the overall reaction kinetics. This sometimes results in a deviation from the law of mass action. Effect of anomalous diffusion on such systems have been well studied by earlier workers (Gefen *et al*, 1980; Ben-Avraham and Havlin, 1982; Gefen *et al*, 1983; Havlin *et al*, 1983; Kopelman *et al*, 1984; Newhouse *et al*, 1984; Meakin and Stanley, 1984; Klafter *et al*, 1984; Anacker and Kopelman, 1984, 1987; Argyrakis and Kopelman, 1984, 1990a, 1990b; Newhouse and Kopelman, 1985; Robillard and Tremblay, 1986; Duran *et al*, 1986; Lopez-Quintella *et al*, 1987; Zumofen *et al*, 1989; Clement *et al*, 1989, 1990a, 1990b; Lindenberg *et al*, 1990; Albano, 1990; Klafter *et al*, 1990). In chapter 3, we have studied the *A + B --> inert* case on static and mobile (*fractile*) fractal surfaces. Selectivity studies have also been carried out.

1.3.2   Analysis of Protein Shape

Stapleton *et al* (1980) analyzed the electron spin data from five ferric proteins in terms of the fractal model of protein structure. Their results led to a characterization of protein structures by a single parameter, the fractal dimension (Allen *et al*, 1982). Various methods have been developed to determine the fractal dimensions of proteins (Isogai and Itoh, 1984; Helman *et al*, 1984a, 1984b; Farin *et al*, 1985; Cates, 1985; Stapleton, 1985; Lewis and Rees, 1985; Wagner *et al*, 1985; Colvin and Stapleton, 1985; MacDonald and Jan, 1986; Elber and Karplus, 1986; Wang *et al*, 1990).

The methodologies discussed earlier can be applied to characterize protein surfaces as well. The calculation of protein surfaces was pioneered by Richards (1977) who used variations of the above algorithms to define the outer surfaces of a macromolecule. The molecular surface of a protein was determined by rolling a probe of known radius over the van der Waals surface of a protein. There are two standard methods for defining a macromolecular surface: the solvent accessible surface, ie., the boundary of the surface accessible to the center of a probe sphere; and the molecular surface, which refers to the boundary of the volume accessible to the surface of the probe sphere. The molecular surface as defined by Connolly (1983), consists of three parts: the contact surface, the reentrant surface and the saddle surface. These surfaces differ in the number of degrees of freedom available to the probe molecule on the protein surface (2, 1 and 0 degrees of freedom, respectively). The sum of these three surfaces constitutes the molecular surface.

To calculate the fractal dimension of protein surfaces one must calculate the surface area of the protein using different probe radii. Figure 1.10 illustrates three examples of dependence of surface area on probe radii of lysozyme, ribonuclease and superoxide dismutase. Since proteins are real objects, boundary limits have to be imposed to calculate their fractal dimensions. The probe sizes vary from 1.5 to 4 A^{O}. Referring to the figure we can see that beyond these resolution limits, the molecular surface area is only marginally dependent on the probe size. Within these resolution limits the fractal dimension is given by the relationship

$$D = 2 + |m|$$

where 2 is the topological dimension and m is the slope of the log-log plot of the surface area with the probe size. If we take an average value of D within these resolution limits, we find that D = 2.4 for all three proteins. The values of D vary with the proteins and the maximum dimension of D are as high as 2.8 (Lewis and Rees, 1987). Figure 1.11 shows a more explicit dependence of D on probe radii.
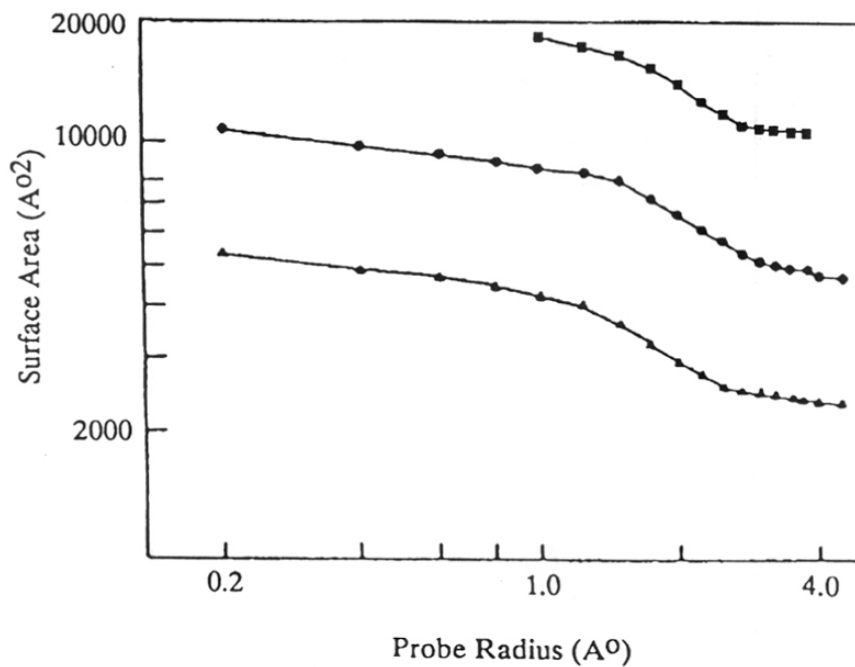
FIGURE 1.10

Dependence of molecular surface on probe radii for lysozyme (●), ribonuclease (▲; areas divided by 2), and superoxide dismutase (■ ; areas multiplied by 2).
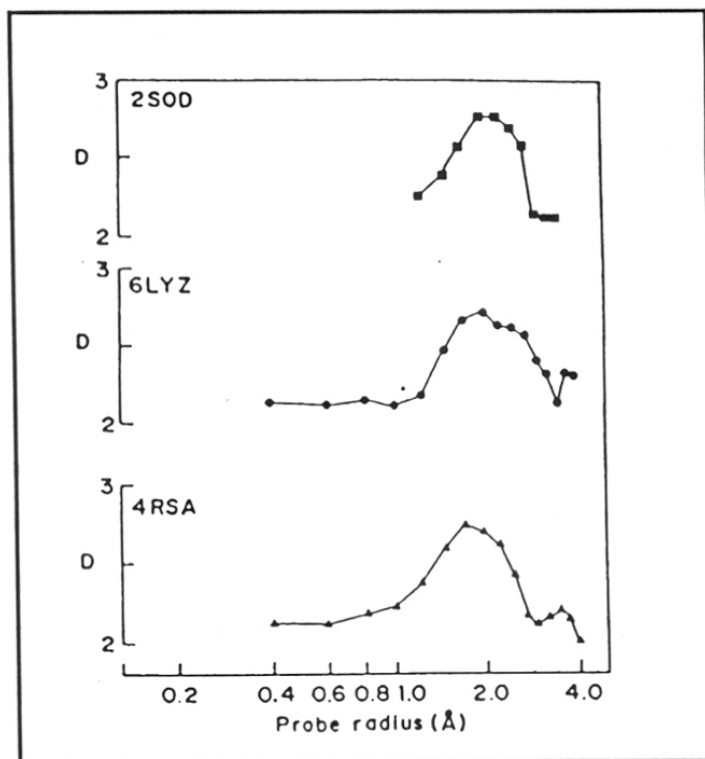
FIGURE 1.11

Dependence of D on probe radii for the same proteins as in figure 1.10. The equation $D = 2 + |m|$ was used to evaluate D as a function of probe radii. Average values of D evaluated for probe radii in the range 1.0 to 3.5 Å were 2.44, 2.44, 2.43 for lysozyme, ribonuclease and superoxide dismutase structures respectively.

In chapter 5 an algorithm is presented which enables visualization of the entire protein surface in two-dimensions. The distribution of various properties on the surface can be seen and comparison of similar proteins is facilitated. Three, new indices have been introduced which help characterize a protein almost completely, and are based on local relationships. Various other indices, including the fractal dimension, have also been calculated for a variety of proteins. Chapter 6 is a special case study on subtilisins and their surface properties.

1.3.3   Dynamics of Fractal Networks

Although the concept of fractal geometry is useful for the definition of static structural properties, it can also have utility when describing the dynamical properties of fractal networks. These could arise either directly, as vibrations of the atoms that make up a fractal structure, or in terms of the diffusion or flow of particles along paths constrained to fractal geometry (Alexander and Orbach, 1982; Orbach, 1984, 1986; Keyes and Ohtsuki, 1985).

1.4   HOW IMPORTANT ARE FRACTALS ?

Like for the theory of chaos, it is too early to say for sure, but the prospects are favorable. Many fractals have already had an important cultural impact and have already been accepted as works of a new form of art. Some are representational while others are totally unreal and abstract. It must come as a surprise to both mathematicians and artists to see this kind of cultural interaction.

To the layman, fractal art seems to be magical. But no mathematician can fail to try to understand its structure and its meaning. Much of the underlying equations would have

been regarded as part of being pure mathematics, without any applications to the real world, had its visual nature not been seen. Most important, many of the most active uses of fractals are in physics, where they have helped tackle some very old problems and also some altogether new and difficult ones (Mandelbrot, 1990).

EFFECT OF FRACTAL NATURE
ON ENZYMATIC REACTIONS

Immobilized enzymes have been modelled as a fractal object in the form of a DLA and each enzyme molecule as another fractal object in the form of a percolation cluster. Simulations have been carried out to test the performance for a sequence of elementary reactions and transport on the surface. The results show that non-idealities in the performance, such as multi-stationarity and substrate inhibition, can also arise in this simple description.

CHAPTER 2

2.1   INTRODUCTION

The most remarkable and highly specialized proteins are enzymes. They are the functional units of cell metabolism and have extraordinary catalytic power, which is generally far greater than that of synthetic catalysts. Enzymes have therefore become important practical tools, not only in medicine but also in the chemical industry, in food processing, and in agriculture (Lehninger, 1984). For cost effective use of enzymes, they have been immobilized on various matrices (Chibata, 1978; Mawal et al, 1990).

Several kinds of regular backbone conformations of proteins have been discovered by careful, but subjective and qualitative, observations of the tertiary structure. The objective and quantitative analysis of the conformations is desirable, but is hindered by the irregularity of protein molecules. The classical Euclidean geometry and differential-geometry have been the common tools for dealing with regular forms, while the extremely irregular forms, such as the trajectory of a particle under Brownian motion and the protein conformation have remained beyond these traditional tools.

Mandelbrot's fractal geometry provides a descriptive and mathematical way to model many of the seemingly complex forms found in nature (Mandelbrot, 1983). Although the fractal dimensionality is but a single parameter, it is nevertheless a useful indicator of protein conformation because it provides a quantitative measure of the degree to which a structure fills the space in which it resides (Wako, 1989).

The rate of substrate arrival (by diffusion) at a biological receptor depends very much on whether the diffusion space is 3-, 2- or 1-dimensional. The maximum rate of a

reaction will depend on the encounter probability of the components. The diffusion process can be treated in terms of Brownian motion, or the random walk process (Feder, 1989). It has been shown in the case of lysozyme that substrate molecules close to the surface are trapped and then migrate along the surface to the active site (Pfeifer *et al*, 1985). Such diffusion on complex proteins with fractal structures may have important biological implications (Voss, 1988).

Enzymatic reactions often involve interaction with charged substrates. Enzymes have localized charged density over their surface. An analysis of the consequences of this surface distribution has been done in chapter 6. Such charges can often result in protein-substrate interactions at locations other than the active site (Regnier, 1987; Kucerova *et al*, 1986). An enzymatic reaction, in which the substrate molecules can attach to certain points on the enzyme surface, other than the active site, and then diffuse towards the active site, has been considered. The amount of substrate that can attach to the surface will greatly depend on the fractal dimension of the surface, surface localization of charges, surface area of enzyme exposed to the medium and the size and bulkiness of the substrate. On reaching the active site, the reaction occurs and the substrate is converted to product. Either the intrinsic rate of conversion of the substrate or the availability of it due to surface diffusion would then determine the rate of the reaction. Diffusion on fractal structures is known to be anomalous (Blumen and Kohler, 1989; Argyrakis and Kopelman, 1990a, 1990b) and a particularly simple illustration of a random fractal is a percolation lattice (Hoshen and Kopelman, 1976; Stauffer, 1985). If movement is allowed from one site of the percolation cluster occupied by the substrate only to a nearest neighbor which is also occupied, the motion is restricted. The aim of this work is to elucidate the effect of the fractal nature of enzymes, and surface diffusion on them, on rates of enzymatic reactions.

2.2 MATERIALS AND METHODS

The enzyme agglomerate was assumed to be in the form of a DLA cluster and each individual enzyme molecule as a percolation cluster at the threshold (figure 2.1). A 2-dimensional DLA cluster with $\sim 10^4$ lattice points (fractal dimension ~ 1.7) and a 2-dimensional percolation cluster with $\sim 2.5 \times 10^3$ (fractal dimension ~ 1.89) were computed for the present study. Certain sites on the percolation cluster were labeled as the active site. 10 lattice points on all four sides of this cluster were kept vacant to facilitate the random walk of the substrate.

2.2.1 *Generation of DLA Cluster*

Generation of the two-dimensional DLA was carried out essentially by the way of Witten and Sander (1981). The initial state is a seed particle at the center of the lattice. A second particle is added at some random site at large distance from the origin. This particle walks randomly until it visits a site adjacent to the seed. Then the walking particle becomes part of the cluster. Another particle is now introduced at a random distant point, and it walks randomly until it joins the cluster, and so forth. If a particle, in its random walk, touches the boundaries of the lattice, it is removed and another one introduced.

2.2.2 *Generation of Percolation Cluster*

For simulation purpose we begin with a percolation cluster at its threshold value p_c (0.5928). The percolation cluster was generated essentially by the way of Stauffer (1985). In the usual process, each point on the lattice is occupied randomly with a probability p and left unoccupied with a probability $(1-p)$, independent of what its

37
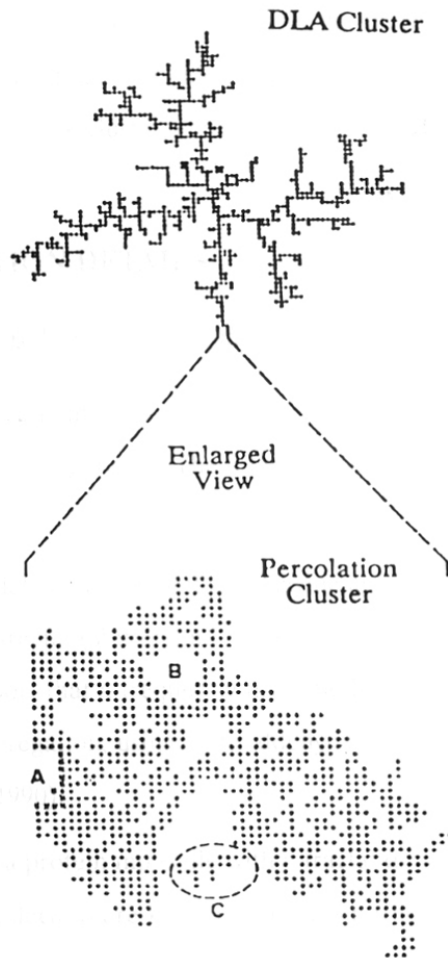
FIGURE 2.1

The immobilized enzyme system as depicted by a DLA cluster. The individual enzyme molecules are represented by a percolation cluster at the percolation threshold.

A   Region of active site.
B   Lattice size unoccupied by percolation cluster.
C   'Dead Zone'.
x   Percolation cluster sites representing the active site.

neighbor is. A *cluster* is a group of neighboring occupied sites. For some probability p, larger than some threshold p_c, one *infinite cluster* appears besides many *finite* clusters, whereas for p below p_c all clusters are finite in the thermodynamic limit. A infinite cluster will therefore touch all four sides of the lattice grid that contain it. In all the simulations only the infinite cluster, generated at p_c was utilized.

2.3   SIMULATION DETAILS

2.3.1   *Assumptions Made for Simplification of the Simulation*

Considering attachment of a substrate molecule to the enzyme surface, the reaction mechanism is depicted in figure 2.2. The following assumptions were made to simplify the simulation:

1) We have modelled an immobilized enzyme aggregate as a DLA cluster, which is a random fractal (Witten and Sander, 1981; Feder *et al*, 1984). This follows from the report that a frequently used method for enzyme immobilization is chemical aggregation, using glutaraldehyde as a bifunctional reagent (Khare and Gupta, 1990).

2) We consider a protein molecule with a fractal dimension of ~1.89. A number of protein molecules are known to possess a fractal dimension and a number of investigators have reported such a dimension for different proteins (Allen *et al*, 1982; Lewis and Rees, 1985; Li *et al*, 1990). It is known that different conformations of proteins may give rise to the same value of fractal dimension (Voss, 1988). Therefore we can generally represent such a protein as a percolation cluster with the same fractal dimension.

3) There is no interaction between individual substrate molecules.

39
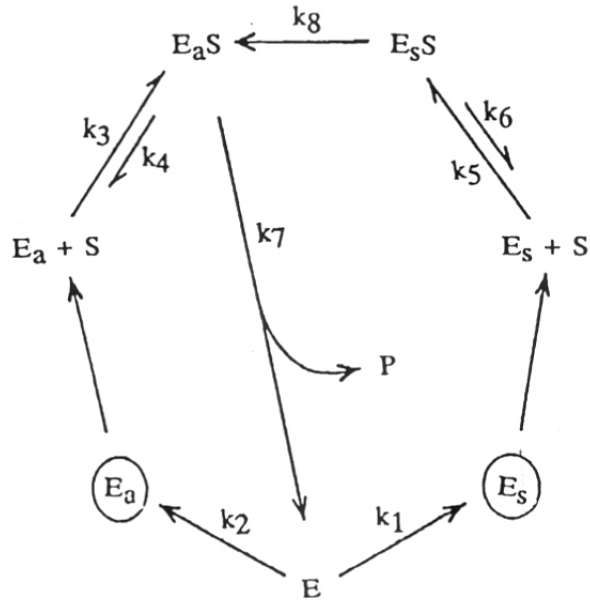
FIGURE 2.2

A schematic representation of the reaction mechanism, where

E_a represents the enzyme active site.

E_s represents the enzyme surface other than the active site.

E_aS represents a complex of the substrate at the enzyme active site.

E_sS represents a substrate molecule attached to the enzyme surface.

P   represents the product.

k_1, k_2 are proportional to the surface area of the enzyme other than the active site and the enzyme active site, respectively.

k_3 is proportional to the probability of colliding at the active site and attaching there.

k_5 is proportional to the probability of attachment to the enzyme surface on colliding there.

k_4, k_6 are proportional to the dissociation constants of E_aS and E_sS, respectively.

k_7 is proportional to the reaction probability on complex formation.

k_8 is proportional to the surface diffusion coefficient and the number of surface bound substrate molecules.

4) The substrates can attach only to the edges of the percolation cluster to account for the fact that only certain patches on the enzyme surface are capable of interacting with the substrate.

5) Once the substrate is bound to the surface, it moves towards the active site through the shortest available distance.

6) The dissociation constants for the complexes formed are low.

2.3.2   Simulation Methodology

The reaction mechanism was simulated using the Monte Carlo method. Particles were released from outside of the region occupied by the DLA cluster and followed a random walk trajectory on the lattice. If the particle reached the end of the lattice, it was rejected. On reaching a point on the DLA cluster, that point was magnified as a percolation cluster. The particle then continued its random walk towards the percolation cluster. If the particle reached the end of this lattice, it was again allowed to walk on the lattice of the DLA cluster. On reaching the percolation cluster, the particle was allowed to follow a biased random walk towards the active site by the shortest available distance. Diffusion of substrate particles bound on the enzyme surface was simulated simultaneously. If a particle tried to attach to a position where another substrate was already present, it was rejected. If one particle had all four nearest neighbors occupied, then it did not move at that instant. On reaching the active site, the complex was formed and reaction took place with a certain high probability. Assuming different surface diffusion coefficients (D), in the range of 0.005 to 8, product formation was studied as a function of time.

Similar simulations were performed on a perfect square lattice (with the same number of lattice sites as the percolation cluster) in place of a percolation cluster to delineate the effect of the fractal nature of the surface. Variation of rate of product formation with substrate concentration was studied for both the cases.

2.4   RESULTS AND DISCUSSIONS

Many chemical and biochemical reactions in nature exhibit complex characteristic behavior patterns which require the use of highly nonlinear rate models to explain the observations (Sadana *et al*, 1981). In reality, however, the behavior may have its origin in other non-idealities such as fractional dimensions of the system and the rate and transport processes on them. In the present study we have tried to analyze this effect by considering a sequence of elementary bioreactions on the enzyme molecules. The analysis, however, can also be carried out for any other heterogeneous system.

Profiles for product formation as a function of time, for different diffusion coefficients, are shown in figure 2.3a (percolation cluster) and figure 2.3b (perfect lattice). The presence of regions over periods of time where the product formation is relatively slow can be discerned in this figure. This is especially clear if we examine the profiles for lower diffusion coefficients. This is, however, not the case for a perfect lattice as seen in figure 2.3b.

This can be explained using the following observations during the simulation: At the very beginning of the reaction, very small amount of substrate is bound to the enzyme surface. If diffusion is fast, these substrate particles can reach the active site faster than they could have in the case of slow diffusion.
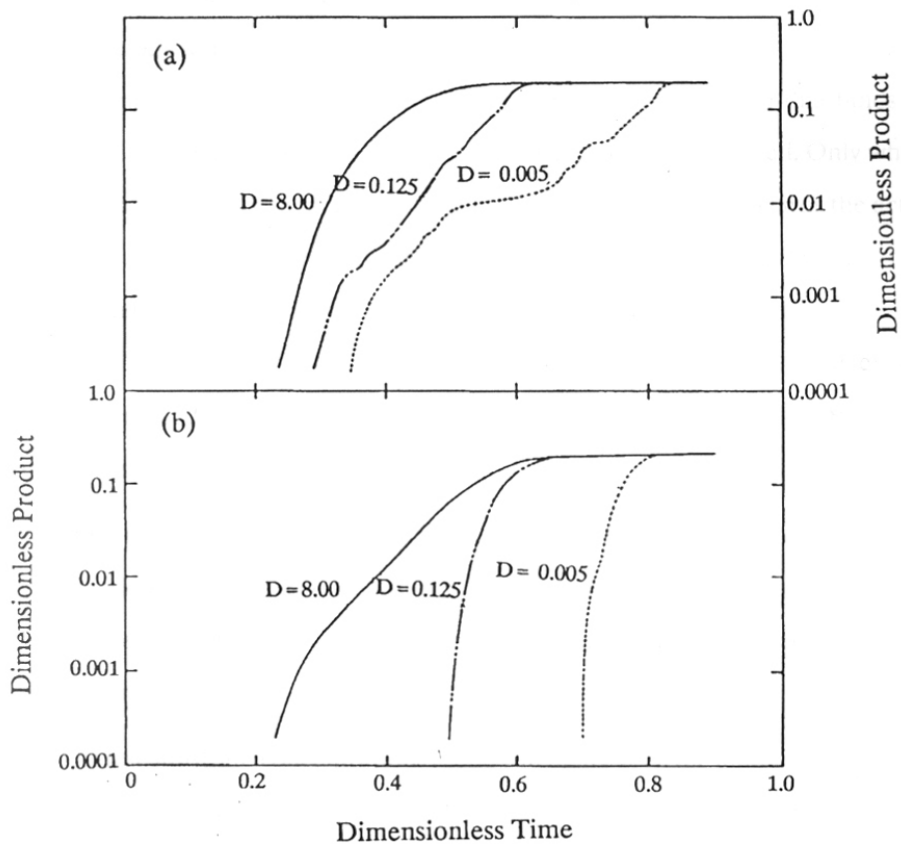
FIGURE 2.3

a) Profiles depicting product formation as a function of time for reaction on a percolation cluster.

b) Profiles depicting product formation as a function of time for reaction on a perfect square lattice.

After lapse of some time, more substrates bind but the hindrance to their movement is not very high. As time proceeds, the surface is almost saturated with the substrate and resistance to diffusion is high. Due to the presence of lattice sites unoccupied by the percolation cluster (shown in figure 2.1), achievement of equal distribution of substrate over the enzyme surface takes time. The large amount of substrate that binds initially takes time to reach the active site and further attachment is hindered. Only when most of these have reacted can more substrate bind and diffuse slowly towards the active site. This gives rise to regions of relatively slow product formation. On a perfect square lattice, achievement of a more or less equal distribution of substrate on the surface is faster than on a percolation cluster. Under conditions of high diffusion coefficients, lattice sites unoccupied by percolation cluster do not cause resistance to movement and the surface also does not get saturated.

Figure 2.4 depicts the profiles for the amount of substrate attached to the surface as a function of substrate concentration. To delineate the effect of the fractal nature of the surface, profiles for reaction on a percolation cluster have been compared with that on a square lattice.

At low substrate concentrations (zone 1 in figure 2.4), the amount of substrate that can bind to the surface will not be affected by the perimeter. This is because at this concentration of the substrate, the ratio of the surface area occupied by the substrate, in comparison to the overall area to which the substrate can bind, both in the case of a square lattice and a percolation cluster, is small. Movement is facilitated on the square lattice and so rate of reaction is higher than that on the percolation cluster (zone 1 in figure 2.5).

At intermediate substrate concentration (zone 2 in figure 2.4), the amount of substrate that can bind to the surface will now depend on the perimeter and surface
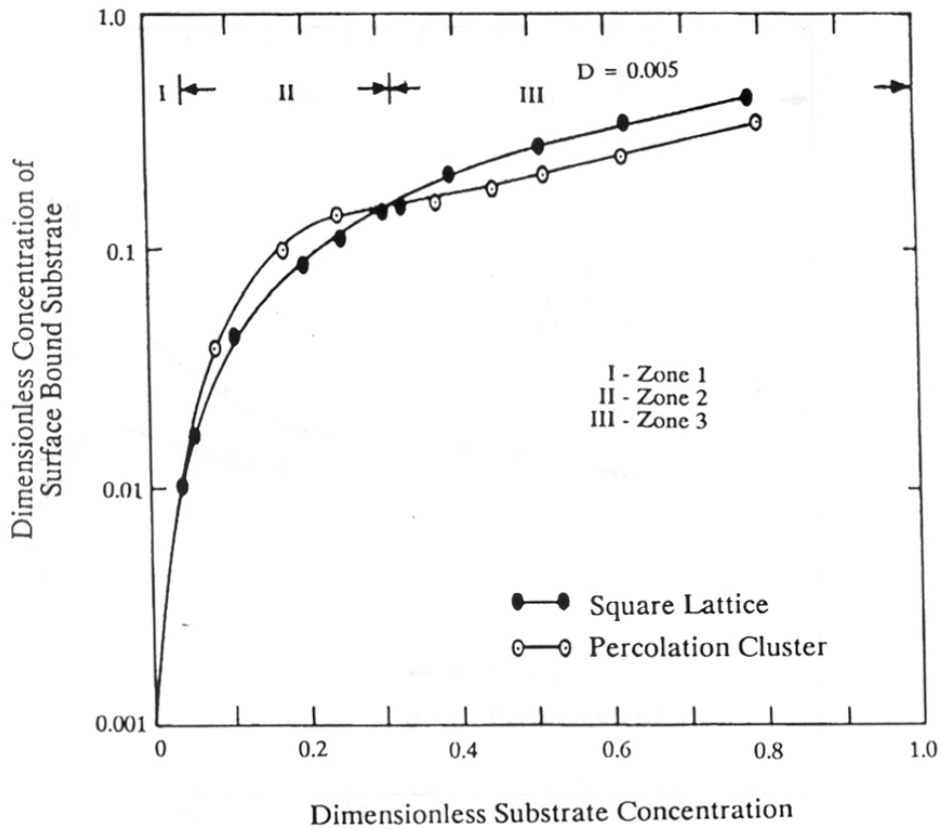
FIGURE 2.4

Profiles showing amount of surface bound substrate as a function of substrate concentration, on a square lattice and on a percolation cluster.
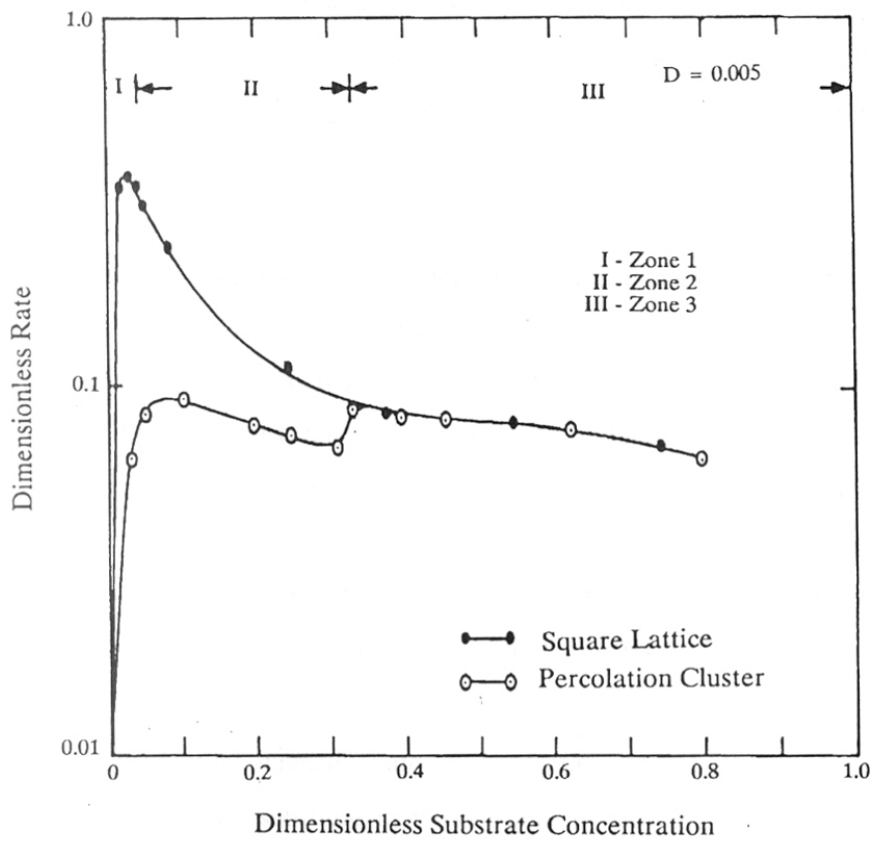
FIGURE 2.5

Profiles of rate of reaction as a function of substrate concentration, on a square lattice and on a percolation cluster.

area available for movement towards the active site. In the case of a percolation cluster, the perimeter is larger than that of the square lattice. Thus, the amount of substrate that binds to the cluster is larger. It faces restrictions in its movement and so the rate starts falling (zone 2 in figure 2.5). The fall in rate of reaction on the square lattice is faster as it undergoes a larger change from less surface bound substrate to saturation of the surface (from zone 2 to zone 3 in figure 2.4) and has a greater tendency to get saturated with the substrate.

At high substrate concentration, the average amount of substrate that can bind to the surface of the percolation cluster is lower even though the perimeter of the same is larger than that of the square lattice (zone 3 in figure 2.4). This is because the restriction to movement on the percolation cluster is larger due to presence of unoccupied sites. Thus the perimeter is not made vacant easily and further attachment is hindered. On the square lattice less substrates bind initially, but move easily over the surface facilitating further attachment. The surfaces of both the percolation cluster and the square lattice tend to get saturated and the fall in rate can be attributed to the inhibition in movement towards the active site caused by the binding of this excess of substrate. The rates coincide as seen in zone 3 of figure 2.5.

The profiles of reaction rate versus substrate concentration, as shown in figure 2.5, depict significant substrate inhibition, both in the case of a square lattice and a percolation cluster. In the case of a percolation cluster, the same rate of reaction is observed at four different substrate concentrations. This phenomenon is not noticed in the case of a square lattice. The reasons for this can be attributed to the complex kinetics arising from the fractal nature of the surface. In the case of a percolation cluster, at high substrate concentration, the *dead zones* get completely saturated and hence the movement of substrate to the active site is facilitated without it getting stuck there. This

also probably contributes to the double-humped nature of the curve in figure 2.5. *Dead zones* are defined as regions in the percolation cluster which are connected to other regions by constricted sites and do not have a direct access to the active site. *Dead zones* are clearly depicted in the figure 2.1. These are also responsible for the product formation being less than one in case of reaction on a percolation cluster.

2.4   CONCLUSIONS

The analysis indicates that substrate inhibition in certain cases can be attributed to slow surface diffusion of substrate particles towards the active site. Rate multiplicity attributed to date to complex reaction kinetics on a homogeneous surface may be attributed to the heterogeneous (fractal) nature of the surface, as seen here in case of an elementary reaction.

CHAPTER 3

CAN MOBILE SHAPES OF FRACTALS CAUSE RATE ENHANCEMENTS ?

The concept of mobile fractal shapes *(fractiles)* is introduced and applied to biological processes. Systems like biological membranes, proteins and nucleic acids, which can be described as fractals, exhibit significant dynamism in their shapes. Numerous such examples also exist in other physical and chemical systems. The effects of this dynamism or mobility have been studied on the overall physical, chemical and biological process. Theoretical simulations for a model system indicate that mobility can drastically affect the rate constants of such processes.

CHAPTER 3

3.1   INTRODUCTION

During the last few years, increasing attention has been focused on the dynamic aspects of protein and nucleic acid structure and function (McCammon and Harvey, 1989). It has long been inferred from a variety of experimental studies that substantial structural fluctuations occur in these molecules, and that these fluctuations are essential to biological activity (Linderstrom-Lang and Schellman, 1959; Koshland, 1963; Edsall, 1968).

The last chapter considered an enzymatic reaction with the enzyme taken as a static fractal. This may not give the complete picture of many biological molecules which are actually dynamic in nature. This chapter deals with biological molecules modelled as mobile fractals. Simulation studies on fractal sets wherein the dimension of the system may or may not undergo a change have been performed. The results indicate the implications of mobility in biosystems as well as certain physical and chemical systems.

Biological systems like membranes, proteins and nucleic acids, which can be described as fractals, show considerable change in their shapes. Their activity is related to the mobility of their components i.e. their dynamic behavior. It is known that different fractal sets with different appearances or textures (*lacunarity*) may have the same fractal dimension (Voss, 1988). If a reaction occurs on a fractal shape whose lacunarity evolves with time, the rates of the reactions may be drastically different. We define *fractiles* as fractal objects which change their shapes, with or without maintaining a constant fractal dimension (Shinde *et al*, 1990).

3.1.1 Applicability of Fractiles in Real Systems

Fractile systems do occur in practice frequently and the example of cell membranes may help to familiarize the concept in simple terms. Biological membranes are organized sheet-like assemblies consisting mainly of proteins and lipids. The functions carried out by them are indispensable for life. Membranes are highly selective semipermeable barriers which contain specific molecular gates and pumps. These transport systems regulate the molecular and ionic composition of the intracellular medium. Cell membranes are frequently described as fractals with non-integer dimensions (Kopelman, 1986). Though membranes are fractal in nature, their fractal dimension has not been calculated to date. The protein and lipid units in the membrane plane are known to undergo diffusion and the rates of their movement are dependent upon various factors such as the composition of the lipids and the protein to lipid ratio. Furthermore, external factors like temperature, pH etc also affect the diffusion of the components (Tocanne *et al*, 1990). The proteins and lipids which form the lattice points that describe a fractal shape can themselves be in motion. This leads one to the notion of a mobile fractal. The activity of certain membrane associated proteins is known to be affected by the lipid composition around it. As mobility of the membrane lipids is high, the local concentration around any protein may undergo a constant change as a result of which the activity of the protein can be affected.

Other examples include DNA-protein complexes (von Hippel *et al*, 1989) and reactions on catalytic surfaces. During the DNA-protein interaction (which depends on the environment (Shakked *et al*, 1989)) intermediate complexes are formed. It is known that the regulatory protein in such complexes can bind to sites that are quite far apart along the DNA contour. However, they are brought together transiently by the segmental diffusion of individual loops of the DNA double helix (Berg *et al*, 1981). This again

suggests that a fractal describing DNA can experience changes in its shapes (for pictorial representation see Stryer (1988)). In a broader sense, mobility of the individual components of the membrane will amount to a change in the fractal shape.

A closer look at most systems reveals mobility in one form or another (McCammon, 1984; Duprez et al, 1990; Hopkins et al, 1990). It is known that a number of enzymes have mobile surface loops that change conformations to allow ligand entry and to secure the ligand in place (James and Sielecki, 1983; Anderson et al, 1979; McCammon and Northrup, 1981). X-ray analysis of several enzymes also indicate large scale structural changes upon sorption of substrate (Anderson et al, 1978; Bennet and Steitz, 1978). The presence of external fields, indirectly inducing mobility, is also known to enhance the rates in some other systems (Vayenas et al, 1990; Weaver and Astumain, 1990).

The past decade has witnessed vigorous activities in applying the concept of fractals to various problems in as diverse areas as chemistry, biology, geology, solid state physics, astrophysics and atmospheric sciences (Sander, 1986, 1987; Smirnov, 1990; Kopelman, 1988; Goldberger et al, 1990). The literature is replete with information regarding the results of several different types of experimental systems and theoretical tools to compute the rates of transport and reactions on fractals. Despite this fact, the effects of mobility of the fractal shapes have not so far been investigated. This becomes more relevant when one notices that a large number of experimental systems with rate exceeding the limit set by the diffusion controlled nature of the process by orders of magnitude are known (see experiments of Riggs et al (1970)). In fact the question of how systems of different sorts might transcend the rate limits set by three-dimensional diffusional control has been an unresolved question despite the flurry of theoretical investigations and the experimental papers coming from as varied disciplines as mathematics to physical chemistry to biology. The possible explanations offered and the progress in

some of these areas has been recently reviewed (von Hippel *et al*, 1989).

3.2   SIMULATION STUDIES OF ELEMENTARY REACTIONS ON FRACTILES

The present work undertakes to explore the effects of mobility of the fractal on the behavior of the system. The consideration of mobile fractals leads to the question as to whether the fractal dimension of the system itself would change or not. Such a question should be answered on a case to case basis. Our interests here are to first establish the qualitative effects and, thus, for the time being we begin with a fractal object of specified dimension and allow its shape to change (at different speeds) while maintaining the same fractal dimension. Further, similar studies have also been performed for cases where the fractal dimension is allowed to change to assess its effect. Simulations have also been performed on a more complex reaction scheme to assess the effect of mobility on the selectivity (Meakin, 1986; Tambe *et al*, 1990)

We consider a system for which extensive Monte-Carlo simulations have been carried out (two-particle annihilation process, $A + B \text{--}>$ inerts, with *initial pair-correlated and random distribution* (Ben-Avraham, 1987)) and the results known. This will help in clearly identifying those effects that come about due to mobility of the fractal and, in the limiting case of no mobility, will also provide a test for the validity of the simulated results.

In a random type of distribution, for two-particle annihilation on a fractal surface, the particles A and B are allowed to adsorb on the surface in a way such that there exists absolutely no relation between the position acquired by a particle A and the position of a particle B. In the case of distribution of the initial pair-correlated type, the

distribution of a particle A is such that it is within a short and defined distance of a particle B and *vice versa*. Generally, this is achieved by distributing species A and B as pairs on the fractal surface.

3.2.1 Movement of Cluster

For simulation purpose we begin with a percolation cluster at its threshold and identify particles which can move. The possible attachments of particles and allowed movements are shown in figure 3.1. Four pivots at the four edges are identified. These are not allowed to move to ensure same fractal dimension all through the simulation. Each particle capable of movement (labelled CY in figure 3.1), except for the singly attached ones, is identified and allowed to move to a neighboring site not occupied by the cluster but being itself a nearest neighboring site to a point on the cluster. The singly attached particles (labelled Y in figure 3.1) are allowed to random walk and attach to a cluster site with a certain probability. Particles labelled N are not allowed to move as this would lead to a break in the percolation cluster. Open circles are nearest-neighbors of the particles being considered for movement (shown as solid circles in figure 3.1). These rules for mobility can be considered random within spatial limits and can be related to the relative movement of membrane components or residues of a protein molecule. The evolution of the fractal surface with time is shown in figure 3.2.

3.2.2 Reaction Simulations and Random Walk on a Fractile of Constant Dimension

To simulate diffusive annihilation on a 2-D percolation cluster, sites on the cluster are picked up and occupied with particles, either A or B, in a way to avoid multiple
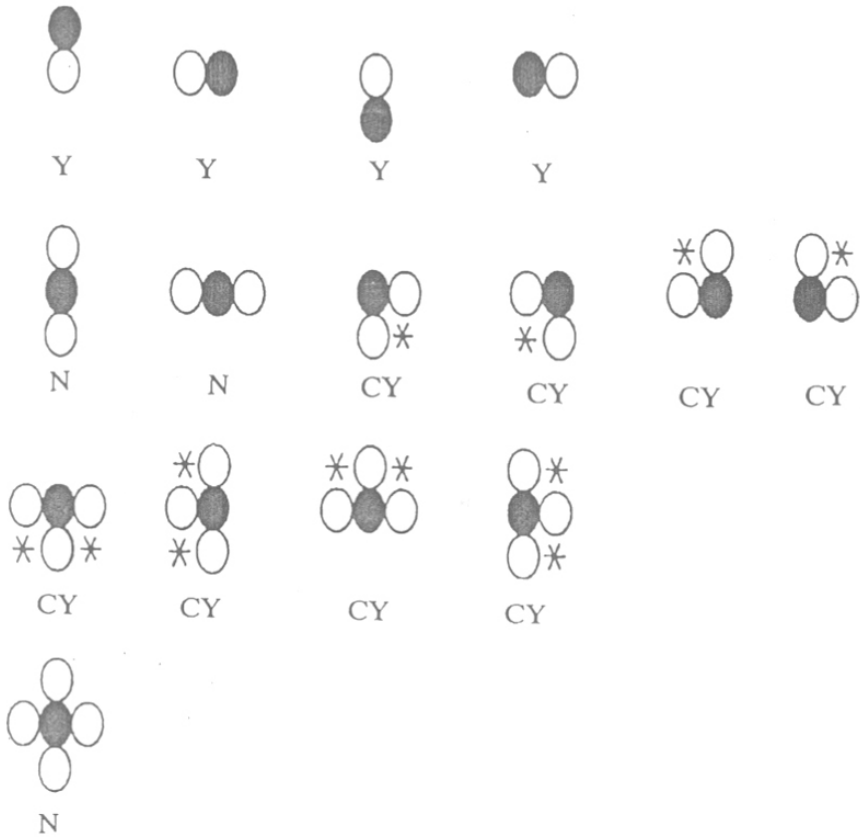
FIGURE 3.1

Schematic diagram showing possible ways of particle attachment and conditions for movement.

Solid circles depict the particle being considered for movement.

N ------ cannot move at all.

Y ------ can move randomly anywhere on the lattice but the new position should have at least one nearest neighbor as a part of the fractal.
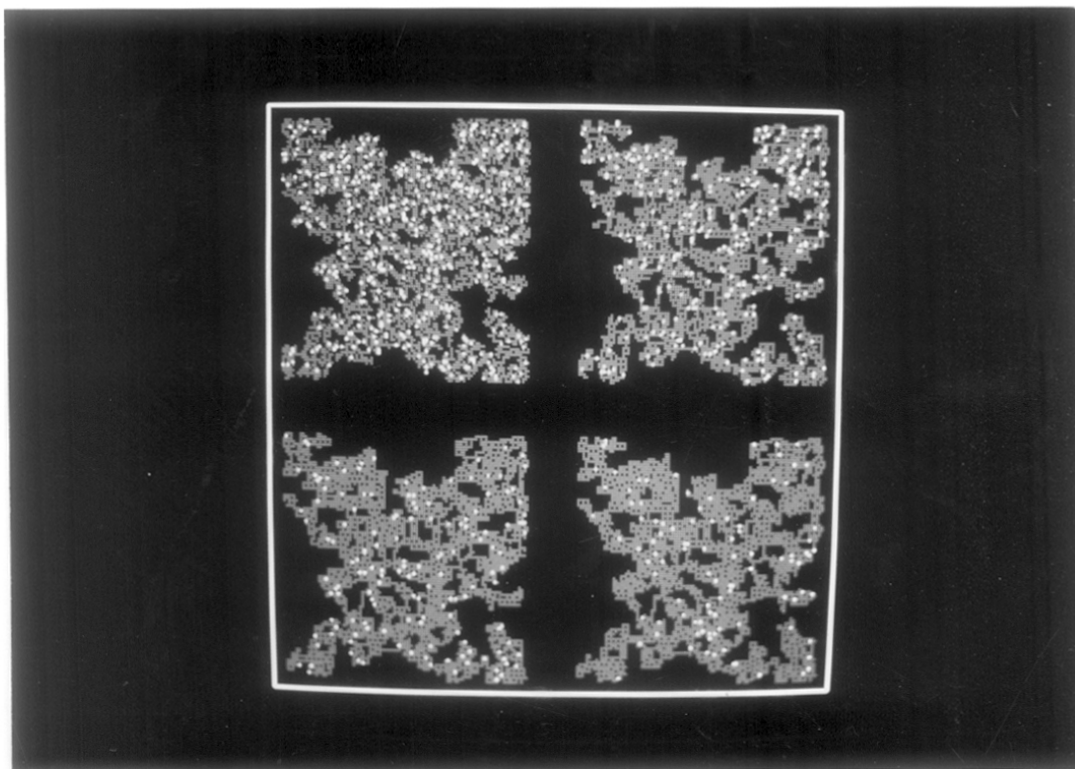
CY ------ can move a distance of one lattice point if

(a) the position(s) marked '*' is/are a part of the fractal.

(b) the new position has at least one nearest neighbor as a part of the fractal.
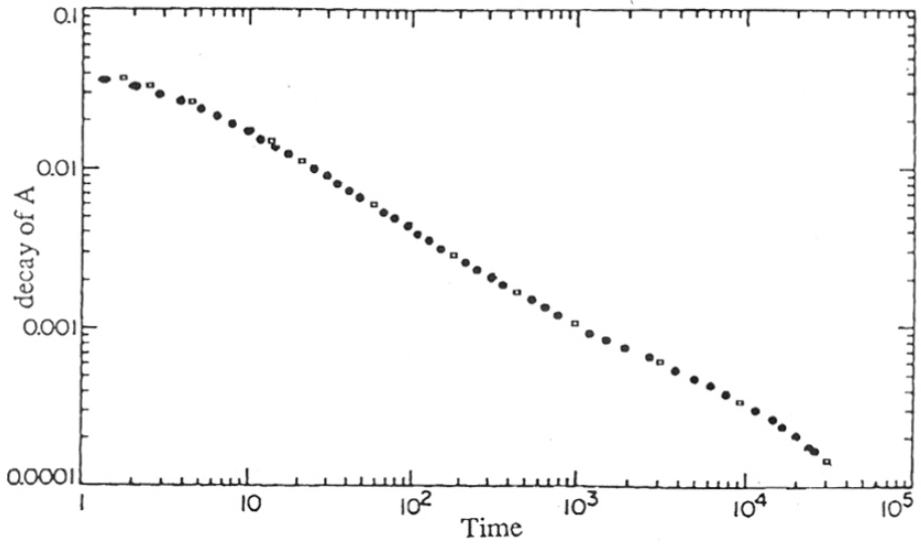
FIGURE 3.2

Evolution of the fractal shape with time: stage 1-top left; stage 2-top right; stage 3-bottom left; stage 4-bottom right.

occupancy until a desired concentration of particles has been achieved. The particles are then selected at random and moved to a randomly selected nearest-neighbor site. The reaction occurs if two antiparticles are nearest-neighbors of each other. The simulations were, thus, carried out using standard procedure (Meakin and Stanley, 1984) and the results compared and validated with the results obtained for the reaction on a static fractal using a large lattice size (1000 X 1000) (figure 3.3). However, for computational reasons and for relative ease in engineering fractal mobility, we preferred conducting the simulations on a smaller lattice (100 X 100). The effect of smaller lattices on reaction profiles have been noted by earlier workers (Toussaint and Wilczek, 1983). These would not affect the qualitative results as finite size effects would be observed in case of both the static and mobile fractals. Additionally periodic boundary conditions were employed in the simulations. Hence a comparison between the two would still give a reasonable indication of the effects of fractal mobility on the reaction kinetics.

The lattice points describing the fractal are moved to gauge the effect on the reaction. After all the particles have attempted to move once and A and B are found to be nearest neighbors, the number of product formed is incremented by N_A * k1, where N_A is the number of A molecules with B as nearest neighbors (pair) and k1 is the rate constant. Each time this value exceeds an integer one pair of A and B is selected, at random, and converted to inert product. Varying values of the rate constant were used for all the different cases studied.

The variation of the rate constant for the reaction $A + B$ --> inerts, as the reaction proceeds on a mobile fractal surface (percolation cluster), was established by the following simulation at different mobilities. Sites on the fractal surface are picked at random and occupied with A and B particles (avoiding multiple occupancy) till a desired initial particle concentration has been reached. After all the particles have attempted

FIGURE 3.3

Particle density in the particle-antiparticle model ($A + B$ --> inert) in two dimensions for an initial particle density of 0.05. The solid circles depict the results of Toussaint and Wilczek (1983), whereas the empty boxes show our results. The lattice size in both cases is 1000 X 1000.

to diffuse once and A and B are found to be nearest neighbors, the number of product formed is incremented by N_A * k1, where N_A is the number of A molecules with B as nearest neighbors (pair) and k1 is the rate constant. Each time this value exceeds an integer one pair of A and B is selected, at random, and converted to inert product. The rate constant at each time was evaluated as the ratio of the product formed to the reactant concentration.

3.2.3   Reaction Simulations and Random Walk on a Fractile of Changing Dimensions

The following two case studies were also simulated with the same reaction scheme to assess the effect of the change in fractal dimension of the base during the course of the reaction.

(i) the fractal base is randomly changed between a DLA and a percolation cluster (with same number of lattice sites occupied) so that the dimensionality changes values between ~ 1.7 and ~ 1.89.

Randomly picked sites on the fractal surface are occupied with A and B particles (avoiding multiple occupancy) till a desired initial particle concentration has been achieved. After diffusion and reaction, all the reactants are picked up, a fractal surface is decided on randomly and the reactants are allowed to occupy sites here for continuation of the reaction. Similar reactions occurring only on a DLA cluster and only on a percolation cluster were also studied.
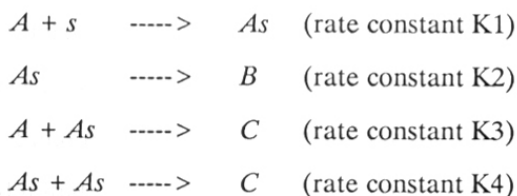
(ii) the fractal base is a percolation cluster (200 X 200) which is allowed to move such that its dimension can change during the course of the reaction.

Cluster sites are randomly picked and occupied with reactants (avoiding multiple occupancy) until a desired initial particle concentration is reached. After diffusion and reaction, the cluster is allowed to move as earlier with the variation that there are no pivots, the surface may not remain a percolation cluster during the entire course of the reaction and the fractal dimension might change from ~1.89.

To simulate the diffusive annihilation process, A and B particles are moved to a randomly selected vacant nearest-neighbor site on the cluster. All particles are allowed an attempt to diffuse. Both A and B particles are removed if they occupy the same lattice site. If a randomly selected move would cause a lattice site to be occupied by more than one A particle or more than one B particle, the move is rejected. This reaction was studied at varying values of the rate constant for both the above mentioned cases.

3.2.4   Selectivity Studies on a Fractile of Constant Dimension

To study the selectivity behavior on a mobile percolation cluster of constant fractal dimension, the following multistep reaction scheme was simulated.

$$A + s \quad -----> \quad As \quad \text{(rate constant K1)}$$
$$As \quad -----> \quad B \quad \text{(rate constant K2)}$$
$$A + As \quad -----> \quad C \quad \text{(rate constant K3)}$$
$$As + As \quad -----> \quad C \quad \text{(rate constant K4)}$$

C is the desired product and B is the undesired product. Selectivity, a relative measure defined as the ratio of number of molecules of C formed to the number of molecules of B formed, was studied at steady state on a static and a mobile fractal. A constant flux of A particles is launched at each time interval. If they land on a point of the percolation cluster unoccupied by any other particle, they get adsorbed to form the

species As. These are allowed to diffuse freely over the surface. If A particles land on adsorbed A particles, a C molecule is formed with rate constant K3. Conversion of As to B molecules is assumed to have a rate constant K2. If two adsorbed A particles come to occupy the same site, a C molecule is formed with rate constant K4. The different cases studied were (i) varying flux of A onto the fractal surface (ii) varying mobility of the fractal and (iii) varying value of rate constant K2 with constant values of K3 and K4. The movement of the fractal base was as allowed earlier, keeping the fractal dimension constant.

3.3   RESULTS AND DISCUSSIONS

Figures 3.4-3.6 depict profiles for the *two-particle annihilation* on a mobile fractal base with constant fractal dimension. Figures 3.7 and 3.8 depict profiles for a similar case study on a mobile fractal with changing fractal dimension. Figure 3.9 depicts profiles for the selectivity studies on a mobile fractal base of constant fractal dimension.

Figure 3.4a shows that the mobility of the fractal leads to greater product formation (case of a random initial distribution) in the *two-particle annihilation* process with spatial inhomogeneities. The mobility of the fractal causes *surface renewal* resulting in bringing more and more of A and B particles together and facilitating the reaction. In the case of a pair-correlated initial distribution, however, a lower amount of product is formed when compared to reaction on a static fractal surface. The mobility of the surface in this case tends to restructure the pairing, thus losing A to B contact, and results in low product formation. Figure 3.4b shows decay of reactants as a function of time.

The effects of mobility as seen here are in a way similar to the effects of stirring observed in the work of Argyrakis and Kopelman (1989) and the effects observed by
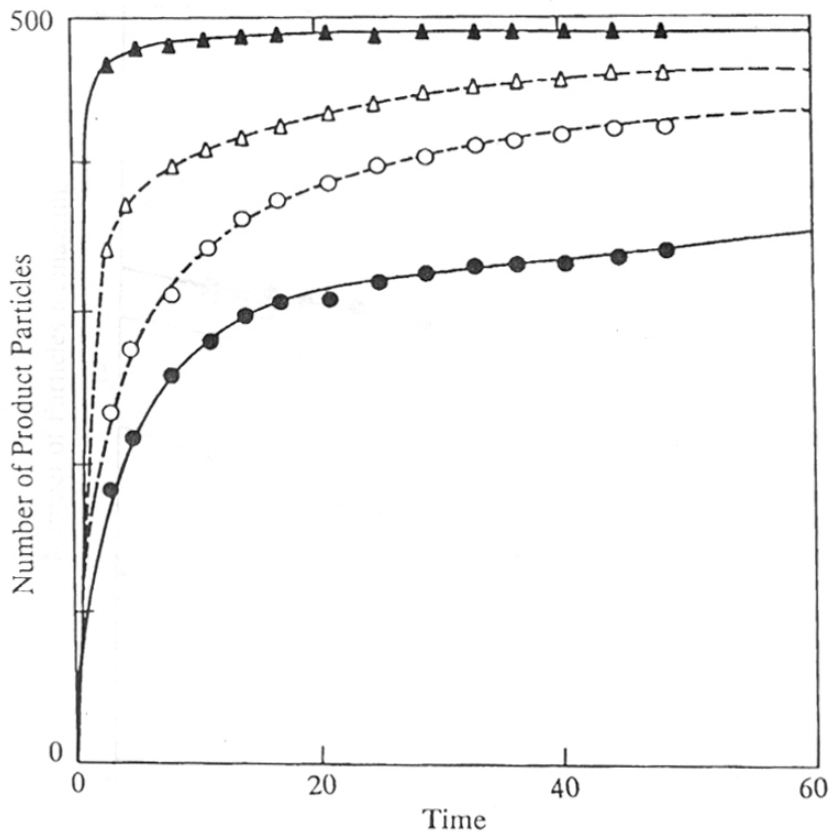
FIGURE 3.4a

Profiles of number of product particles formed versus time with a random initial distribution on a static fractal (●), on a mobile fractal (○), with a pair-correlated initial distribution on a static fractal (▲) and a mobile fractal (△).
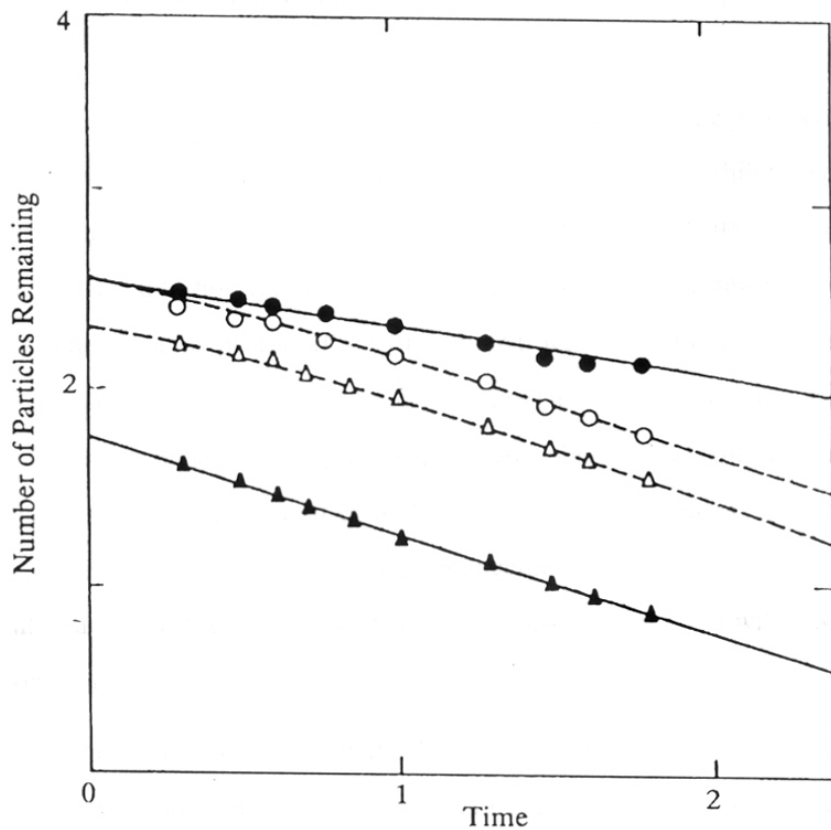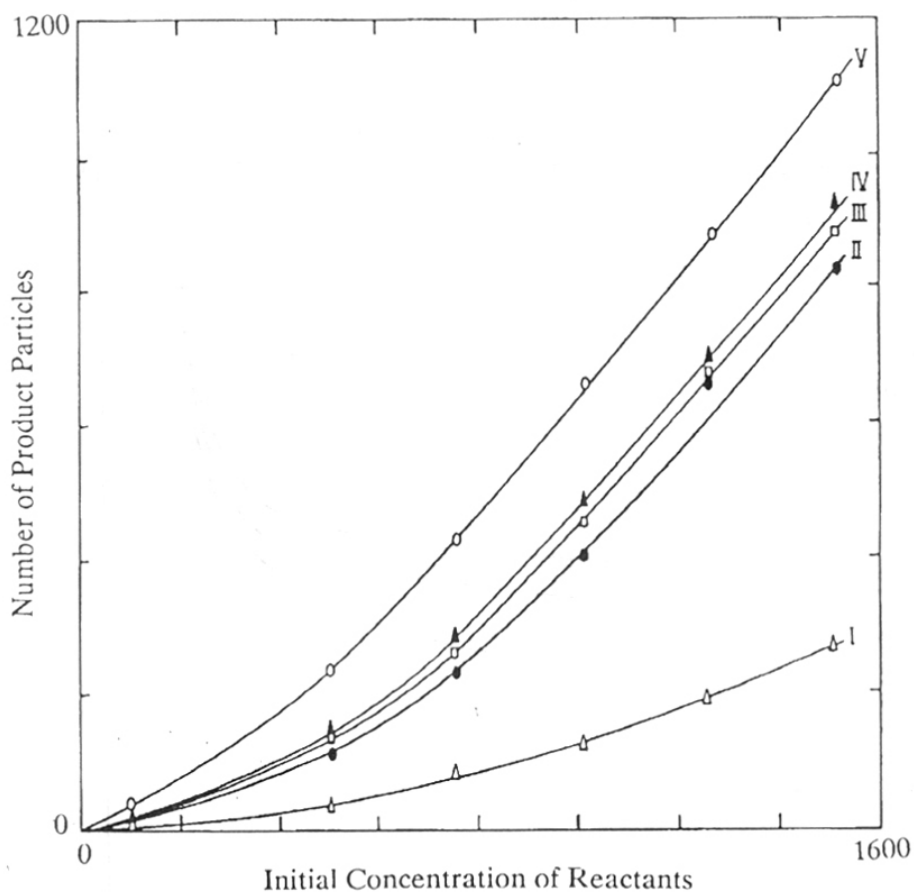
FIGURE 3.4b

Profiles depicting the decay of 'A' particles with time with a random initial distribution on a static fractal (●), on a mobile fractal (○), with a pair-correlated initial distribution on a static fractal (▲) and a mobile fractal (△).

Harrison and Zwanzig (1985) in the use of a dynamic percolation model. There are, however, some essential differences that in both the cases, though some amount of dynamism does exist, the past, present and future states are totally unrelated. In the present case the fractal surface takes the shape that is permissible as per the scheme defined in figure 3.1 and therefore a definite relation exists between the past and present shape.

Figure 3.5 shows the effect of fractal mobility on the amount of the product formed as a function of initial concentration of A and B for the two-particle annihilation process. Profile IV in this figure corresponds to behavior on a static fractal (rate constant = 1) while profiles II, III and V show the behavior on a fractal surface with different mobilities. If we were to reproduce the profile 'II' say on a static fractal, we observe that we would need a rate constant which is about 100 times larger. This is equivalent to saying that on a mobile fractal corresponding to profile II, we have observed a 100-fold increase in the rate. Qualitatively, higher extent of mobility leads to higher rates of reaction. A quantitative correlation of magnitude of rate enhancement with the magnitude of shape change would vary with the kind of system under consideration and will have to be attempted on a case to case basis.

Profiles of rate constant with time are shown in figure 3.6. As expected for fractal kinetics it can be observed that the rate constant changes during the course of the reaction. It tends to achieve a stable value at high mobilities.

Figure 3.7a, shows that the extent of product formation increases with an increase in the rate constant. Figure 3.7b shows the amount of product formed as a function of initial number of reactants present, for various values of the rate constant. In figure 3.7c we see product formed versus initial amount of reactants profiles, with varying rate constants, for reaction occurring only on a DLA cluster. Figure 3.7d shows similar profiles

FIGURE 3.5

Profiles showing the number of product particles formed as a function of initial number of reactants present for reactions on a fractal with constant fractal dimension.

I ------ reaction on a static fractal with reaction rate constant 0.1.

II ------ reaction on a mobile fractal (moved forty five times) with a reaction rate constant 0.01.

III ------ reaction on a mobile fractal (moved five times) with reaction rate constant 0.1.

IV ------ reaction on a static fractal with reaction rate constant 1.0.

V ------ reaction on a mobile fractal (moved once) with reaction rate constant 1.0.
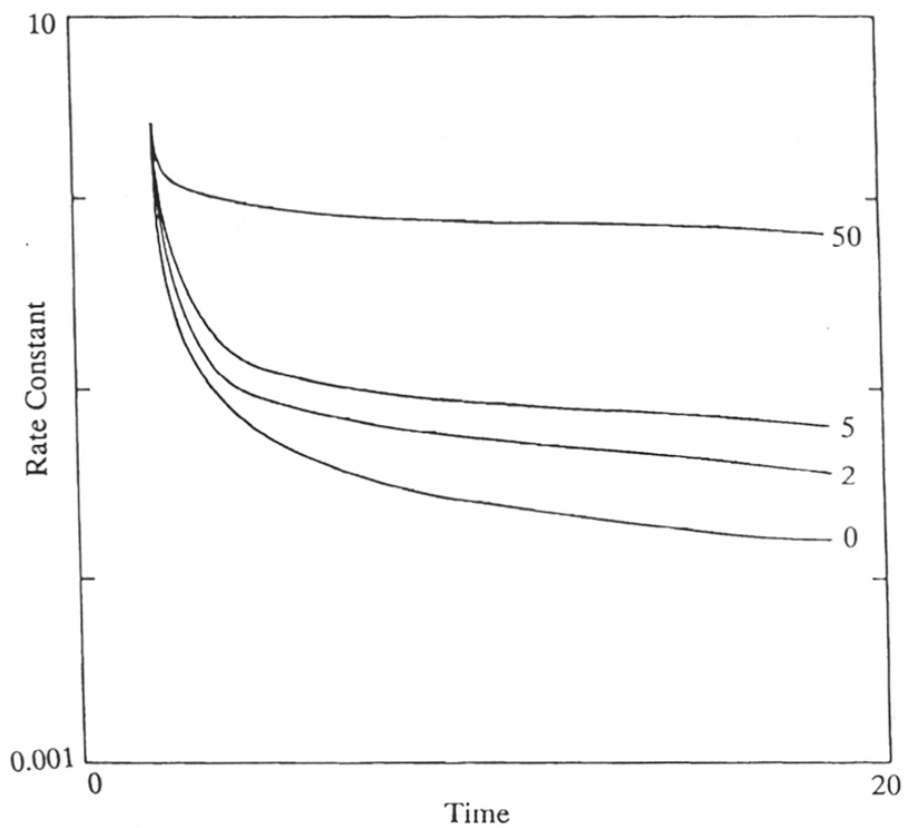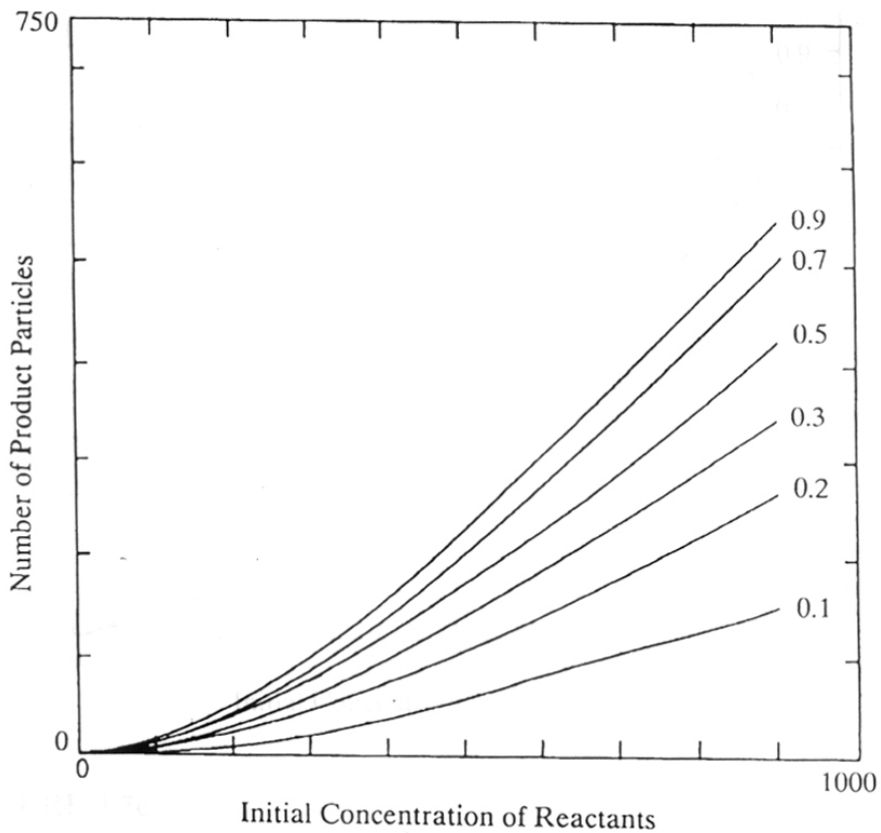
FIGURE 3.6

Profiles showing change in the rate constant during the course of the reaction as a function of time on a mobile fractal of constant fractal dimension. The figure shows the cases when the fractal was static (moved 0 times) and mobile (moved 2, 5 and 50 times).
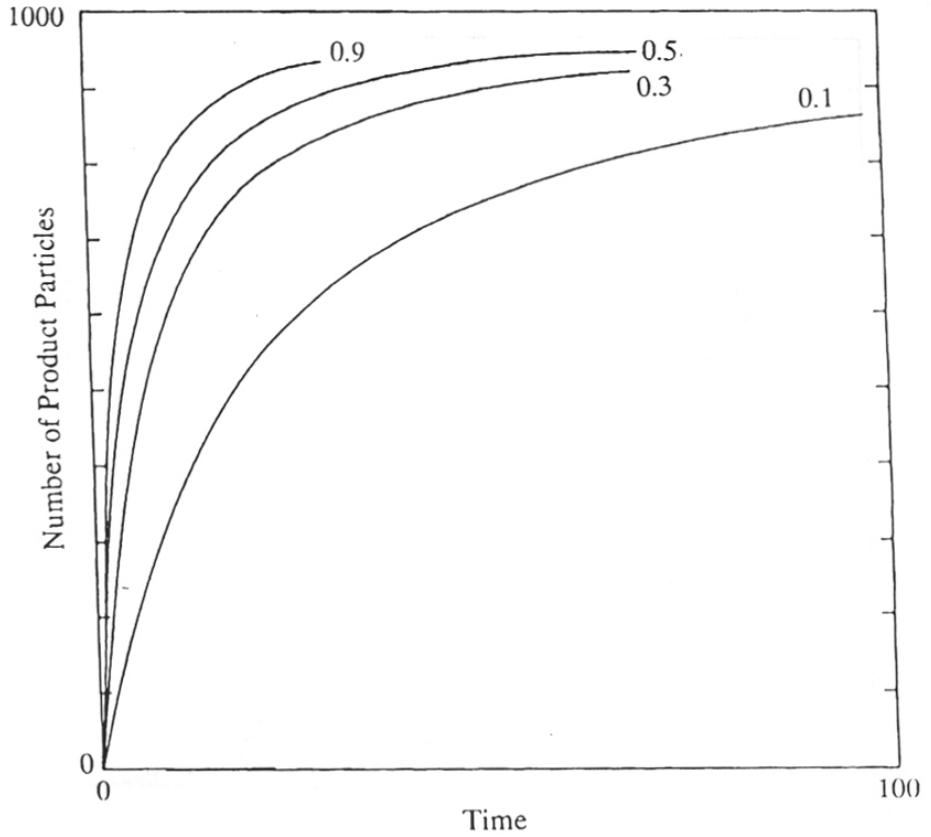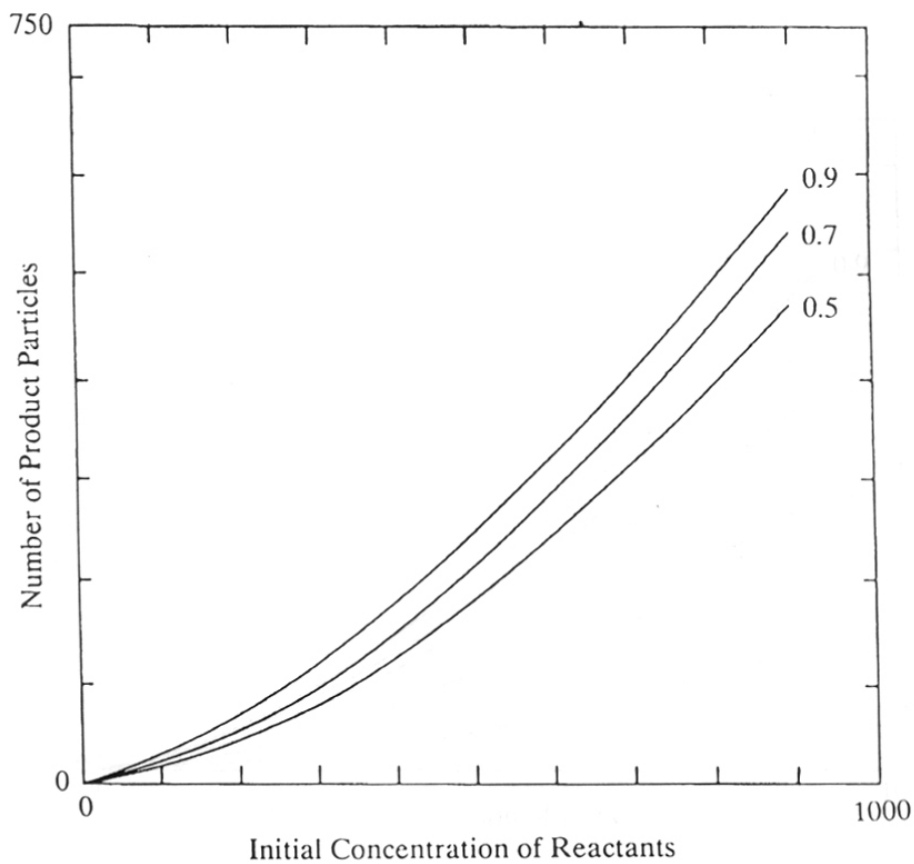
FIGURE 3.7a

Profiles of number of product particles formed versus time for the reaction on a DLA and a percolation cluster, with different reaction rate constants (0.1, 0.3, 0.5, 0.9).
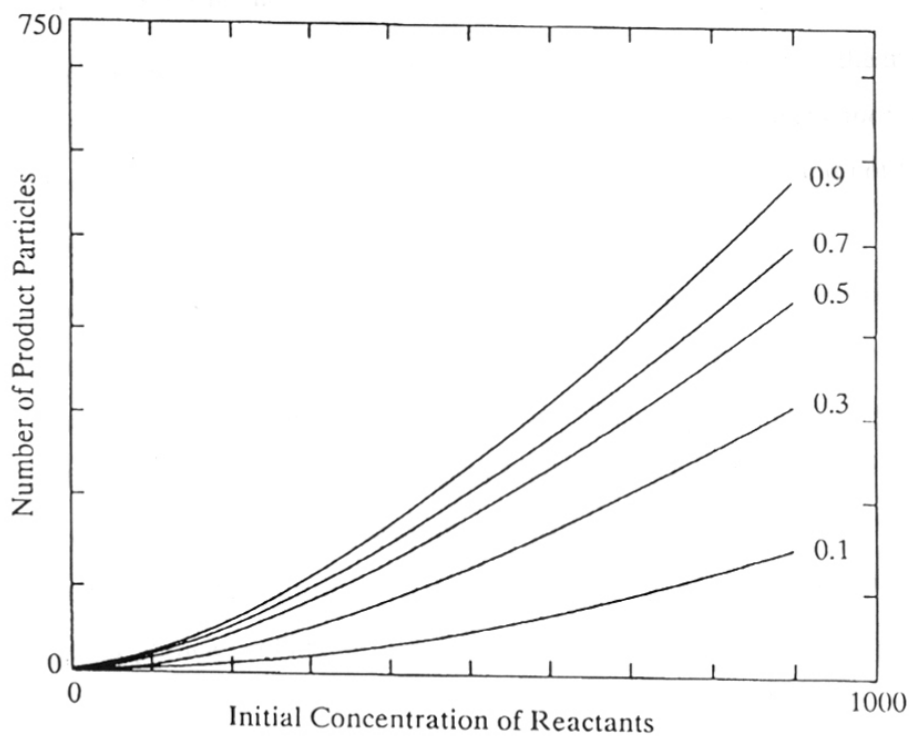
FIGURE 3.7b

Profiles showing the number of product particles formed as a function of initial number of reactants present for the reaction on a DLA and a percolation cluster, with different reaction rate constants (0.1, 0.2, 0.3, 0.5, 0.7, 0.9).

FIGURE 3.7c

Profiles showing the number of product particles formed as a function of initial number of reactants present for the reaction only on a DLA, with different reaction rate constants (0.5, 0.7, 0.9).

FIGURE 3.7d

Profiles showing the number of product particles formed as a function of initial number of reactants present for the reaction only on a percolation cluster, with different reaction rate constants (0.1, 0.3, 0.5, 0.7, 0.9).

for reaction taking place only on a percolation cluster. As can be observed, not much change is seen in the count of products formed, whether the reaction takes place only on a DLA, only on a percolation cluster or on a surface which changes its fractal dimension between that of a DLA (~ 1.7) and that of a percolation cluster (~ 1.89).

Figure 3.8 shows that there is a negligible change in the fractal dimension of the surface as it moves during the course of the reaction.

The mentioned studies indicate that the change in fractal dimension of the mobile surface does not contribute significantly to rate enhancements. Thus, the enhancements in rate reported earlier can be attributed to the mobility of the surface and not to the change in fractal dimension.

For the selectivity studies, increasing the flux of A particles onto the fractal surface brings about an increase in the selectivity (figure 3.9a). An increase is also observed with an increase in the mobility of the fractal surface (figure 3.9b). Selectivity falls as the value of rate constant K2 increases (figure 3.9b). It is seen in figure 3.9b that for a fixed value of K2, as the mobility increases, selectivity tends to achieve a stable value which would be attained at high mobilities. In the case studied here, the probability that two adsorbed A particles collide increases with mobility, causing an increase in the C to B ratio. This ratio tends towards a high stable value at large mobility.


3.4   CONCLUSIONS

In summary, the general results of analysis verify the known results for the case of static fractals, thus validating the methodology, and provide a measure of the effects of the mobility. It is interesting to note that rate enhancements to the tune of several hundred-fold seem possible, although in certain cases (pair-correlated distribution) the
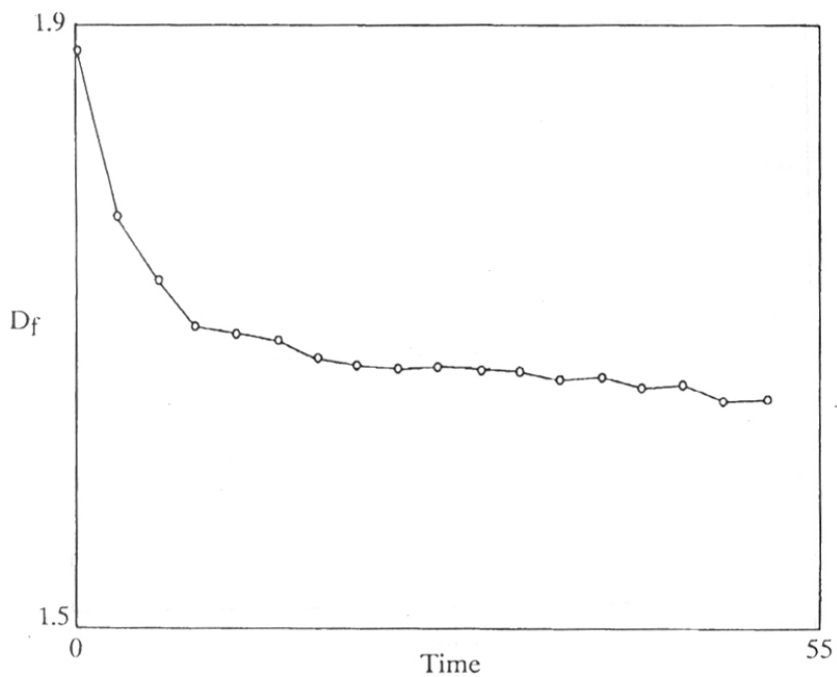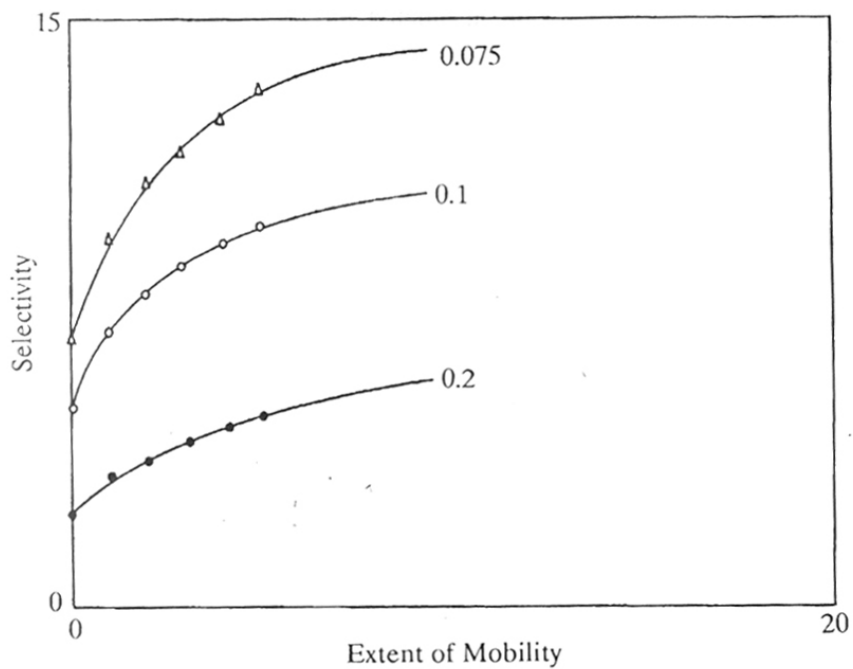
FIGURE 3.8

Profile showing the change in fractal dimension of the base (Df) as it moves
during the course of the reaction.
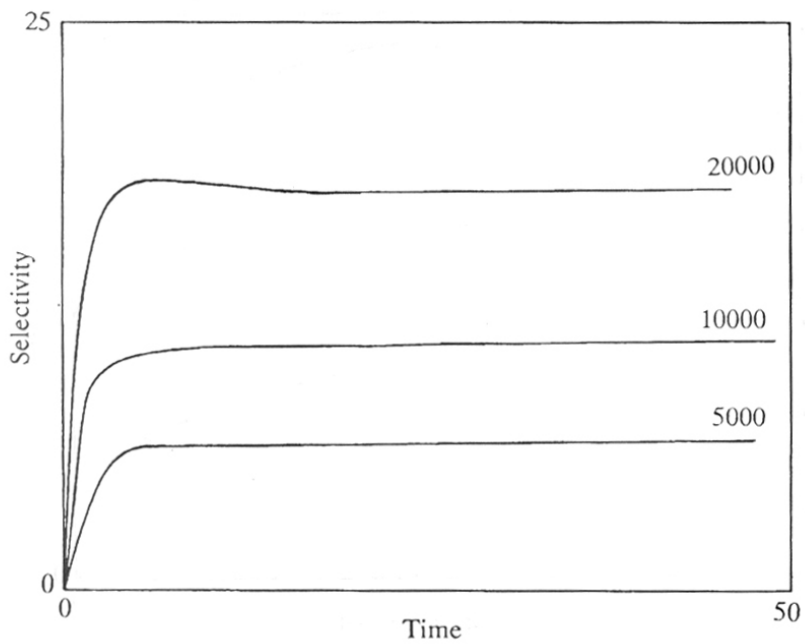
FIGURE 3.9a

Profiles depicting the effect of flux of 'A' particles (5000, 10000, 20000) on the selectivity of the reaction on a static fractal as a function of time.

FIGURE 3.9b

Profile showing the effect of extent of mobility and rate constant K2 (0.075, 0.1, 0.2) on the selectivity of the reaction at steady state.

overall effect may be deleterious. The mobile fractal shapes seem to provide another way for explaining rate enhancements in the range observed in some systems and can have wide implications in understanding several biochemical as well as physical and chemical systems. It is also interesting to note that the change in fractal dimension does not lead to any significant rate enhancement.

PATTERN FORMATION
IN BACTERIAL COLONIES

Simple iterative rules have been framed for the growth of cells giving rise to various pattern formations in bacterial colonies, taking into account the sticking and rotation probabilities, thickness of the medium, concentration of nutrients and the yield coefficients. The existing models assign arbitrary probability values for growth in different directions to produce various shapes and patterns. The model presented in this chapter allows for correlating the parameters used above with actual biochemical mechanisms and thus claims advancement over existing models.

CHAPTER 4

4.1   INTRODUCTION

The previous chapter dealt with the study of reactions on *fractiles* as a possible explanation to the rate enhancements observed in biological systems as against those expected from calculations. In this chapter, the growth of bacterial colonies has been studied. This is known to be a rather complicated process (Shapiro, 1987) and the morphology of the entire colonies of bacteria grown under certain conditions has recently been shown to be self-similar (Fujikawa and Matsushita, 1989; Matsushita and Fujikawa, 1990).

Pattern formation has fascinated mankind for many years. Recently the study of growing structures has developed greatly, mainly due to the introduction of the concept of fractal geometry and computer simulations. Some of the interest shown in this subject has surely been excited by the construction of complex and beautiful spatial patterns from very simple computer algorithms, as well as by the close match between the theoretical model results and the observations of natural pattern formation phenomena. Physical pattern formation phenomena have many interesting analogies in biology, and it is worthwhile to apply the computational methods which have proven successful in physics to the more complex problems in biology.

Problems of biology are more difficult than problems of physics in the sense that the vast complexity of biological systems prevents us from describing the processes at work in any phenomenon in terms of simple equations. Although biological growth must involve the production, transport, and chemical transformation of biologically active molecules, the specific processes and their rates are unknown. This ignorance forces us

to attack the problem of growth indirectly. When simulations are found which match observed patterns, we assume that we have discovered a logical structure in the growth rules which is possessed by the actual biological process. We may then speculate on the biochemical processes underlying the successful growth rules. In the absence of detailed knowledge of the mechanisms, the plausibility of the model will be determined by its simplicity.

4.1.1   Study of Colony Morphologies

Colonial morphology, which is a function of many parameters, has been used as an aid to identify bacteria since the time of Koch. Examination at high magnifications reveals variations in arrangement of the organisms in different colony types and in different areas of the same colony (Whittaker and Drucker, 1970). The finer details of growth vary, sometimes almost spectacularly with the nature of the strain, the concentrations, the presence of adsorbent substances added to the agar and other conditions (Cooper et al, 1968; Belisle and Brennan, 1989).

4.1.1.1   Growth of Bacterial Colonies

Bacterial colonies of a given species differ in size, rate of development and structure according to the environmental conditions and the biochemical history of the particular strain, including mutational and adaptive changes. In a rudimentary way a colony constitutes a tissue, the growth of which is determined partly by diffusion and partly by its inherent character, and it is capable, in a simple way, of morphogenesis and differentiation (Cooper et al, 1968).

When cells first begin to proliferate on a solid medium they do so at rates which differ according to the strain in much the same way as they would in a liquid containing the same nutrients. There will be lag phases, which are shown to bear a relation to the size distribution among colonies on plates at different stages of development. The gradual outward growth of the colony takes place according to different quantitative laws depending on the stage of growth and on the density of colonies on the plate. At first diffusion of nutrients, buffer or waste products are not rate-determining, but diffusion, chiefly affecting pH rather than nutrient, becomes more and more the dominant factor as growth becomes protracted. This condition occurs especially with large single colonies which can grow eventually to very large areas (Cooper *et al*, 1968).

The dynamics of microcolony formation of *E. coli* at $37^{\circ}C$ appear to depend primarily on the fact that growth is in the direction of the longitudinal axis of the bacterium. The naturally undisturbed order, therefore, would be that of a chain of bacteria. The bacterial microcolony, once palisading is initiated, may be regarded as a spatial distortion of a single chain of bacteria. When the palisading movements have established three or more columns of bacteria, the exterior organisms will continue to form new palisades, but the interior columns will develop unbroken because of constraint by the adjoining organisms (Hofmann and Frank, 1961).

With the normal *Aerobacter* strain on the normal agar medium the course of events in the development of a single colony have been described and shown to have a distinctly floral form with petal-like processes separated by narrow fjord-like channels (Cooper *et al*, 1968). As the petals grow they put out secondary processes until the whole has a fern-like appearance. The secondary fronds of the fern represent a small-scale repetition of what has occurred in the formation of the primary ones. This is similar to a fractal

structure (figure 4.1). Furthermore, bacterial colonies of a given species differ in size, rate of development and structure according to the environmental conditions and the biochemical history of the particular strain.

4.1.1.2   Experimentally Observed Morphologies of Bacterial Colonies

S. pneumoniae gives smooth or rough colonies depending on whether the cells are capsulated or not (Whittaker and Drucker, 1970). *S. mutans* OMZ61 shows plano-convex colonies on blood agar but raised, irregular colonies on mitis salivarius agar (Whittaker and Drucker, 1970). Organisms in the central depressed area of the *S. mutans* colonies are seen in some cases to be arranged in chains grouped together to form broad intercommunicating buttresses with spaces between producing a sponge-like effect (Whittaker and Drucker, 1970). In domed colonies of *C. albicans* fine filamentous strands associated with the surfaces of the organisms are evident (Whittaker and Drucker, 1970). Colonies of *S. pyogenes* are characterized by steep sides (Springer and Roth, 1972). Irregular edges of *B. megaterium* colonies might be due to long filaments growing out from the edges (Drucker and Whittaker, 1971). The macroscopical appearance of *Nocardia* colonies show well separated, tangled filaments, growing vertically as well as laterally and are no doubt responsible for the rough appearance of colonies of this organism (Drucker and Whittaker, 1971).

4.1.2   Application of Fractal Analysis to Colonial Morphology

Fractal analysis (Mandelbrot, 1983; Voss, 1988; Feder, 1989) introduced to microbiology to describe growth patterns is of fundamental importance: morphological differences correlate with pathogenicity as well as with growth, metabolic activity,

FIGURE 4.1

Single colonies of normal (top) and methylene-blue resistant (bottom) strains of *Aerobacter* after 20 days growth (Cooper *et al*, 1968).
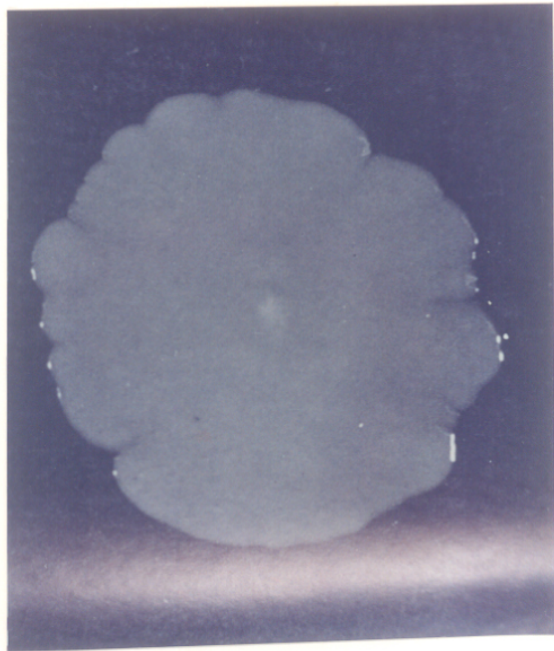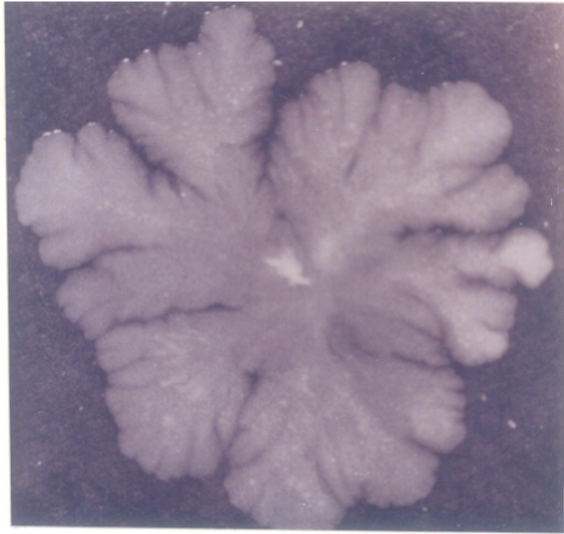
enzyme production, and pigmentation in cases of bacteria and fungi. Because of the complex structure of colonies, a geometric, pattern-oriented description, which leads to a measure of irregularity, was impossible without the development of fractal geometry.

4.1.2.1   *Earlier Studies Reveal the Fractal Nature of Microbial Colonies*

Experimental studies have revealed the fractal nature of microbial colonies (Matsuyama *et al*, 1989), and a few attempts have been made at developing simulation models of biological growth.

Thus, Obert *et al* (1990) have applied the fractal concept to the growth patterns of two microbial species, *Streptomyces griseus* and *Ashbya gossypii*, and is the first example showing fractal aggregates in biological systems. They find that the global structure of sufficiently branched mycelia can be described by a fractal dimension, D, which increases during growth upto 1.5. The mycelial structure changes during growth from a mass fractal to a surface fractal.

Matsushita and Fujikawa (1990) grew colonies of *Bacillus subtilis* and found them to grow two-dimensionally and self-similarly on agar plates through diffusion-limited processes in a nutrient concentration field. They obtained a fractal dimension of the colony patterns of D = 1.73 + /-0.02, very close to that of the two-dimensional DLA model, and confirmed the existence of the screening effect of protruding main branches against inner ones in a colony, the repulsion between two neighboring colonies and the tendency to grow towards nutrient. Their findings imply the importance of physical properties of the environment for the morphology of bacterial colonies in general.

Young and Corey (1990) have shown that very simple iterative rules for the growth of cells on a two-dimensional lattice can simulate biological-growth phenomena realistically. They discuss random cellular automata models for the growth of fern

gametophytes, branching fungi and leaves, and for shape transformations useful in the study of biological variation and evolution. The growth rules in various directions are necessarily empirical in that different probability distributions are assigned in different directions of growth. It may become difficult then to relate them to actual biochemical mechanisms.

Vicsek *et al* (1990) have studied the scaling behavior of the surface of *Escherichia coli* and *Bacillus subtilis* colonies growing on agar plates. They present the first experimental evidence for the self-affine fractal nature of the shape of a biological system. They conclude that regardless of the complexity of bacterial colony formation, there are some common basic mechanisms which determine the behavior of the surfaces obtained in both the experiments on the growth of bacterial colonies and the simulations of aggregation models.

4.2   THE MODEL

Simple rules are employed to simulate growth of bacterial colonies and explicit account is taken of *sticking probability*, yield coefficients and *rotational probability*. The three-dimensional nature of the medium is also recognized explicitly. The values to various parameters are assigned and varied with a view to generate different structural patterns. The advantage of such an approach is that the values to various parameters such as *sticking probability*, *rotational probability* etc. can be correlated with the actual biochemical mechanisms.

Thus for instance it is known that at 37°C, some bacteria are highly motile, so that any aggregations are soon disrupted. In case of *Escherichia coli*, smooth-phase daughter pairs tend to separate easily, while rough-phase organisms have a high tenacity of

attachment (Hofmann and Frank, 1961). The motility of cells, or in other words the persistence of attachment, has been incorporated in the model in terms of a *sticking probability*.

Similarly, when microorganisms are grown on solid surfaces migrating and rotating colonies associated with some members of the genera *Proteus, Clostridium, and Bacillus* are observed (Codner, 1969). Further, palisading is the primary post-fission movement in the rough- and smooth-phase of *E. coli* but the rates at which palisades develop is much slower than in smooth-phase cultures (Hofmann and Frank, 1961). Another facet of microbial growth is incomplete separation of the two daughter cells (Codner, 1969). Typically, the first division of the original bacterium of the colony gives rise to a 2- or 3-membered chain. Continued growth along the long axis of the chain finally leads to a horizontal displacement of the proximal ends of a bacterial pair, and the bacteria then begin to grow past each other. Depending upon the extent of separation will be the tendency of rotation of individual cells comprising the colony and thus the formation of circular or irregular colonies. The extent of incomplete separation or palisading and relative sliding has been incorporated in the model in terms of a *rotational probability*.

4.3   ALGORITHM FOR SIMULATION OF GROWTH

A lattice of 200 X 200 was used in all the simulations. Each lattice point was considered as a site which can be occupied by one living microbial cell. In the present model yield coefficients (number of cells produced for every nutrient consumed) have been incorporated. When the stipulated number of cells are produced, the nutrients closest to the bacterial colony are identified and removed. This is because microbial

cells are known to grow in the direction of the closest nutrient (Matsushita and Fujikawa, 1990). Three-dimensional growth of cells is not considered as it drastically increases the computational time.

The gel on the surface of which the cells grow was considered to be a three-dimensional lattice (200 X 200 X thickness of gel). Nutrients were allowed to diffuse in three dimensions. To begin simulations the initial inoculum consisted of five cells at the center of the lattice. A cell was picked at random. The nutrient closest to this cell was identified and the cell allowed to grow towards that nutrient. If the site where the cell can grow was already occupied then a new cell was picked upon for growth. The nutrient closest to it was likewise identified. The tendency of certain species to remain in a chain-like formation while certain other daughter cells to separate immediately after division can give rise to significantly different morphologies. In certain cases growth is in the direction of the longitudinal axis of the bacterium (Hofmann and Frank, 1961). This concept has been introduced in the model in terms of *rotational probability* for cells and the value lying between zero and one determines the extent to which a cell can grow in a certain direction. The direction towards which each cell grows was maintained the same till the random number generated has a value less than the value assigned to *rotational probability*. If the random number generated had a value greater than the *rotational probability*, the nutrient closest to the last cell formed was identified and the new direction for growth was determined. This procedure of growth continued by randomly picking up cells for growth. The motility of the cells was also accounted for in terms of *sticking probability*. This term determines the extent to which lateral diffusion of cells can occur. Random numbers were generated to determine lateral diffusion for each cell. If the random number generated had a value less than the *sticking probability* then the cell was allowed to diffuse.

Simulations were performed by varying the *sticking probability* of the cells, their *rotational probability* and the thickness of the gel. The fractal dimension of the resultant colonies was calculated using the well-established *box-counting method* (Obert *et al*, 1990).

4.4   RESULTS AND DISCUSSIONS

A colony does not expand uniformly but for a size below the threshold of visibility, it can be treated as a regular disk of approximately constant thickness. With a considerable number of colonies on the plate, there is usually no perceptible distortion of this circular pattern. But as the number diminishes so that growth can be protracted and a larger area reached, new phenomena make their appearance. They begin with an instability of the perimeter, which loses its smooth circular form and develops undulations. These become more and more exaggerated as time goes on, but more or less follow a pattern depending upon the strain of organism, the composition of the solid substrate and the buffer concentration. Furthermore, as any protuberance grows it reaches a richer and less contaminated medium which may favour faster growth except in so far as growth-promoting intermediates may be produced by the cells themselves (Cooper *et al*, 1968). Formation of such circular colonies as well as distortions of it have been observed in our simulations. Figure 4.2 shows the time evolution of a bacterial colony. The change from an evidently circular colony to one with undulations of the perimeter can be clearly seen.

Figure 4.3 shows the twelve representative different possible shapes of a bacterial colony obtained by taking three different values of *sticking probabilities* and four different values of *rotational probabilities* for cells during growth. These parameters are equivalent to the preference of some cells to stick together and the time taken for growth,

Time = 0	Time = 15	Time = 30
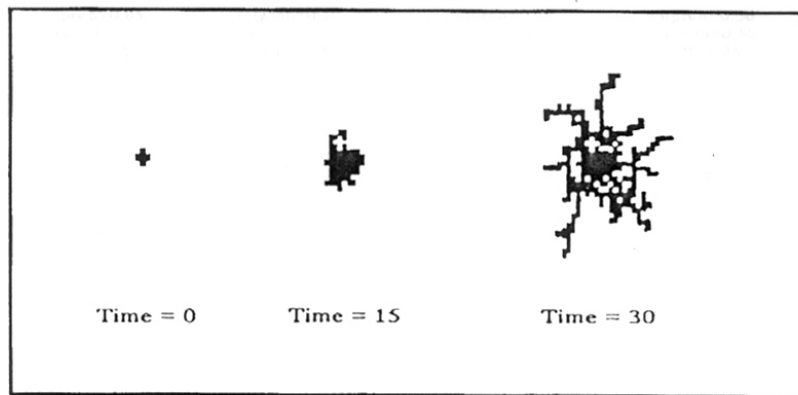
FIGURE 4.2

Shapes of colonies at different times during growth depicting the appearance of undulations of the perimeter as time proceeds in case of single colonies growing on the plate.
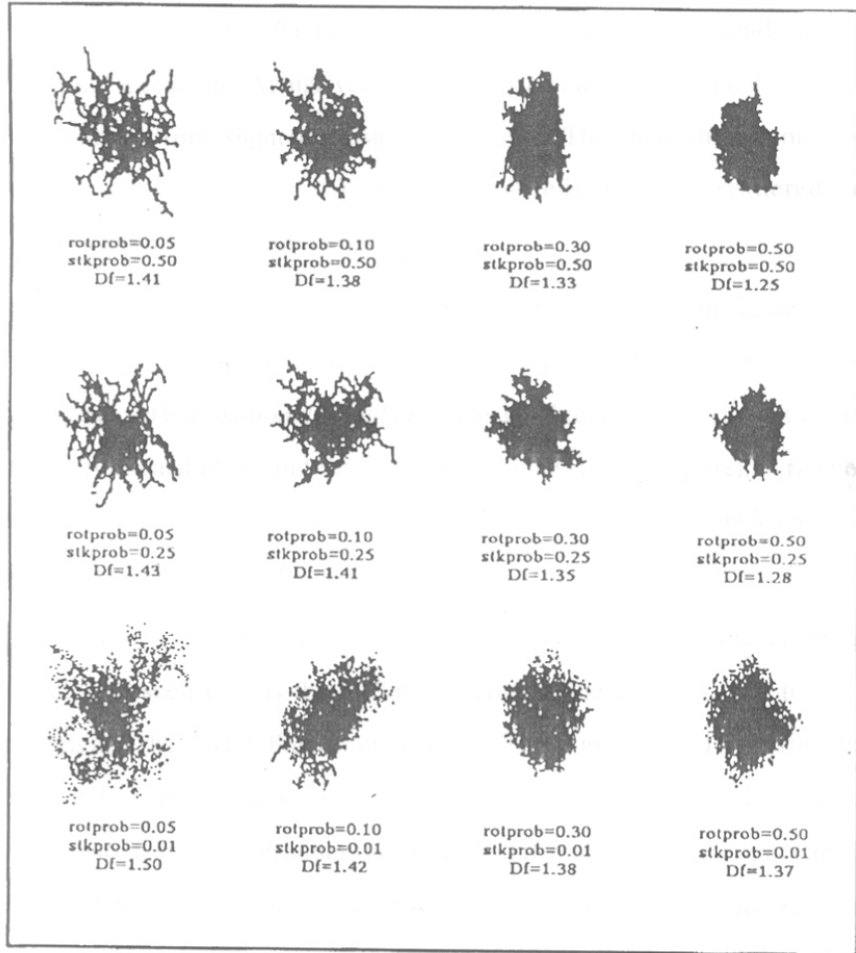
FIGURE 4.3

Twelve representative colonies obtained by simulations considering three different values of *sticking probability* (stkprob) and four different values of *rotational probability* (rotprob). Df stands for the fractal dimension.

respectively. If the cells have a high tendency to stay together then their diffusion is considerably less. Also more is the time taken for growth more is the time available for separation and tendency to do so.

As the *sticking probability* for the cells decreases the colonies tend to be become dispersed and spread out. At high values of *sticking probability* the colonies appear more or less circular with only slight protrusions at the edges. The fractal dimension is expected to increase with decrease in *sticking probability* of cells due to the scattered nature of the colonies and this is as seen in the figure.

The effect of change in *rotational probability* is also seen in figure 4.3. As the tendency for rotation increases the colonies tend to be circular with few protuberances from the edges. At low *rotational probabilities* the daughter cells will appear to be partially separated from each other and the resultant colonies are highly irregular. The fractal dimension in such cases is expected to be greater than for colonies which appear more regular. This can be seen in figure 4.3.

In figure 4.4 are shown the different colony shapes as a result of change in thickness of the gel. It is seen that as the thickness increases the colonies tend to have more protrusions and the fractal dimension increases. This is as expected because it has been experimentally seen by earlier workers that agar depth has a marked effect on radial growth of colonies as it determines the effective nutrient concentration in each layer of the gel. It has been found that doubling the standard glucose concentration gives smaller and more or less circular colonies (Cooper *et al*, 1968). The spikes in the colonies can be understood in terms of tendency of the microbial cells to seek out the nutrient medium in the surroundings where lower concentrations of it are present. Similarly, as the yield coefficient rises the colonies tend to have more spikes and are more spread out. More nutrient is depleted for lesser number of bacterial cells formed and less nutrient is

Thk = 3   Thk = 10   Thk = 20
Df = 1.29   Df = 1.31   Df = 1.34
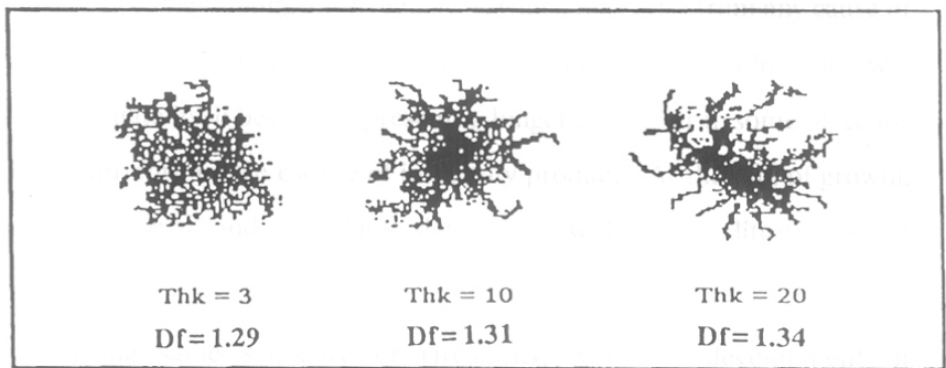
FIGURE 4.4

Effect of gel thickness (thk) on colony morphology. As the thickness increases the colonies tend to have more protrusions and the fractal dimension increases. Df stands for the fractal dimension.

available for further growth. Microbial colonies of different colonies observed experimentally by other workers are shown in figure 4.5. Varying morphologies are evident and some bear similarity to the colonies obtained by the simulations.

Several lines of evidence suggest strongly that the instability develops after the growth has become diffusion-limited. It would in any event be expected. The circular perimeter being of minimum length any incipient bulge will allow more rapid supply and greater growth which in turn will accentuate the bulge. Moreover, protrusion of part of the colony into less depleted medium will allow that part to grow out still further. Once diffusion has become limiting any irregularity, which may arise from any cause or may have been inherent in the imperfect circularity of the initial inoculum site, will progressively accentuate itself because it presents a longer perimeter in some place for the reception of nutrients, or the escape of inhibitory products. At the end of growth, complex conditions prevail and the minute details vary with the conditions present (Cooper *et al*, 1968).

In general, the same sequence of circularity, waviness, development of protuberances is probable with all the strains, but with the slower growing ones may never develop very far. Moreover, the degree of localization of the protuberances varies in a remarkable manner, and conditions have been found where the normal strain may be induced to put out a few very long spikes, seeking as it were more favorable medium. These themselves develop secondary spikes so that the phenomenon would appear to be basically the same, although the same is quite different.

Other factors of interest in studying colony shapes under different conditions are the concentration and diffusibility of nutrients and the yield coefficient for growth of cells. These factors would have a considerable effect on colony growth. The standard diffusion equations apply well enough to justify the calculation which indicates, with
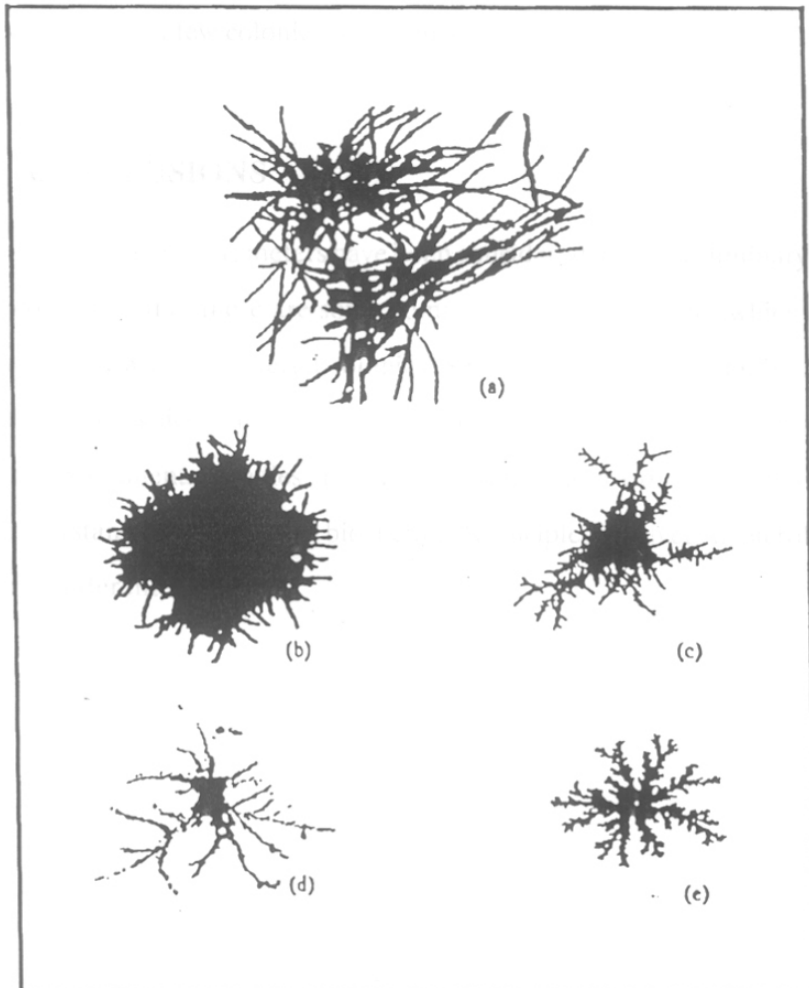
FIGURE 4.5

Digitized images of microbial colonies of different organisms observed experimentally by other workers: (a) Mycelial clumps of *A. pullulans* (Auer and Seviour, 1990). (b) Mycelial of *A. gossypii* 60h after inoculation (Obert *et al*, 1990). (c) Mycelial structure of *A. gossypii* (Obert *et al*, 1990). (d) Colony of *C. albicans* (Jansons and Nickerson, 1970). (e) Colony of *Bacillus subtilis* (Matsushita and Fujikawa, 1990).

some margin of safety, that rate of diffusion, whether of glucose or buffer, upto the colony is likely to determine the rate of increase of colony diameter on plates with the protracted growth of a few colonies on a sparsely covered plate.

4.5   CONCLUSIONS

The effects of a few parameters have been considered in this preliminary case study It can be concluded that there are some common basic mechanisms which determine the behavior of growth of bacterial colonies. Simple iterative rules can be framed for the growth of cells which can give rise to various pattern formations, similar to those observed in experimental studies. Further theoretical and experimental studies will enhance understanding of the actual biochemical principles involved in microbial colony formation of different species.

CHAPTER 5

AN ALGORITHM
TO DESCRIBE THE ENTIRE PROTEIN SURFACE
IN TWO DIMENSIONS

An algorithm has been developed which enables visualization of the entire protein surface in a plane along with the distribution of various properties on the surface. Three new, global indices have been introduced which help in characterizing a protein almost completely and are based on local relationships. These and certain other indices presented by earlier workers have been computed for a variety of proteins. Plots of change in these indices as they vary along the surface are reminiscent of fractal Brownian functions. R/S analysis has been carried out for these fractal Brownian function-like plots to calculate the Hurst exponent.

CHAPTER 5

5.1   INTRODUCTION

The present chapter reports the development of an algorithm, using interactive graphics, which can describe the entire surface of the protein in two-dimensions. The primary aim is to be able to visually compare protein surfaces. Three global indices which characterize proteins have also been introduced.

"The surface was invented by the devil," said the illustrious physicist Wolfgang Pauli. Pauli's frustration was based on the simple fact that the surface of a solid serves as the boundary between it and the outer world. Whereas an atom within a solid is surrounded by other atoms, an atom at a surface can interact only with other atoms on the surface, with atoms beyond the surface or those immediately under it. The properties of the surface of a solid therefore differ radically from those of the interior. For instance, to minimize energy, surface atoms often arrange themselves differently from the other atoms in a solid. The resulting complexities of surface structures have long thwarted efforts to derive precise experimental and theoretical descriptions of them (Binnig and Rohrer, 1985).

It is through the association of complementary surfaces that protein-protein recognition occurs. One of the important problems in structural biology is, therefore, the origin of specificity and recognition of surfaces involved in molecular interactions. An essential step in this process is the contact between approaching molecular surfaces (Lee and Richards, 1971). An enzyme-substrate interaction is an extremely complex one and not only involves steric complementarity at the active site but also at regions on the surface neighboring the active site. Domains several angstroms away from the active site may interact with cofactors that can not only induce activity but also change substrate

specificity. The topology of the surface of a protein, therefore, is intimately related to its function as well as its conformation, and parts of the surface that are directly involved in interactions with other molecules (Miller, 1990). Furthermore, domains in proteins carry out specific functions and it has been suggested that they are units of protein evolution as well as protein structures. (Edelman *et al*, 1969; Rossmann and Liljas, 1974).

It can be argued that location of structural domains by visual inspection suffers from subjectivity. Objective definitions and algorithms to find domains from atomic positions are therefore useful (Crippen, 1978; Rose, 1979). The criteria of surface area to detect structural domains as regions of the protein structure where most of the interactions between atoms or residues within the regions and least without, have proved to be quite useful in identifying limits of structural domains (Wodak and Janin, 1981). Visual inspection relies on a subjective estimate of the extent to which parts of the protein molecule interact. In order to study the structure-function relationship of proteins it is desirable to define precisely the outer surface of a macromolecule. It is this part of the molecule that interacts with other macromolecules (Connolly, 1983).

Surface area is a geometric concept. A geometrical definition of domains may not coincide with biochemical or functional definitions. Yet, a correlation established previously between accessible surface areas and hydrophobic free energies (Hermann, 1972; Chothia, 1974) provides a link between the two. The *hydrophobic effect* (Kauzmann, 1959; Tanford, 1980) is thought to be a major force driving the protein-folding process. Consistent with this idea, the average surface area that residues lose upon folding is found to scale linearly with hydrophobicity (Rose *et al*, 1985). These compact, low-energy substructures are likely candidates to be folding intermediates and to exhibit autonomous structural stability.

Many indices have been defined to characterize structural domains in proteins. A parameter called the *coefficient of compactness* is applied to X-ray-elucidated proteins to identify those continuous-chain regions having the smallest accessible surface area for their volume (Zehfus and Rose, 1986). This is differènt from the familiar idea of *packing density* (Richards, 1977) which is the ratio of summed atom volumes to total protein volume. *Coefficient of compactness* is not a new parameter, having been described previously as a *roughness index* (Richards, 1977), a *globularity index* (Wodak and Janin, 1981), and a possible means of finding protein domains (Wetlaufer, 1973).

It is extremely important to be able to visualize the entire surface of a protein, and characterize it, at the same time, in order to correlate the role of surfaces in molecular recognition. An attempt has been made in the present chapter to visualize, characterize and quantitate protein surfaces. An algorithm has been developed to visualize the surface of proteins in two-dimensions to facilitate their comparison. Three new, global indices have been introduced which characterize proteins based on local relationships.

5.2   MATERIALS AND METHODS

To evaluate and compare the surface of proteins visually, it is necessary to be able to *peel* the surface and display the properties associated with the regions on the surface in two dimensions. It is also necessary to be able to *fix* proteins when displaying them so that a one-to-one comparison can be made. An algorithm has been developed for this and is described below. The crystallographic data on proteins was obtained from the Brookhaven Protein data bank (1990). Sections of the protein are made through the center of mass and the outer contour is traced out. This describes the outer surface of the protein and its length is a measure of the undulations and folds on the protein surface. Sections are cut at different angles in the X-Y plane and, likewise, the entire surface is traced out.

5.2.1   Algorithm for Determining the Surface Properties of Proteins

1) Calculate the center of mass of the protein and transform the coordinates such that the center of mass corresponds to the origin of the cartesian coordinate system under consideration. Thus, the center of mass now has coordinates (0,0,0).

2) Identify the coordinates of the N-terminal α-carbon atom and rotate the molecule such that the N-terminal α-carbon now lies on the Z-axis of the coordinate system under consideration. The new coordinates of the N-terminal α-carbon are now $(0,0,+Z)$.

3) Identify the coordinates of the C-terminal α-carbon atom and rotate all atoms around the Z-axis in a way such that the C-terminal α-carbon now lies in the Y-Z plane and has coordinates $(0,+Y,+Z)$.

4) Determine the equation of the plane passing through the Z-axis and making an angle θ with the Y-axis. The range of θ lies within $0^0 < \theta < 180^0$. Identify those atoms the van der Waals contact radii of which cut the plane under consideration. Compute the extent to which these atoms cut the plane and, thus, calculate the radii of the cross-section and the center of the circle so formed. The projection of these atoms on the plane furnishes a description of the section of the protein. Various properties, depicted in table 5.1, can be displayed, using a color code to indicate the approximate value. The values of the indices are those indicated by Argos *et al* (1982). One such section showing hydrophobicity variation is depicted in figure 5.1a.

TABLE 5.1

COLOR CODES USED FOR PROPERTIES DISPLAYED

AMINO ACID	HYDROPHOBICITY INDEX		HYDRATION POTENTIAL		BULK		POLARITY	
	COLOR	VALUE	COLOR	VALUE	COLOR	VALUE	COLOR	VALUE
GLN	White	0.00	White	0.25	Red	0.94	Red	1.26
SER	White	0.05	Green	0.92	Cyan	0.62	Green	1.10
THR	White	0.05	Green	0.94	Red	1.03	Green	1.03
ASN	White	0.06	White	0.20	Green	0.83	Magenta	1.39
GLY	White	0.07	Blue	2.07	White	0.22	Green	1.08
ASP	Yellow	0.46	White	0.01	Green	0.76	Blue	1.56
GLU	Yellow	0.47	White	0.13	Green	0.88	Blue	1.48
ARG	Yellow	0.60	White	0.00	Red	0.93	Red	1.26
ALA	Yellow	0.61	Blue	2.00	Green	0.75	Cyan	0.97
HIS	Yellow	0.61	White	0.12	Green	0.89	Red	1.25
CYS	Cyan	1.07	Magenta	1.51	Green	0.88	White	0.66
LYS	Green	1.15	White	0.23	Red	1.02	Magenta	1.36
MET	Green	1.18	Red	1.47	Red	1.06	White	0.68
VAL	Green	1.32	Blue	2.00	Blue	1.40	White	0.71
LEU	Red	1.53	Blue	2.06	Blue	1.39	White	0.59
TYR	Red	1.88	Cyan	0.75	Magenta	1.17	Yellow	0.74
PRO	Magenta	1.95	Green	0.93	Magenta	1.13	Cyan	0.96
PHE	Magenta	2.02	Magenta	1.58	Blue	1.29	White	0.62
ILE	Magenta	2.22	Blue	2.03	Blue	1.39	White	0.62
TRP	Blue	2.65	Cyan	0.79	Blue	1.41	White	0.65

FIGURE 5.1

a) A representative section of 2SBT depicting hydrophobicity variation.

b) The same section as in figure 5.1a, but with the adjacent cluster joined.

c) Spanning the section in figure 5.1b to map the *contour*.
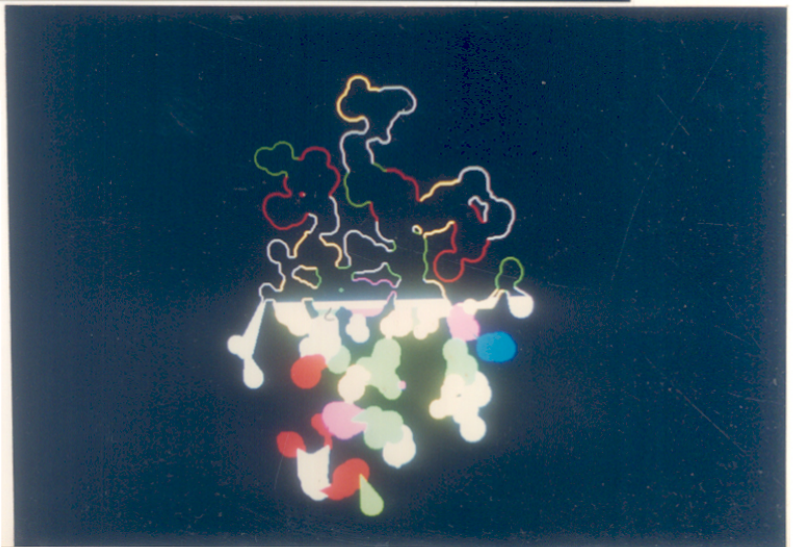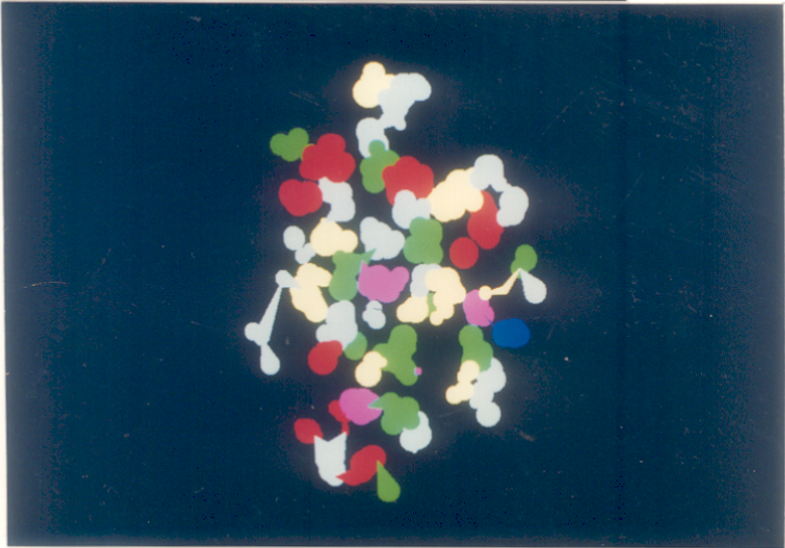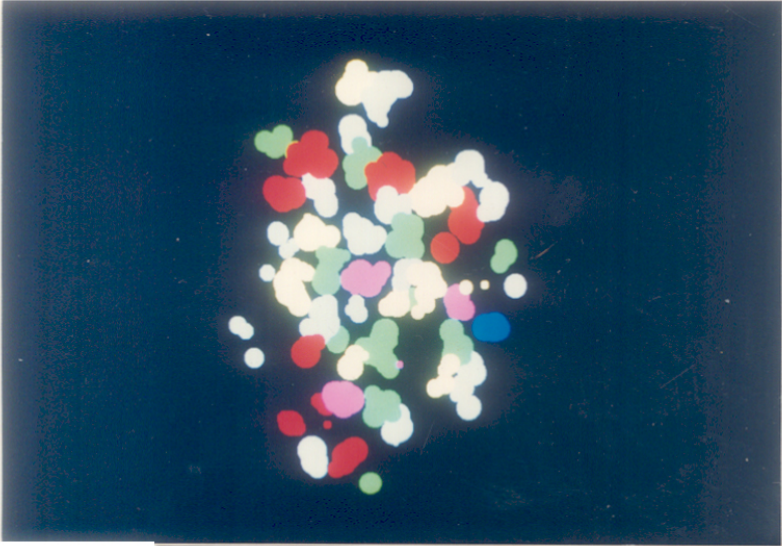
5) Identify isolated clusters of atoms and join them to the closest neighboring atom of another cluster. The joining of clusters is done in such a way that two isolated clusters are joined only once, via the shortest computed distance. One such section is shown in figure 5.1b.

6) Map the *contour* or the edge of the section under consideration for properties, depending on the corresponding amino acid (figure 5.1c). Compute the shortest possible distance of each atom along the edge of the section from the N-terminal α-carbon and also the sign of the Y coordinate of the atom. Map the property of each atom (in color) as a function of distance from the N-terminal, taking into account the sign of the Y coordinate. Contours for different sections are similarly mapped and displayed. A schematic diagram depicting the method followed here is shown in figure 5.1d. The map so obtained describes the property on the surface of the protein in two-dimensions (figure 5.2). A space-filling model of the same protein is shown in figure 5.3.

7) The active site of the protein can be mapped in a similar way and a representative case is shown in figure 5.4.

5.3   RESULTS AND DISCUSSIONS

5.3.1   Calculation of Indices to Characterize Proteins

Three indices have been introduced which will be helpful to characterize proteins and also different regions within them. These are the *roughness factor*, *globularity factor* and *fractality factor*, defined as follows:
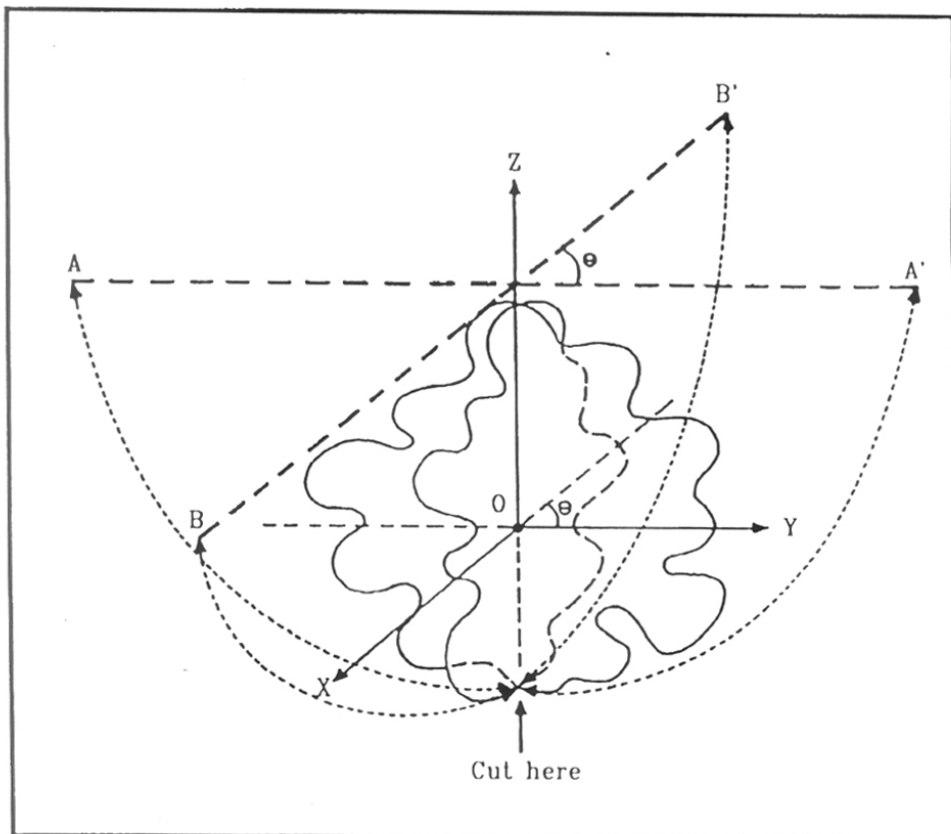
FIGURE 5.1d

Schematic diagram depicting the method for displaying the surface of the protein in two-dimensions. θ depicts the angle between the two sections. O denotes center of mass of the protein and has coordinates (0,0,0). The solid line (- - -) indicates extended contour of protein in the X-Y plane. A-A' indicates opened out contour corresponding to $\theta = 0$ (through the Y-Z plane) while B-B' depicts contour corresponding to angle $\theta = 45$.

FIGURE 5.2

A two-dimensional display of the surface distribution of hydrophobicity of 2SBT. The wedge indicates the Y-Z plane were the C-terminal α-carbon atom lies. The tip of this wedge depicts the N-terminal α-carbon atom.

FIGURE 5.3

A space-filling model of 2SBT depicting hydrophobicity variation.

FIGURE 5.4

The active site mapped for 2SBT depicting hydrophobicity variation on the surface exposed areas. Only the sections which contain the active site have been depicted.
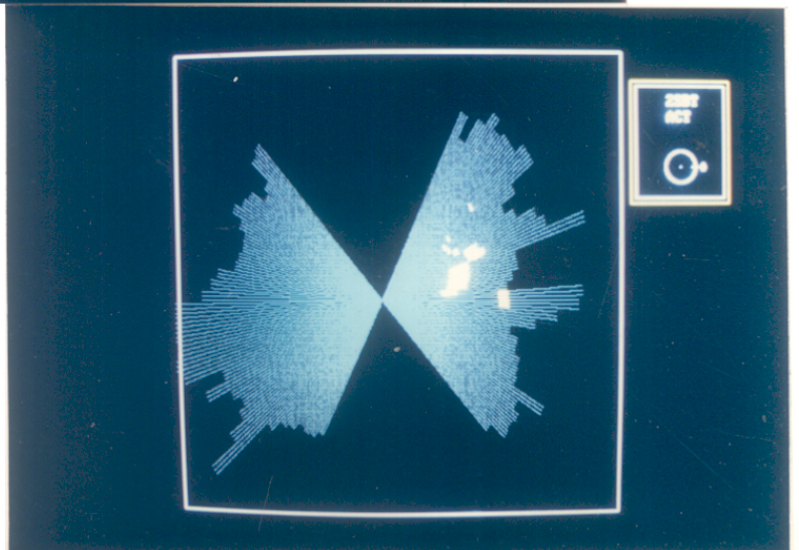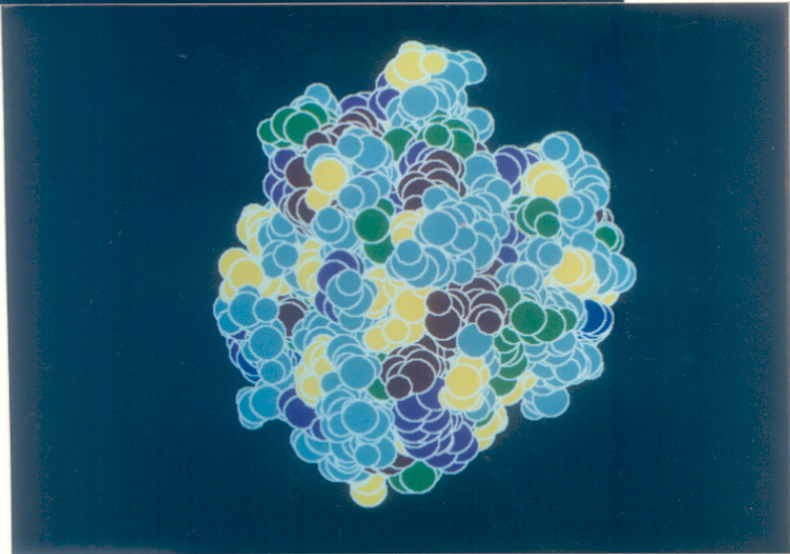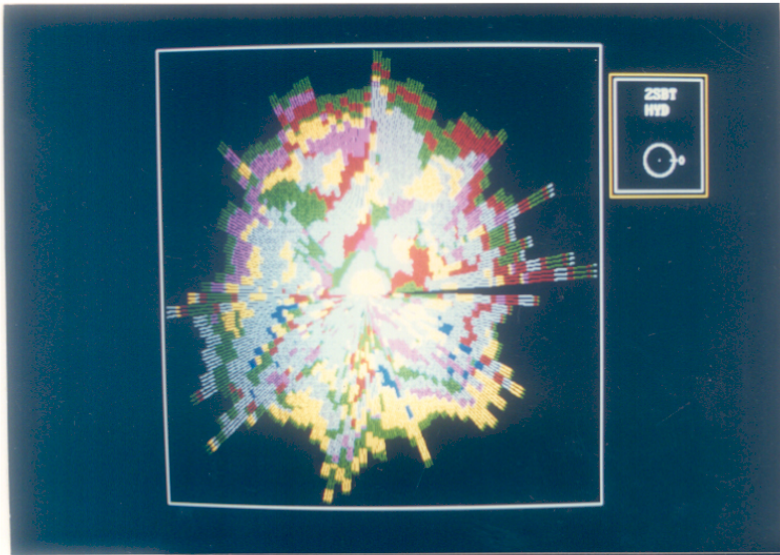
$$roughness\ factor = \sqrt{\frac{\Sigma((lencont/meancont)-1)^2}{ncont}}$$

$$globularity\ factor = \sqrt{\frac{\Sigma((areacont/meanarea)-1)^2}{ncont}}$$

$$fractality\ factor = \frac{(lencont/meancont)/(areacont/meanarea)}{ncont}$$

where,

roughness factor is a measure of the roughness of the protein.

globularity factor is a measure of the globular nature of the protein, taking into account the interstitial spaces.

fractality factor is a measure of the space-filling nature of the protein.

ncont is the total number of contours traced.

lencont is the length of individual contours.

areacont is the area occupied by each contour.

meancont is the circumference of the circle with diameter equal to the largest diameter of the protein.

meanarea is the area of the circle with diameter equal to the largest diameter of the protein.

The calculation of these indices gives an insight into the roughness of the surface of the protein, the globular nature of the protein, and a measure of the extent it fills the space in which it resides. These calculations can also be carried out for parts of the polypeptide chain which may help to identify protein domains, to locate nucleation sites for protein folding, determine the nature of the interfaces between domains, etc. The algorithm enables the calculation of these indices in addition to displaying the entire surface in two-dimensions. Hence, the protein is almost totally characterized.

Various other indices have also been calculated: the globularity index (Wodak and Janin, 1981), packing density (Zehfus and Rose, 1986), the fractal dimension (Lewis and Rees, 1985) and the coefficient of compactness (Zehfus and Rose, 1986). These are explained in detail below. The values obtained have been tabulated in Table 5.2.

Globular proteins follow the law (Janin, 1976; Teller, 1976)

$$A_c = 11.1 M^{2/3}$$

relating the accessible surface area A_c to the molecular weight M. The ratio A / A_c is called the globularity index, where A is the accessible surface area. However, this does not take into account the interstitial spaces which are not occupied by the protein molecule.

Packing density is defined as the ratio of summed atom volumes to total protein volume. However, this is not a good measure for the evaluation of compactness. When packing density is uniform, the overall shape of an object becomes the factor that determines compactness.

To calculate the fractal dimension of a protein surface, the surface area of the protein has to be calculated using different probe radii. Within resolution limits of the probe size, the fractal dimension is given by the relationship

$$D = 2 + |m|$$

where 2 is the topological dimension and m is the slope of the log-log plot of surface area versus probe size.

TABLE 5.2

COMPARISON OF DIFFERENT INDICES USED TO CHARACTERIZE PROTEINS

PROTEIN CODE	INDICES						
	RF	GF	FF	GI	PD	FD	CC
1TON	0.321	0.327	1.912	1.719	0.140	2.531	4.163
5CPA	0.714	0.186	1.941	1.989	0.138	2.676	4.751
2ACT	0.552	0.163	1.378	1.565	0.139	2.575	3.788
2LZM	1.440	0.271	2.374	1.608	0.137	2.486	4.102
3LZM	1.435	0.263	2.375	1.722	0.138	2.717	4.189
2AZA	0.561	0.146	1.803	1.818	0.138	2.584	4.364
1L06	1.541	0.300	2.333	1.625	0.138	2.479	4.135
2ALP	0.548	0.158	1.351	1.524	0.134	2.588	3.605
2CNA	0.896	0.364	1.407	1.850	0.140	2.628	4.486
1GCR	0.738	0.302	1.963	1.690	0.149	2.553	4.248
2B5C	1.644	1.000	1.326	1.474	0.133	2.468	3.466
351C	0.989	0.377	2.758	1.374	0.134	2.477	3.222
1SBT	0.679	0.102	1.582	1.663	0.136	2.624	3.977
1SBC	0.605	0.145	1.434	1.582	0.132	2.589	3.713
2SBT	0.492	0.121	1.624	1.772	0.137	2.714	4.252
2SNI	0.582	0.276	1.270	1.559	0.153	2.580	3.694

RF-roughness factor: GF-globularity factor: FF-fractality factor: GI-globularity index (Wodak and Janin, 1981): PD-packing density (Zehfus and Rose, 1986): FD-fractal dimension (Lewis and Rees, 1985): CC-coefficient of compactness (Zehfus and Rose, 1986).

1TON-Tonin: 5CPA-Carboxypeptidase A: 2ACT-Actinidin: 2LZM-Lysozyme: 3LZM-Lysozyme: 2AZA-Azurin: 1L06-lysozyme: 2ALP-α-lytic Protease: 2CNA-Concanavalin A: 1GCR-γ-II-Crystallin: 2B5C-Cytochrome B5: 351C-Cytochrome C: 1SBT-Subtilisin BPN: 1SBC-Subtilisin Carlsberg: 2SBT-Subtilisin NOVO: 2SNI-Subtilisin NOVO (as in a complex with chymotrypsin inhibitor).

The coefficient of compactness is the ratio of accessible surface area to the surface area of a sphere of equal volume. Geometrically, the *coefficient of compactness* is the surface area of a segment normalized by the minimum possible surface area. Numerically, it is a proportionality constant relating a segment's actual surface area to its minimum volume.

The surface area of the protein using different probe sizes and the protein volume were evaluated by QUANTA, ver 2.1.

5.3.2   *Characterization of Indice versus Angle Graphs by Evaluating the fractional Brownian Motion Exponent or the Hurst Exponent (H)*

Figure 5.5a shows the variation of K1 as a function of angle θ for a representative protein. Figure 5.5b is a plot depicting the variation of K2 as a function of angle θ for the same protein. Figure 5.5c depicts the variation of K3 as it varies with angle θ for the same protein.

where,

$$K1 = ((lencont/meancont) - 1)^2$$

$$K2 = ((areacont/meanarea) - 1)^2$$

$$K3 = (lencont/meancont)/(areacont/meanarea)$$

These plots are reminiscent of a fractal Brownian function.
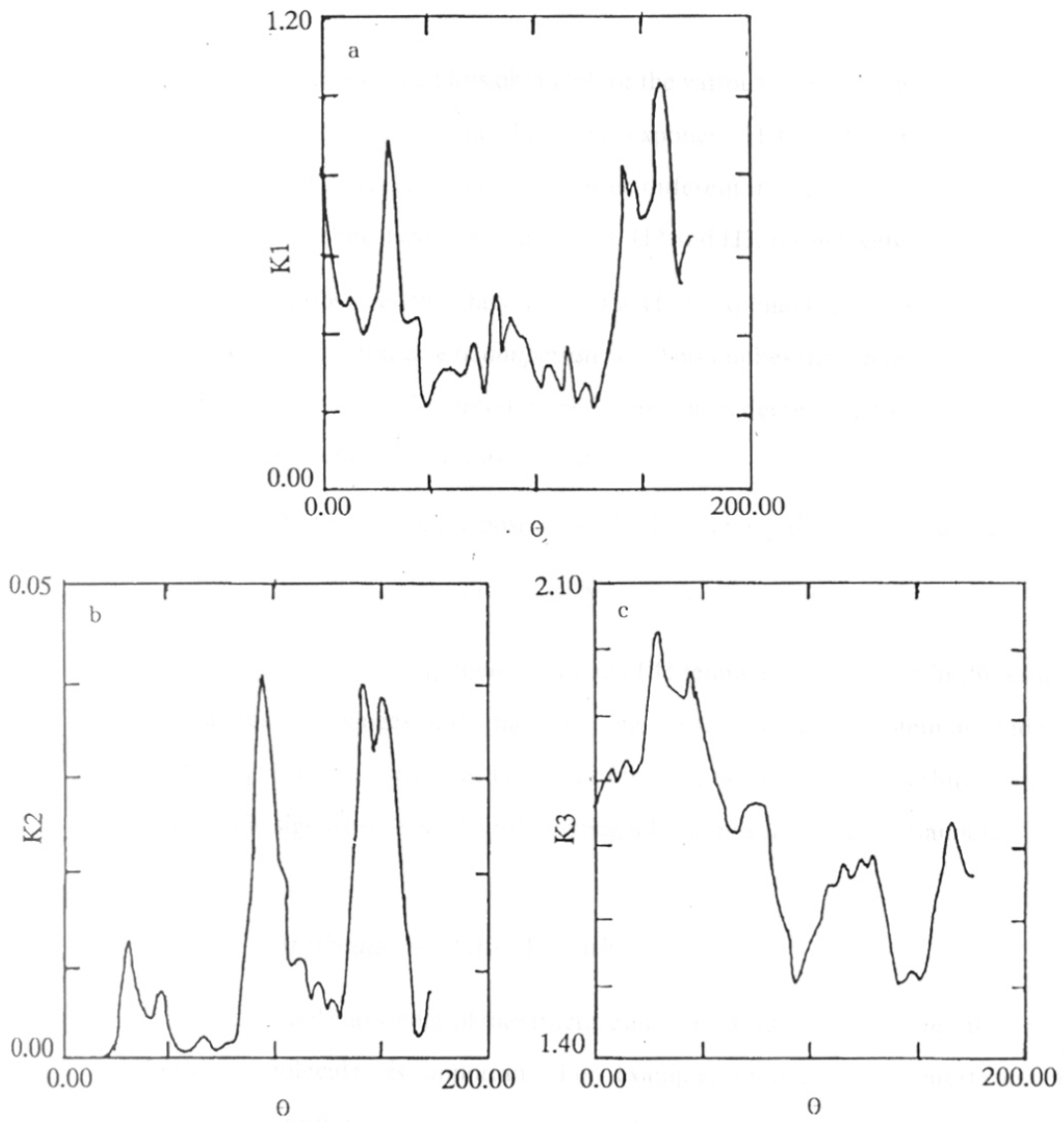
FIGURE 5.5

Plots depicting

a) Variation of K1 as a function of angle θ for 1SBC

b) Variation of K2 as a function of angle θ for 1SBC

c) Variation of K3 as a function of angle θ for 1SBC

115

To characterize the plots obtained for the various proteins examined, R/S analysis was carried out to determine the Hurst exponent H (see Appendix I for details of calculations). The values of H for the three different indices are tabulated in Table 5.3. The three exponents have been called H1, H2 and H3, respectively.

It can be observed that the values of the Hurst exponent are less than 1/2 and tending towards zero. This is a case of *antipersistence*. This implies that an increasing trend in the past indicates a decreasing trend in the future, and a decreasing trend in the past makes an increasing trend in the future probable.

If the increments in the position of the Brownian particle are given by

$$X(t) - X(t_0) \sim \zeta \,|\, t - t_0 \,|^H \quad (t \geq t_0)$$

for any two times t and t_0, then the value of H tending towards zero in this case means that successive changes in the indices along the surface of the protein are independent of the angle. This is correct as the fixing of the angles has been done arbitrarily and bears no specific significance except for aligning all proteins in the same manner.

5.3.3   Applications of the Algorithm

A detailed knowledge of the structure and the interactions occurring at the interfaces between molecules is important. For example, in antibodies, interfaces between associated constant domains are different from those found in protein monomers and therefore the elucidation of the peculiarities of these interactions may afford some insight into the general phenomena of molecular recognition.

TABLE 5.3

VALUES OF THE HURST EXPONENT (H) FOR THE DIFFERENT INDICES

PROTEIN CODE	HURST EXPONENT (H)		
	H1 (x*e-05)	H2 (x*e-05)	H3 (x*e-06)
1TON	3.2291	2.0118	5.0782
5CPA	2.1029	3.2588	6.2796
2ACT	1.5563	2.0935	4.5275
2LZM	1.2736	3.2890	7.2615
3LZM	1.3952	3.4792	7.7227
2AZA	1.0575	1.8357	2.4082
1L06	1.4789	3.4881	7.2114
2ALP	1.3534	1.8447	2.6028
2CNA	1.2538	1.8444	3.0306
1GCR	2.1284	2.0961	0.1098
2B5C	2.1063	2.4863	4.0874
351C	2.9694	2.7161	4.6088
1SBT	1.4608	7.1817	5.1474
1SBC	1.5744	5.0251	2.5347
2SBT	1.9841	2.4332	3.2406
2SNI	1.2322	4.8076	3.0692

The solvent-protein interface is almost certainly related to the structure of the native molecule and the chemical reactivity of the various groups also depend on their relation to this interface. Areas that are on the surface of the protein but are not accessible by the solvent also play a dominant role in reactivity and native protein conformation.

Analyses of proteins of a particular kind that originate from different sources, with the ability to act on the same or similar substrates, can provide important clues for protein engineering. Furthermore, surface description also provides a tool for analyzing regions that are important in subunit-subunit interactions, protein-antibody interactions and protein-solvent interactions.

Studies of this kind will be facilitated with the use of this algorithm as the surface can be easily viewed and compared with those of similar proteins.

5.4   CONCLUSIONS

The algorithm described in this chapter is highly advantageous in that the entire protein surface can be viewed at one time. Various surface properties from different proteins can be easily compared as all the proteins are aligned in a similar manner. The indices calculated help in characterizing a protein almost completely.

CHAPTER 6

DISPLAYING SURFACE PROPERTIES: STUDIES ON SUBTILISINS

Two-dimensional displays showing the surface properties of the subtilisins 1SBT, 1SBC and 2SBT have been analyzed. In addition surface properties distributions of 2SNI, which is the conformation induced in 2SBT on binding to chymotrypsin inhibitor, has also been analyzed. Some unusual observations regarding the distributions have been made and may reflect on the folding process of subtilisins.

CHAPTER 6

6.1   INTRODUCTION

In the previous chapter, an algorithm was introduced which enables one to visualize the distribution of various properties on the surface of a protein. The algorithm also allows evaluation of three new indices which characterize a protein almost completely. In this chapter, the two-dimensional displays obtained from that algorithm have been analyzed, with special reference to subtilisins.

Bacillus subtilis produces two major extracellular proteases, a neutral protease and an alkaline protease (called as subtilisin). The physiological roles of these two proteases are still unclear but have been postulated to play a role in sporulation and be involved as scavenger enzymes (Yang *et al*, 1984). Subtilisins are alkaline serine proteases consisting of a single polypeptide chain of 275 amino acids and possess no disulphide bonds or free Cysteine residues (Boyer and Carton, 1968; Stahl and Ferrari, 1984; Wells *et al*; 1983). There are several other subtilisins produced by a variety of species of *Bacillus*. They are subtilisin BPN' from *Bacillus amyloliquefaciens*, subtilisin Calsberg from *Bacillus Licheniformis* and *Bacillus pumilis*, subtilisin amylosaccharitius from *Bacillus amylosaccharitius* (Markland and Smith, 1971; Ohta and Inouye, 1990).

Because of the special structure of subtilisin among the serine protease family, it has often served as a model for studying a variety of problems in enzyme structure and function. Various studies using subtilisins as model systems, via protein engineering techniques, have been conducted for improving the stability (Estell *et al*, 1985; Wells and Powers, 1986; Bryan *et al*, 1986a, 1986b; Pantoliano *et al*, 1987), changing substrate specificities (Estell *et al*, 1986; Wells *et al*, 1987; Carter and Wells, 1987), and structural

and physicochemical characterization of the enzyme (Thomas *et al*, 1985; Russel *et al*, 1987). These studies have been performed by taking advantage of the X-ray crystallographic data for the enzyme (Wright *et al*, 1969; Drenth *et al*, 1972) and its gene, which has been cloned and sequenced (Stahl and Ferrari, 1984; Wong and Doi, 1986; Wells *et al*, 1983; Vasantha *et al*, 1984; Jacobs *et al*, 1985).

The tertiary structure of subtilisin determined by X-ray crystallography has revealed that the charged amino acid residues are not evenly distributed over the surface (Wright *et al*, 1969; Drenth *et al*, 1972). There is a relatively large surface area adjacent to the substrate binding site where no charged amino acids are located at all. It has been speculated that this hydrophobic surface area is originally covered by the highly charged prosequence (Ikemura and Inouye, 1988; Ikemura *et al*, 1987).

6.1.1   The Subtilisin Prosequence and its Role in Protein Folding

Mature active subtilisins are produced from their precursors, consisting of the presequence of 29 amino acids which serves as a signal peptide, the prosequence of 77 residues, and the mature protease of 275 residues (Wong and Doi, 1983; Stahl and Ferrari, 1984; Jacobs *et al*, 1985; Vasantha *et al*, 1984; Wells *et al*, 1983). The role of the prosequence has been obscure and recent studies on folding have indicated that it is absolutely essential for mature subtilisin to fold into an active enzyme (Zhu *et al*, 1989). Furthermore, the processing is autocatalytic in nature and production of active subtilisin occurs via an autoprocessing mechanism. It has also been shown that exogeneously added prosequence can guide denatured subtilisin to fold into an active state in an intermolecular process (Zhu *et al*, 1989). It can therefore be assumed that specific interactions between the propeptide and mature subtilisin are important during the renaturation process. It is

also noticeable that the subtilisin prosequence is exceptionally long with a very high percentage of charged residues, and mutational studies on it have indicated that almost the entire prosequence is important for its function (Ikemura *et al*, 1987).

A particularly interesting issue in the case of refolding of subtilisins is the rate of the process. Since the protein consists of a single polypeptide chain with no cysteines or cystines, why is the folding process so slow? What limits the rate of folding? What interactions between the prosequence and the mature sequence *induce the fit* or the equilibration?

6.1.2   Role of Prosequences in Secreted Sequences and Peptides

Prosequences are also associated with a large number of other proteins. Among peptide hormones the most prominent example is perhaps insulin in which the C chain is a propeptide and undoubtedly acts as a template for the correct disulphides to form in the A and B chains. The C chain is eventually processed by a proteolytic enzyme. In case of the neutral protease identified in *Bacillus subtilis*, there appear to be 222 amino acids that precede the mature terminus of the protease. Of the 222 amino acids, presumably the first 30 amino acids account for the signal peptide while the rest (about 190 amino acid residues) constitute the prosequence. This prosequence is exceptionally long compared to that of alkaline serine protease (about 70 amino acids). However, the prosequence of both proteases contain a large number of charged residues. The functional role of these sequences is generally uncertain and the following functions can be broadly attributed to the prosequence (Wiren *et al*, 1988).

(1) to ensure correct folding of the protein (Steiner and Clark, 1968)

(2) to provide a minimum length needed for transport across the endoplasmic reticulum

(3) to provide linkage for coordinate translation of related secreted peptides, for example, peptide hormones and neuropeptides (Hebert and Uhler, 1982)

(4) to provide milieu for alternatively cleaved neuropeptides and peptide hormones (Jorgensen *et al*, 1987)

(5) to lead precursors from the rough endoplasmic reticulum (RER) to the golgi apparatus where further processing of the propeptide takes place (Guan and Rose, 1984)

(6) to direct covalent post-translational modification of the mature protein

(7) to act in consort with the signal peptide to optimize signal function (Wiren *et al*, 1988)

Other cases of serine proteases wherein the protein is synthesized as a preprosequence are Carboxypeptidase A, α-lytic protease, renin and HIV protease. This indicates that such structures exist for all major classes of proteases. However, only in the case of α-lytic protease and subtilisin has it been convincingly demonstrated that the prosequence guides folding of the mature sequence to an active enzyme. Data on other serine proteases have so far not indicated the same folding pathway. It is therefore important to study the mechanism in order to find clues which would help elucidate the pathway by which the prosequence guides folding.

The hydrophobic surface area adjacent to the active site has been hypothesized to be originally covered by the highly charged prosequence. What are the interactions that occur between this prosequence and the surface of the protein? To be able to say

something about this it is very important to study the surface properties of subtilisins and move a step closer towards understanding the folding pathway. An analysis of the surface properties of subtilisins has been undertaken in this chapter.

6.2　　MATERIALS AND METHODS

Two-dimensional displays of the surface distribution of properties such as hydrophobicity, hydration potential, polarity and bulk have been obtained from the algorithm described in section 5.2.1 for the different subtilisins under study. These are 1SBT, 1SBC and 2SBT. The active site of these proteins has also been mapped using the same algorithm. Studies have also been carried out for 2SNI which is the conformation of 2SBT induced on forming a complex with chymotrypsin inhibitor.

6.3　　RESULTS AND DISCUSSIONS

6.3.1　　Surface Maps Described by Earlier Workers

There are different ways to calculate and draw a surface map for molecules of globular proteins (Barlow and Thornton, 1986a). Using a specific map, one can observe simultaneously almost the whole protein surface. Barlow and Thornton (1986b) examined charged group distribution using such maps.

Chirgadze *et al* (1989) have used the technique of applying molecular cartography to the analysis of the molecular surface of globular proteins at atomic resolution. Three specific kinds of map were used, superposing each map onto another in order to identify atomic groups forming elevated or deepened regions of the molecular surface.

Holbrook *et al* (1990) have used a database of monomeric protein crystal structures to teach computer-simulated neural network rules for predicting surface exposure from local sequence.

The two-dimensional protein maps presented here have the advantage of being able to show the entire protein surface at one time. They also reflect on the roughness of the surface as the length of the *contours* vary. Various properties can be studied and superimposed to arrive at substantial conclusions.

6.3.2   Analysis of Surface Properties of Subtilisins

Figure 6.1 illustrates differences in the secondary structures of subtilisins 1SBT, 1SBC and 2SBT respectively. It can clearly be noted that 1SBT and 1SBC have very similar secondary structures while 2SBT is fairly different. Both 1SBC and 1SBT have 8 α -helical regions and 5 β -sheets or turns whereas 2SBT has one α -helical region less but has 3 β -turns more. Furthermore, these three β -turns lie from residues 153 to 219, a region which in 1SBT and 1SBC is a random coiled structure. This implies that 2SBT is more organized than 1SBC and 1SBT. This reflects on the stability of 2SBT. It is suggested that α -helices or β -turns are less susceptible to proteolytic cleavage than coiled structures.

The space-filling models of 1SBT, 1SBC, 2SBT and 2SNI are shown in figure 6.2. It can be seen that 1SBT and 1SBC have very similar conformations whereas 2SBT is quite different. Is this difference evident as we move along the surface of the proteins? Figure 6.3 shows the sections of (a) 1SBT, (b) 1SBC and (c) 2SBT at angles of 0°, 45°, 90°, 135° and 180°. The similarities between 1SBT and 1SBC and the difference between 2SBT are clear from this figure.

126
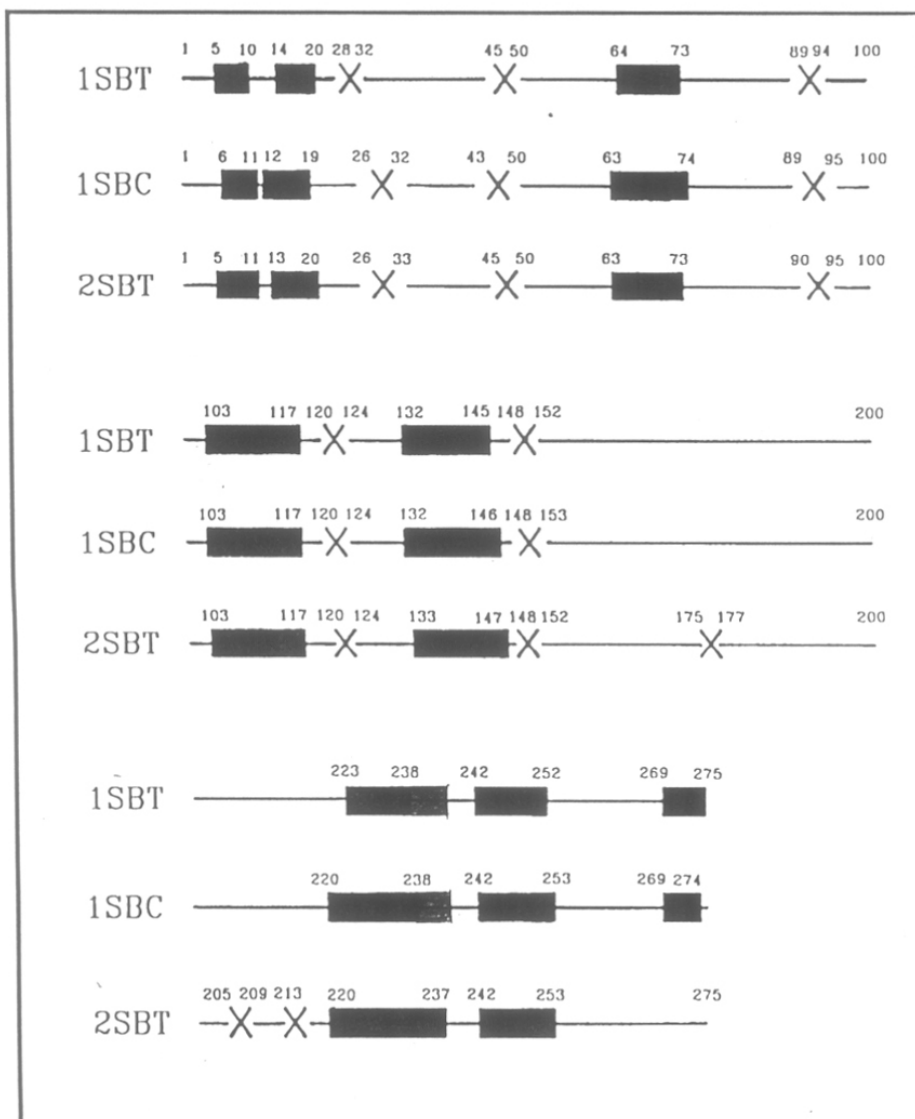
FIGURE 6.1

Schematic diagram depicting the difference in secondary structures of (a) 1SBT, (b) 1SBC and (c) 2SBT. X denote β sheets and filled boxes denote α helices. The residue numbers are indicated.

FIGURE 6.2

Space-filling models of 1SBT (top left), 1SBC (top right), 2SBT (bottom left) and 2SNI (bottom right).
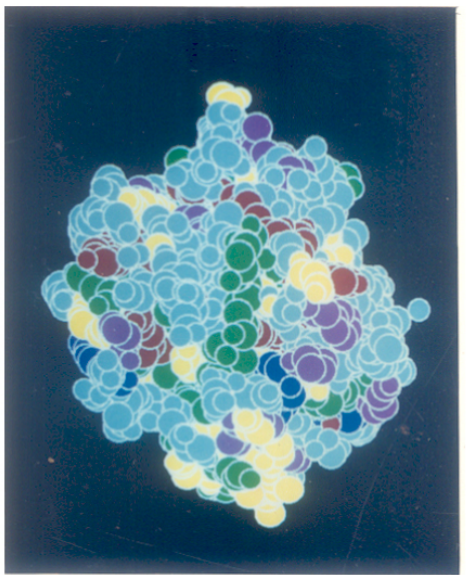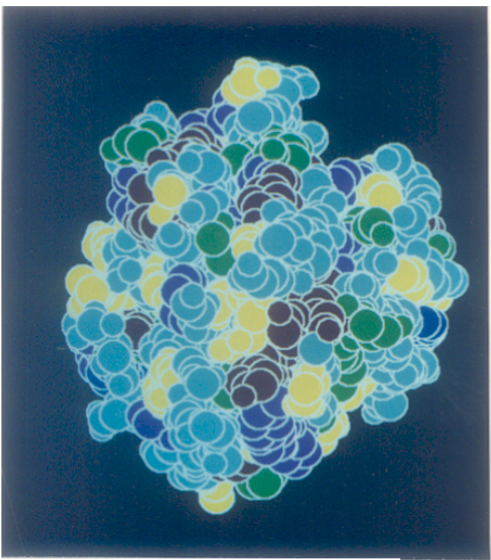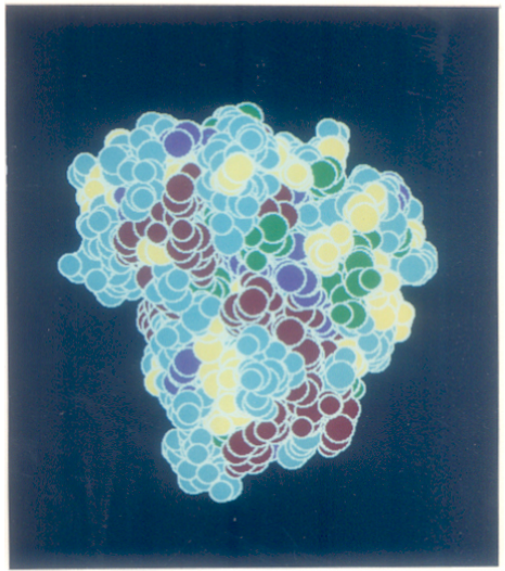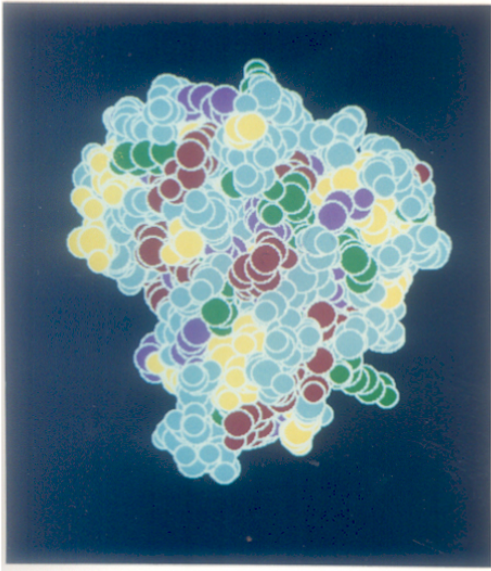
FIGURE 6.3a

Sections through the three-dimensional structure of 1SBT at angles of 0° (top left), 45° (top right), 90° (center left), 135° (center right), 180° (bottom).
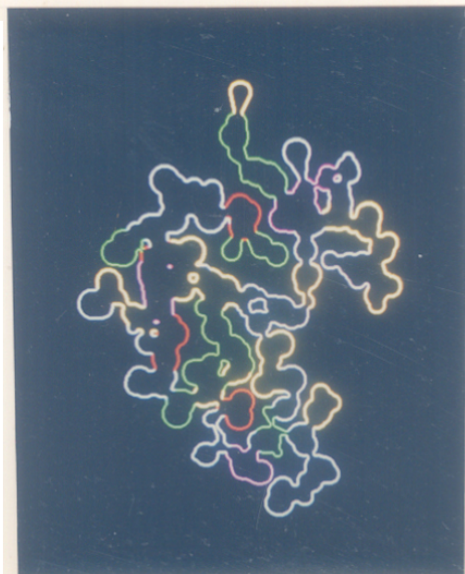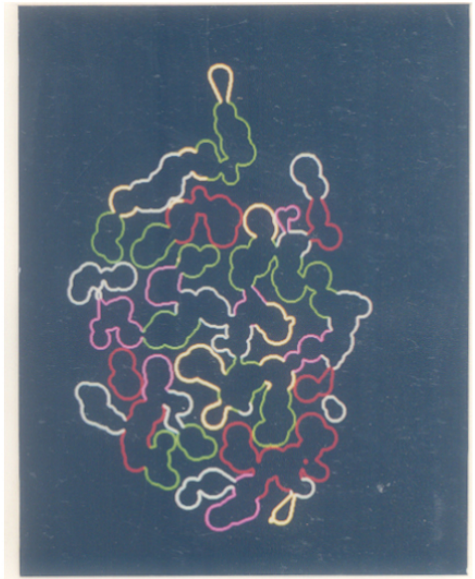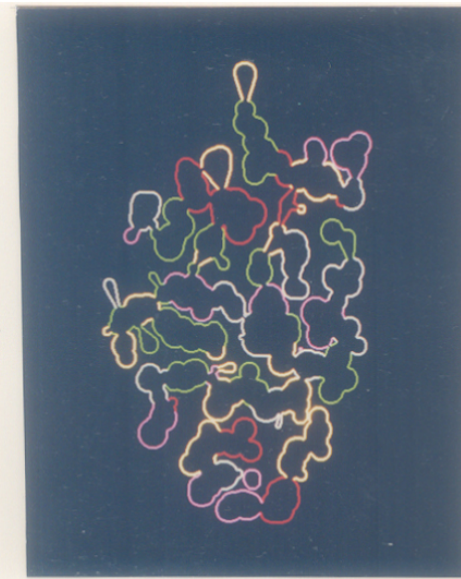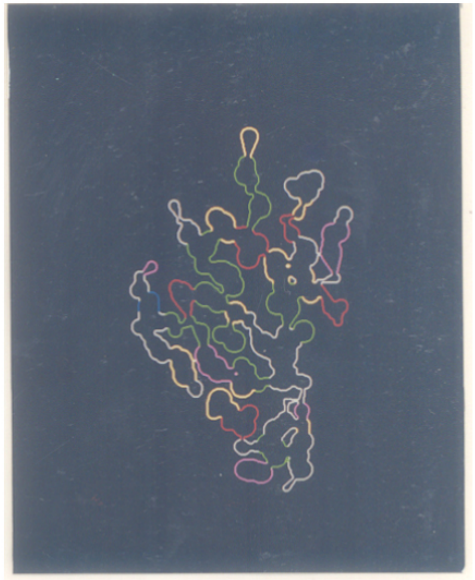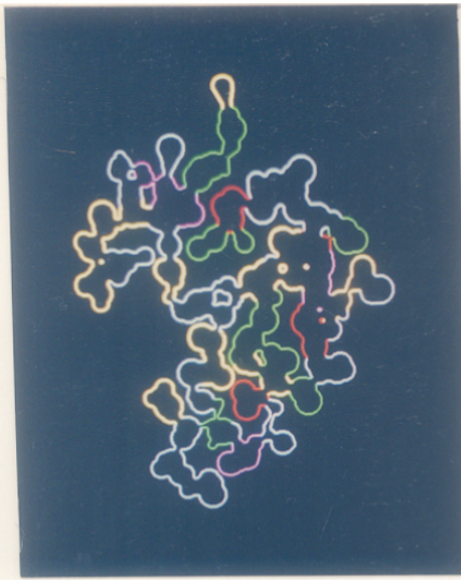
FIGURE 6.3b

Sections through the three-dimensional structure of 1SBC at angles of 0° (top left), 45° (top right), 90° (center left), 135° (center right), 180° (bottom).
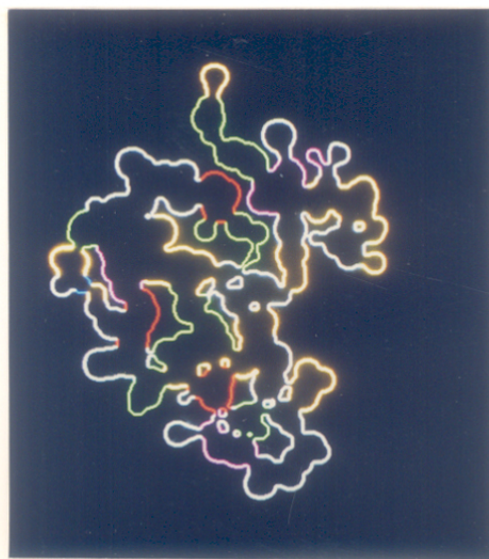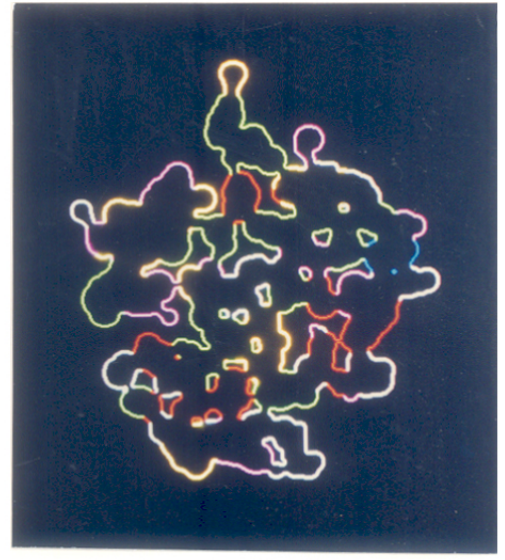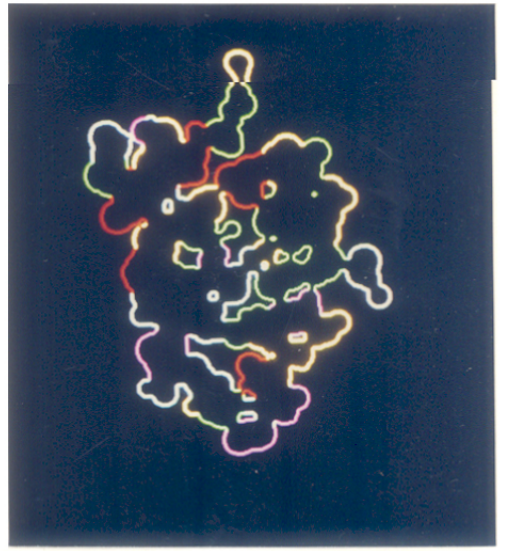
FIGURE 6.3c

Sections through the three-dimensional structure of 2SBT at angles of 0^0 (top left), 45^0 (top right), 90^0 (center left), 135^0 (center right), 180^0 (bottom).
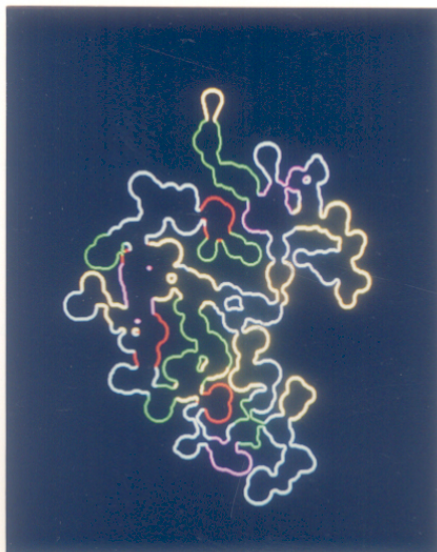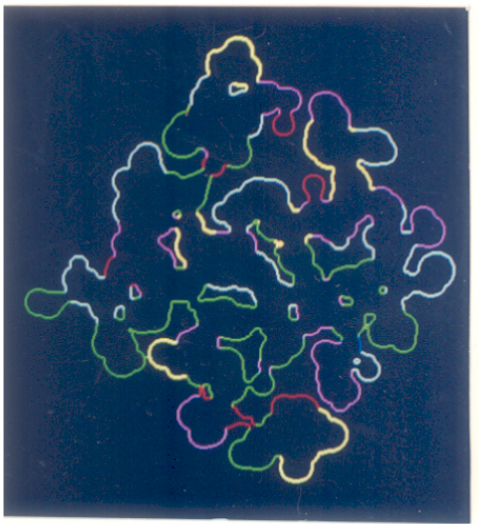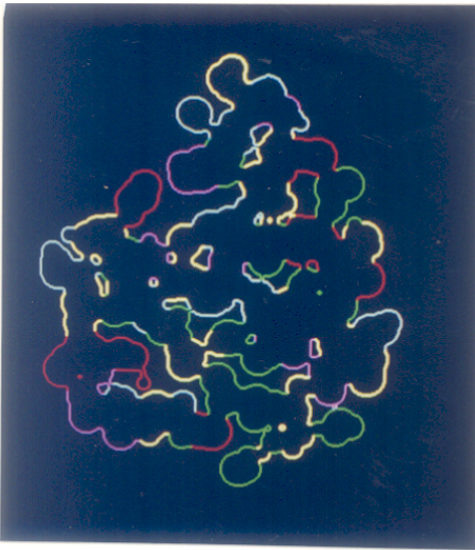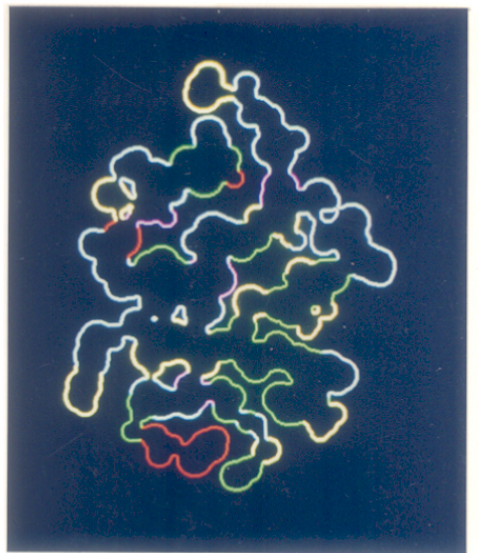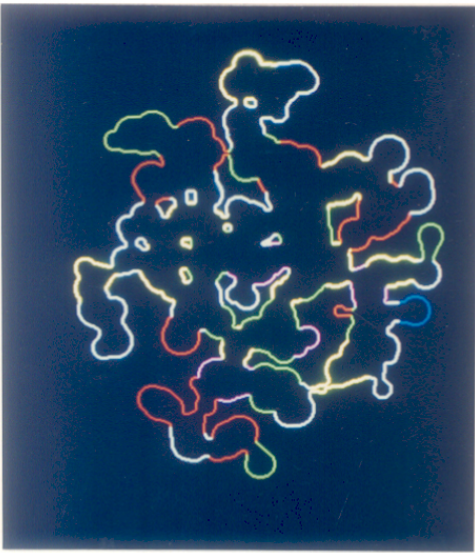
The location of the regions of the active site exposed to the surface is shown in figure 6.4. Only those sections have been displayed which contain the active site residues. This figure depicts the hydrophobicity distribution on the surface. The yellow and white regions depict the region of catalytic residues exposed on the surface of the protein. It is distinctly observed that the region where these catalytic residues are exposed on the surface is flanked on either side by a relatively rough surface indicated by the longer length of the contours. In other words, the cross-section wherein the active site residues are exposed to the solvent are relatively smoother than those neighboring it or, the domain of the active site exposed to the surface lies in a cleft. In all enzymes of known structure, substrate molecules are bound to a cleft or crevice from which water is largely excluded. The *exposed area of the catalytic residues* of 1SBT and 1SBC are similar while that of 2SBT is slightly different. Distances between residues comprising the active site are similar in 1SBT and 1SBC, whereas they are somewhat different in 2SBT. On the whole, this is consistent with the view that all catalytic residues within the same family are conserved during evolution. The sequential conservation around the catalytic amino acids is high and the residues that are near in the three-dimensional structure ($\leq 4\,A°$) are also very highly conserved (Zvelebil and Sternberg, 1988)

In case of subtilisins it has been found from the tertiary structure that there is an uneven distribution of charged amino acid residues on the surface. Also, no charged residues are found over a large surface area adjacent to the active site. Figure 6.5 shows this asymmetric distribution of polarity on the surface of the three subtilisins. But the figure tells more about this distribution. In quadrants 1 and 4 there is an average magnitude of polarity between 1 and 5 o'clock in case of 1SBT, while in 1SBC a similar region is seen only in quadrant 4. In case of 2SBT the area around the active site where it is exposed to the surface is of average polarity whereas in 1SBT and 1SBC this region is relatively more polar, more so in 1SBT. It is known that the active site cleft contains
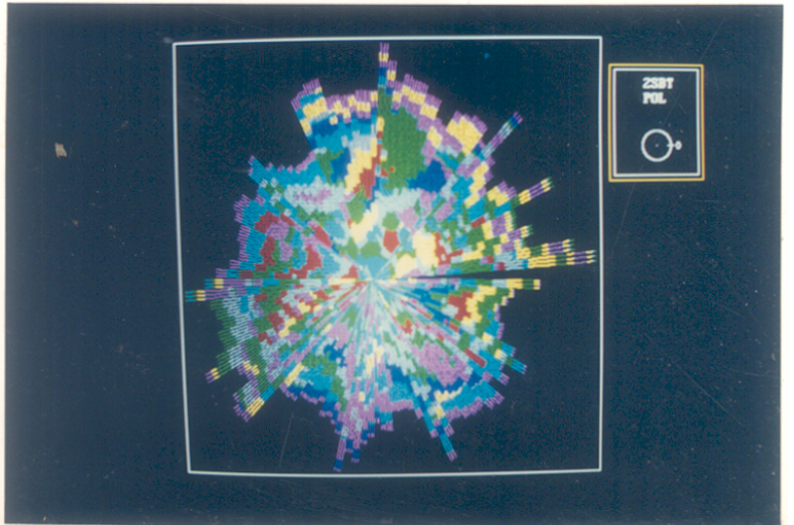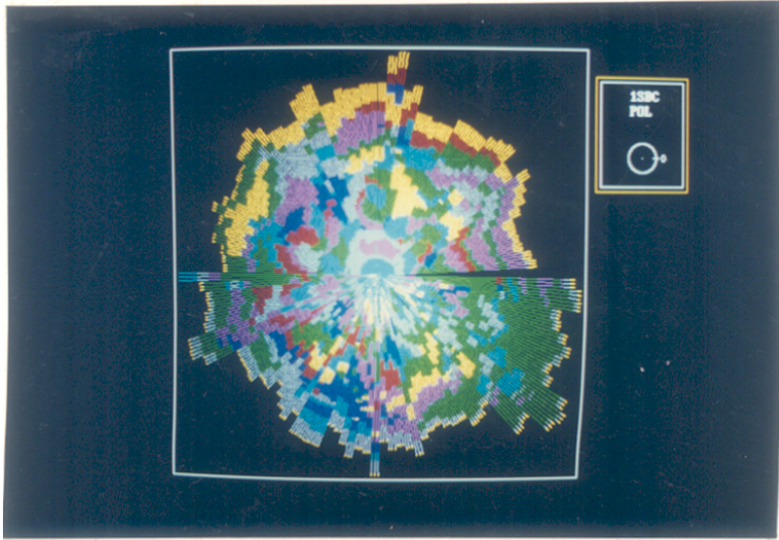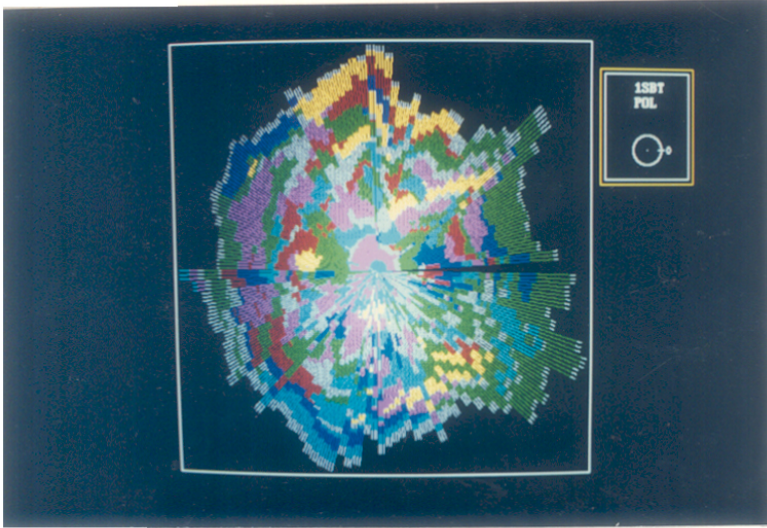
FIGURE 6.4

Location of regions of the active site exposed to the surface for 1SBT (top), 1SBC (center) and 2SBT (bottom).
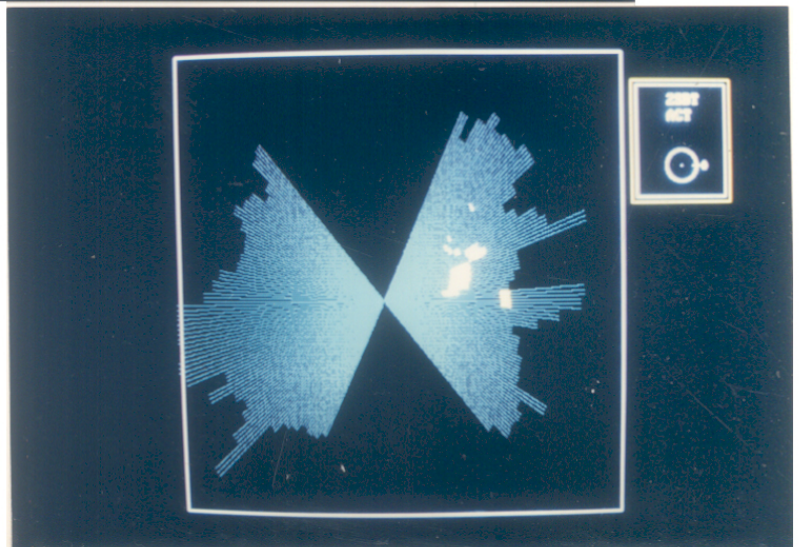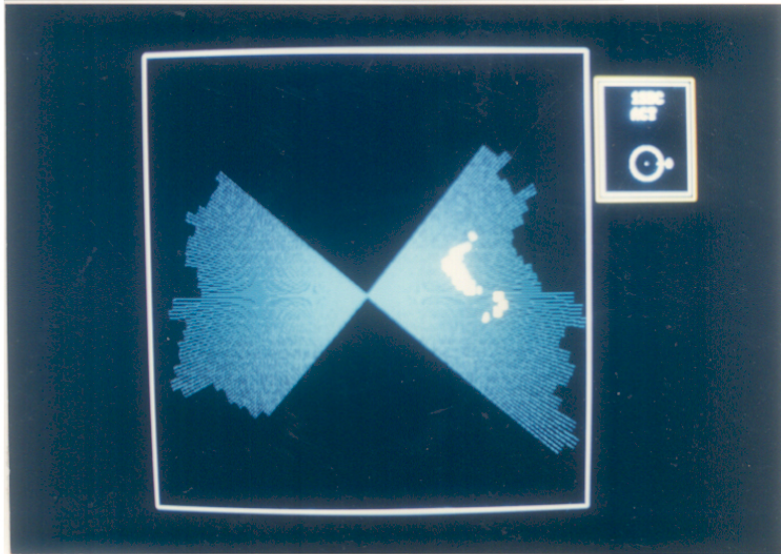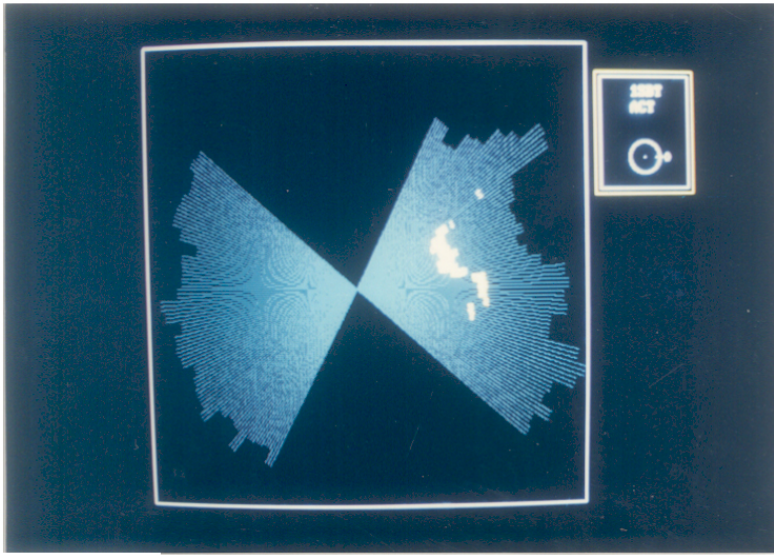
FIGURE 6.5

Distribution of polar amino acid residues on the surface of 1SBT (top), 1SBC (center) and 2SBT (bottom).

several polar residues that are essential for binding and catalysis. In addition, the cleft creates a microenvironment in which certain polar residues acquire special properties essential for their catalytic role.

The surface distribution of hydrophobicity on the surface of the three proteins shows that the distribution is rather random as seen in figure 6.6. The region where the active site is exposed to the surface is not hydrophobic, except in the case of 2SBT where there is a region next to the exposed active site which is hydrophobic.

When the surface distribution of hydration potential is seen, a trend similar to that observed in case of polarity is realized as can be seen in figure 6.7.

Contact surfaces, when individual subunits and domains are associated, are very bumpy, displaying relatively large protuberances and depressions. The extensive use of large side chains would especially exaggerate these interface surface features. In fact, the nine largest amino acids by volume constitute 49% of the interface surface while the same amino acids provide only 38% of the protein exterior of the total composition of proteins in general (Argos, 1988). Therefore, we would expect less bulky amino acid residues to be on the surface and their distribution to be more or less random. But, an interesting distribution is observed when one maps the distribution of amino acid bulk on the surface of the three subtilisins (figure 6.8). There is an drastic segregation of bulky amino acid residues on one side of the protein surface. The active site is located in the region where less bulky amino acid residues dominate. This could be a reason for the low specificity of these enzymes such that substrates of all sizes can be acted upon. This could probably also mean that during the Brownian motion of the protein molecule, the rotation of the molecule around its own axis would be extremely slow. This may imply that the orientation of the active site would be more fixed as compared with other proteins. It would be interesting to study proteins from the same family (i.e., serine proteases) in order to
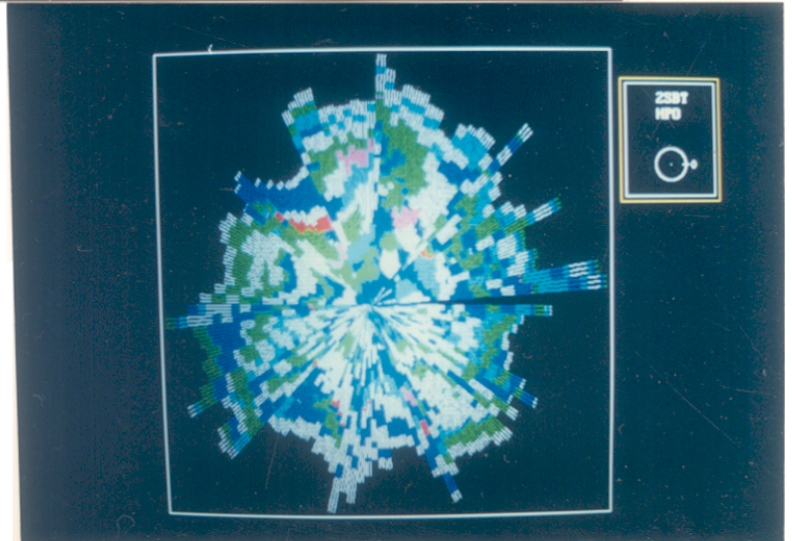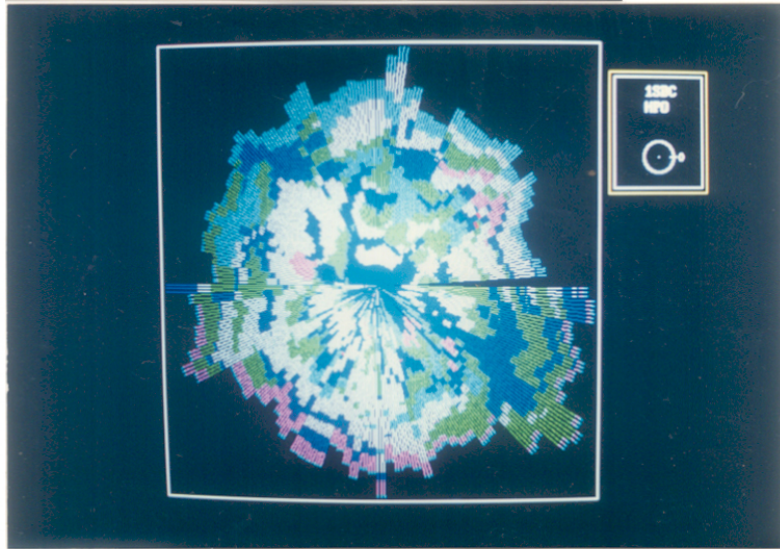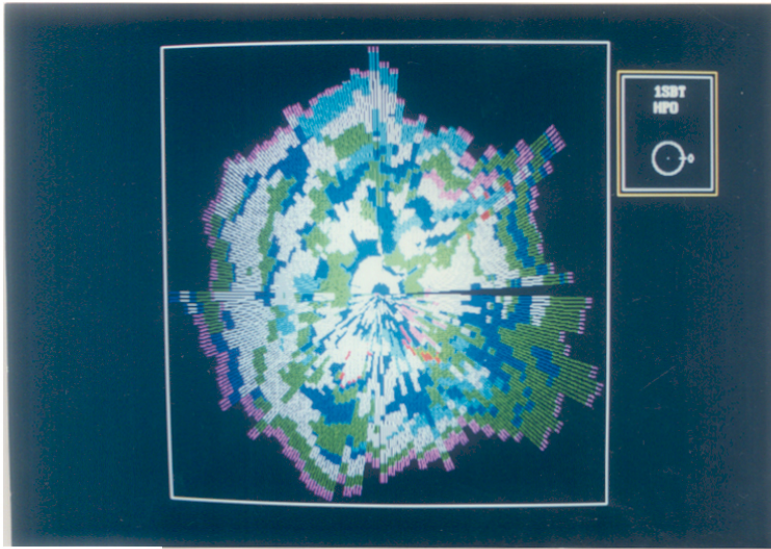
FIGURE 6.6

Distribution of hydrophobic amino acid residues on the surface of 1SBT (top), 1SBC (center) and 2SBT (bottom).
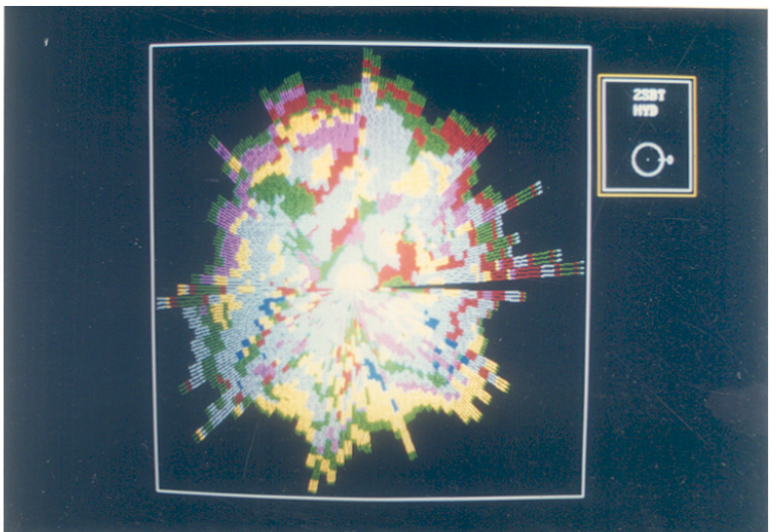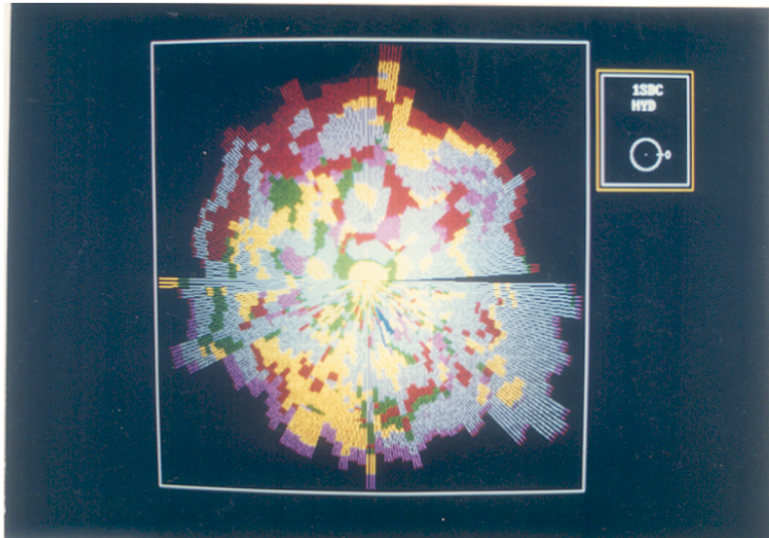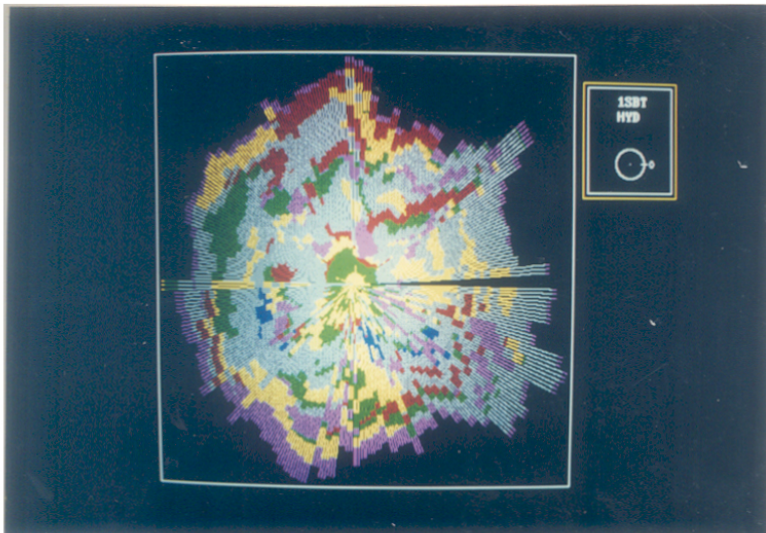
FIGURE 6.7

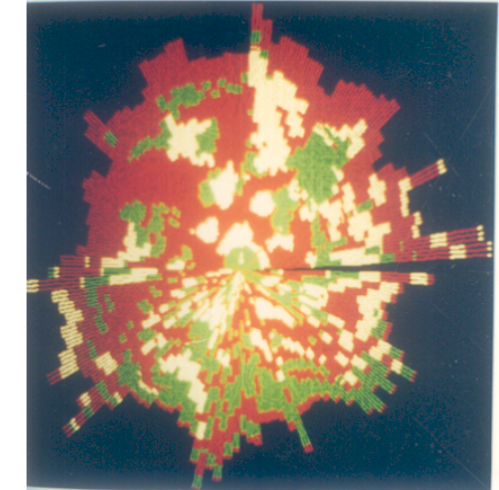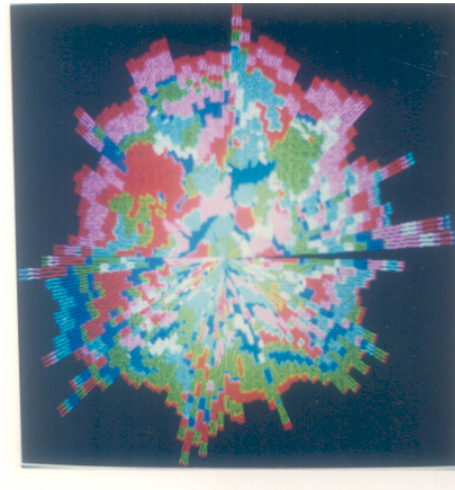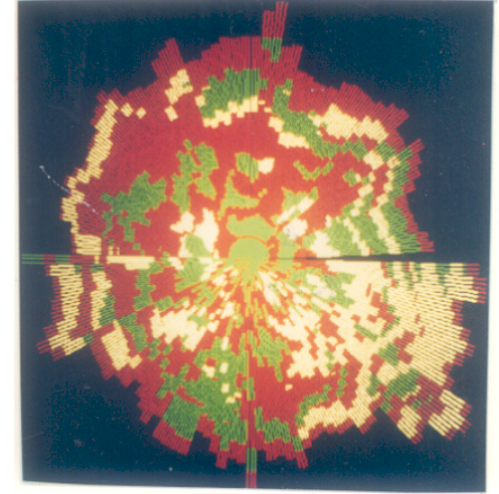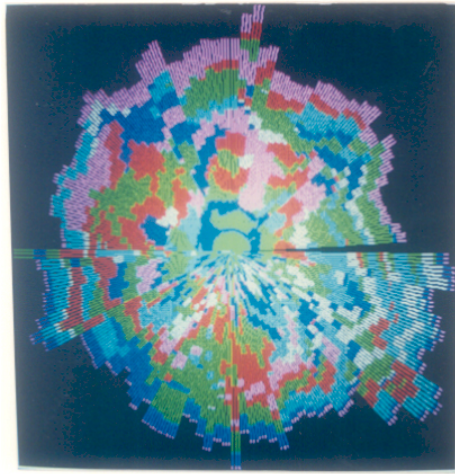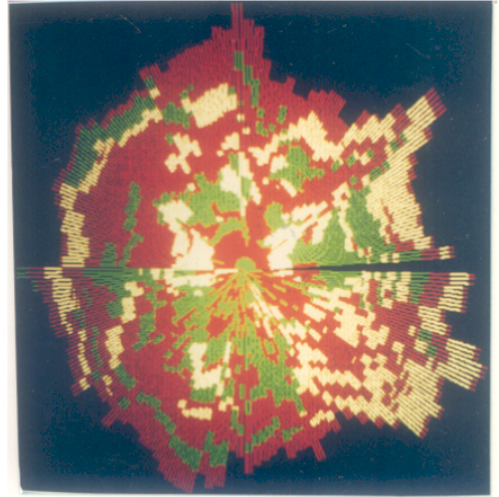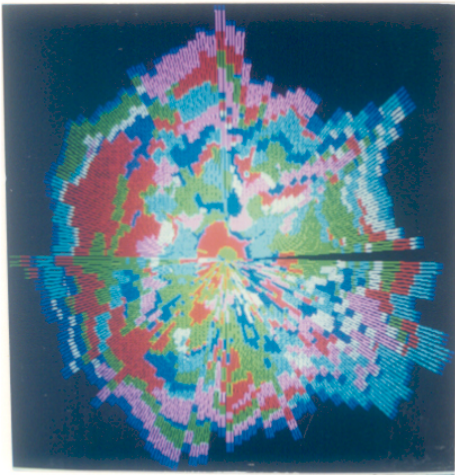Distribution of hydration potential of amino acid residues on the surface of 1SBT (top), 1SBC (center) and 2SBT (bottom).

FIGURE 6.8

Distribution of amino acid bulk on the surface of 1SBT (top), 1SBC (center) and 2SBT (bottom), in the 7 (Table 5.1) and 3 color code (high-red; average-green; low-white).

understand the importance of this asymmetric distribution.

When the distribution of bulk on the surface of Carboxypeptidase A (5CPA), α-lytic protease (2ALP) and Proteinase K (2PRK) was studied (figure 6.9), it was observed that this asymmetry was distinct only in subtilisins and to a lesser extent in 2ALP. In 5CPA and 2PRK such a distribution is absent.

2ALP and subtilisins both have pro-sequences which play a crucial role in protein folding. Could this asymmetric bulk distribution mediate in this process? It is known that the prosequence has a large number of charged residues. Analysis of peptide sequence from DNA coding sequences of subtilisins from different species of *Bacilli* has shown the existence of a common sequence, Tyr-Ile-Val-Gly-Phe-Lys, at the amino terminal of the prosequence (Ikemura *et al*, 1987). These residues are bulky in nature. The region where the active site is exposed to the surface is less bulky than the rest of the surface in case of all the subtilisins, and is polar too. *It is probably this region of the subtilisin molecule which interacts with the prosequence facilitating the folding process.* It is known that inhibitors are not able to inhibit the self-processing of prosubtilisin (Ikemura and Inouye, 1988). The active site must be involved in the process and this is further suggested by the observations of the surface property distribution of these subtilisins.

6.3.3   Comparison Between Structures of 2SBT and 2SNI

2SNI corresponds to the conformation of 2SBT on forming a complex with chymotrypsin inhibitor. There is a drastic change in conformation on this association as can be seen in the active site map (figure 6.10). This is expected as the distances between residues comprising the active site have changed due to the interaction. The exposure of the active site is seen on the diametrically opposite side to that of 2SBT. The exposed

FIGURE 6.9

Distribution of amino acid bulk on the surface of 5CPA (top), 2ALP (center) and 2PRK (bottom), in the 7 (Table 5.1) and 3 color code (high-red; average-green; low-white).
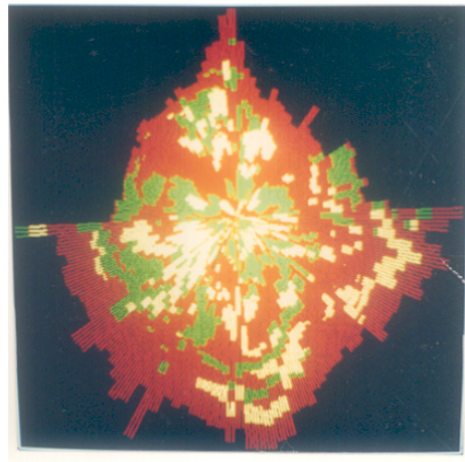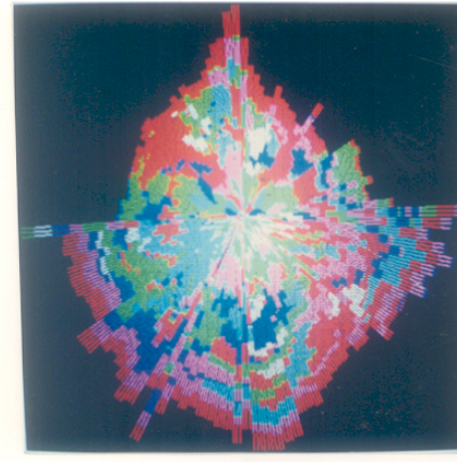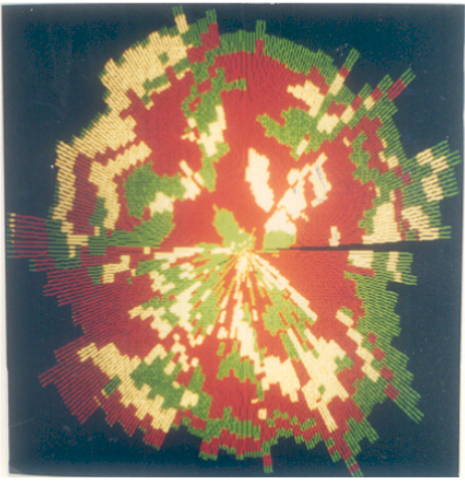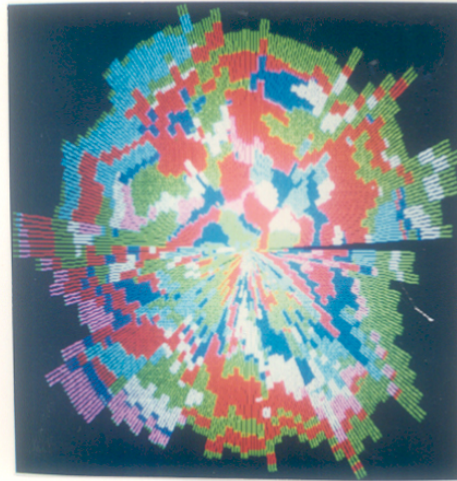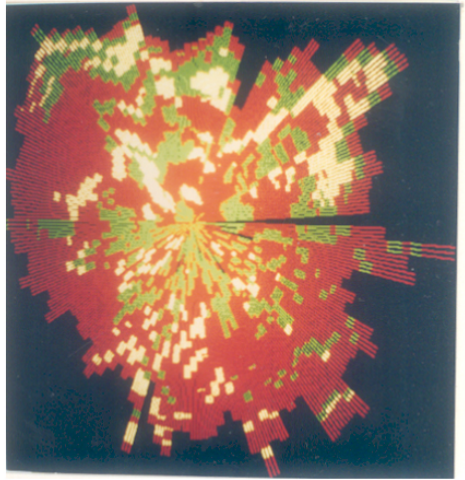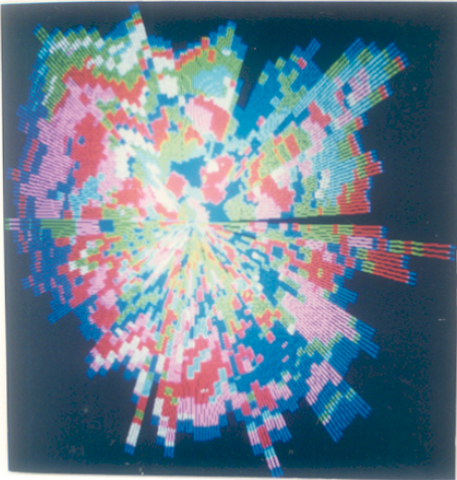
FIGURE 6.10

Distribution of various properties on the surface of 2SNI: active site exposed to the surface (top left); polarity (top right); hydrophobicity (center left); hydration potential (center right); bulk (bottom) in the 7 (Table 5.1) and 3 color code (high-red; average-green; low-white).
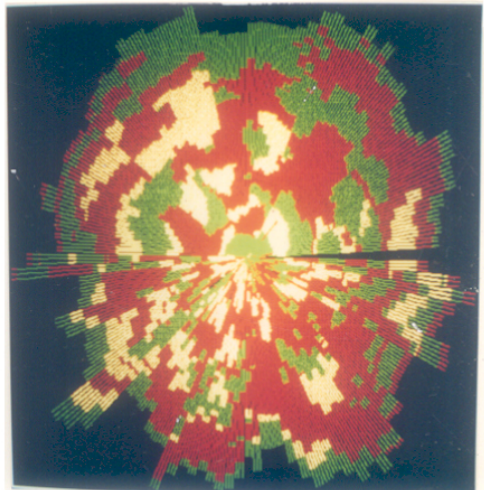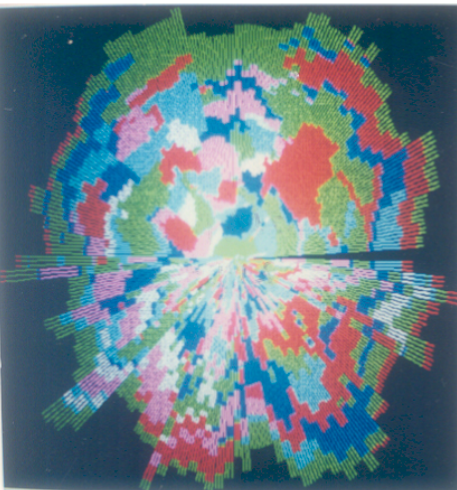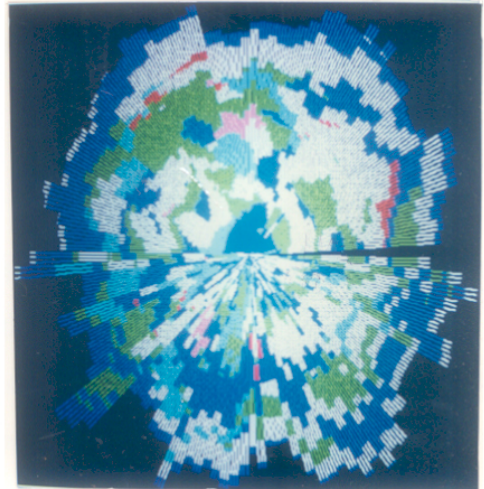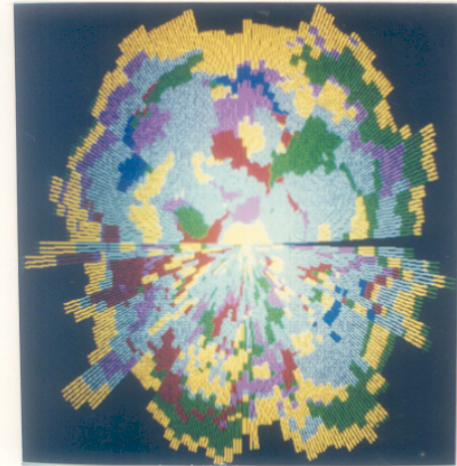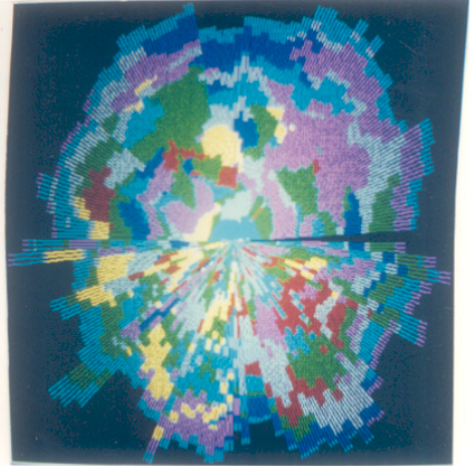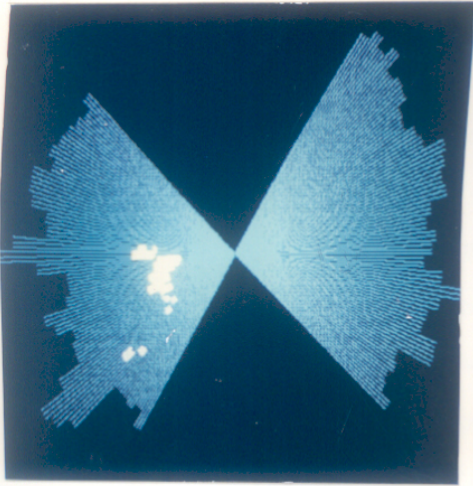
regions here too are flanked by two regions of relative roughness.

The polarity distribution has become segregated. Between 12 and 3 o'clock it is high whereas between 9 and 12 o'clock there is a region of average polarity on the surface. Such a segregation was not observed in case of 2SBT where the distribution was more or less random. Distribution of hydration potential on the surface is also clustered as can be seen with the patches of blue and green colors on the surface map. Hydrophobicity distribution is uneven, but of average or low value as can be seen with the extent of green, yellow and white colour on the surface map. Bulk distribution is relatively more even, although patchy. Figure 6.11 shows the various sections of 2SNI at angles of 0°, 45°, 90°, 135° and 180°. The differences between 2SBT (figure 6.2) and 2SNI can be clearly seen showing the change in conformation on binding of the inhibitor.

6.4   CONCLUSIONS

The results indicate that 1SBT and 1SBC are quite similar in their surface properties whereas 2SBT differs to quite an extent. Drastic conformational changes are evident on binding of inhibitor to 2SBT as seen from the surface properties of 2SNI. How do these differences reflect on the differential stability and activity of these subtilisins? How does the prosequence mediate in the folding pathway? Some part of the answers have been attempted here, but only further studies alongwith biochemical evidence might be able to give the answer.

FIGURE 6.11

Sections through the three-dimensional structure of 2SNI at angles of 0° (top left), 45° (top right), 90° (center left), 135° (center right), 180° (bottom).
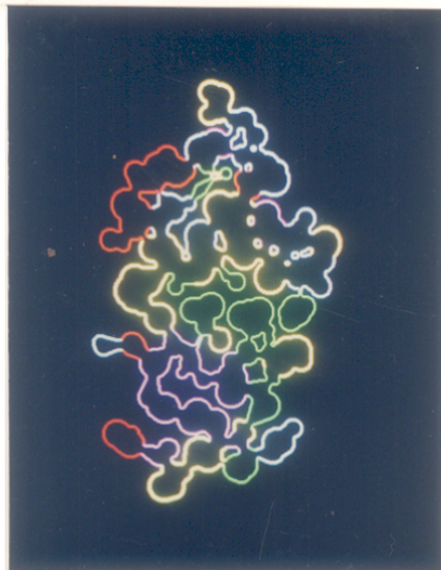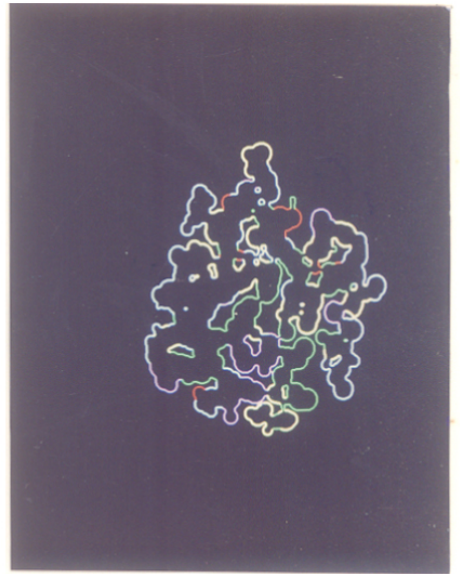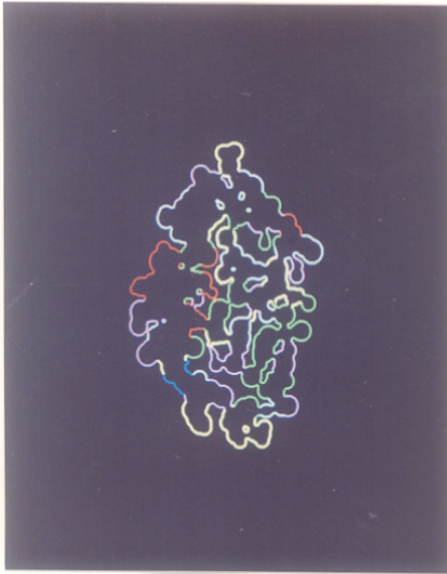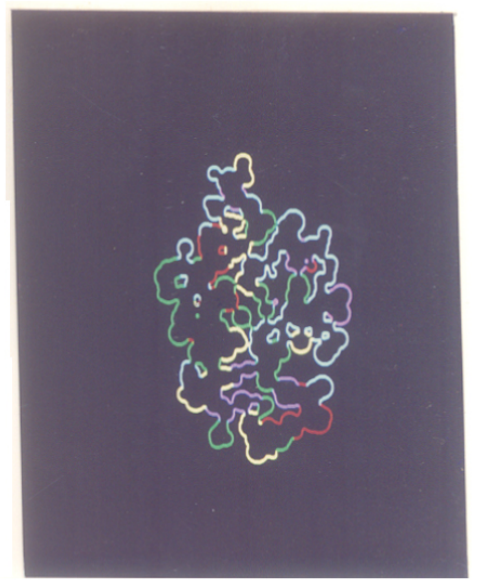
CHAPTER 7

CONCLUSIONS

CHAPTER 7

Biological reactions are extremely complex and are usually explained by considering complex reaction kinetics and interactions between the reacting species. By considering the biological macromolecules to be fractals this can now be explained in a simple manner. Application of the concept of fractals to biological systems in order to analyze structure-function relationships, understand and explain the complexity of biological organization and reactions has been attempted in the present thesis. This is the concluding chapter of the thesis. A summary of the earlier chapters is presented and also the scope of further work and applications.

In the first chapter the subject matter of the thesis was introduced along with a survey of the literature on fractals. Relevant analysis of biological systems was also discussed.

In the second chapter an analysis was made of the effects of fractal nature of enzymatic reactions where the results indicated that non-idealities in their performance can arise due to their fractal nature. As an extension to this work, similar simulations can be done on real enzyme molecules by considering the X-ray crystallographic data. Specific interactions between substrate molecules can also be taken into account.

Biological membranes and protein molecules have been described as fractals. With the consideration of the constant motion of regions which constitute the fractal, the concept of mobile shapes of fractals or *fractiles* emerged. The effect of mobility on reactions was considered in chapter three. Reactions on *fractile* surfaces when the overall dimension of the system may or may not undergo a change were critically analyzed. Selectivity behavior on *fractile* surfaces was also discussed. These studies could provide

an answer to the baffling observation that many reactions occur at rates which exceed the calculated values (considering three-dimensional diffusion control) by factors of thousands.

Reasons why bacterial colonies take diverse shapes under different environmental conditions were evaluated and subsequently simulated in chapter four. The time based change in the fractal shape and dimension of bacterial colonies was calculated. Critical effects of concentration of nutrients, their rates of diffusion, thickness of the gel and yield coefficients of cells per unit substrate had been studied. The effects of a few parameters were considered in this preliminary case study. Further theoretical and experimental studies will enhance understanding of the actual biochemical principles involved in microbial colony formation of different species.

An algorithm was described in chapter five for evaluating the properties on protein surfaces. Three new global indices were introduced which characterize a protein almost completely and are based on local relationships. These and other indices described by earlier workers were calculated for some proteins. R/S analysis was performed on the fractal Brownian function-like plots of the change in these indices as they vary along the protein structure. This algorithm and the indices introduced will be of great help in evaluating the properties of the surface which determine so many of the functions of biological macromolecules.

In chapter six, the two-dimensional representation of protein surfaces was analyzed. This facilitates one in comparing the surface of different proteins in order to understand the effect of surface topologies on protein-substrate, protein-protein and protein-ligand interactions. Special attention was given to subtilisin, a serine protease, in an attempt to understand differences arising in species from different sources. More analyses of this kind substantiated by biochemical evidence will help in unfolding the mysteries of the folding process of subtilisins.

APPENDIX

APPENDIX I

FRACTIONAL BROWNIAN MOTION

Mandelbrot has introduced the concept of *fractional Brownian motion* as a generalization of the random function X(t) by changing the exponent from H = 1/2 (for ordinary Brownian motion) to any real number in the range $0 < H < 1$ in the equation

$$X(t) - X(t_0) \sim \zeta \, |t - t_0|^H \quad (t \geq t_0)$$

for any two times t and t_0. This equation gives the increments in the position of the Brownian particle for a normalized independent Gaussian random process $\{\zeta\}$.

For H > 1/2, we have *persistence*. In this case, if we for some time in the past have a positive increment, i.e., an increase, then we also have on the average an increase in the future. Therefore an increasing trend in the past implies an increasing trend in the future. Conversely a decreasing trend in the past implies on the average a continued decrease in the future.

Antipersistence is the term for the case H < 1/2. In this case an increasing trend in the past implies a decreasing trend in the future, and a decreasing trend in the past makes an increasing trend in the future probable.

DEFINITION OF THE STATISTIC R/S

In continuous time t, define

$$X^*(t) = \int X(u) \, du$$

$$X^2*(t) = \int_0^t X^2(u)\,du$$

$$X*^2 = (X*)^2$$

In discrete time i, define

$$X*(t) = 0$$

$$X*(t) = \sum_{i=1}^{[t]} X(i)$$

with [t] the integer part of t. For every d > 0, called the lag, define the *adjusted range* of $X^*(t)$ in the time interval 0 to d, as

$$R(d) = \max_{0 \le u \le d}\{X*(u) - (u/d)X*(d)\} - \min_{0 \le u \le d}\{X*(u) - (u/d)X*(d)\}$$

Then evaluate the *sample standard deviation* of X(t),

$$S^2(d) = \frac{X^2*(d)}{d} - \frac{X*^2(d)}{d^2}$$

The expression Q(d) = R(d)/S(d) is the R/S *statistic*, or *self-rescaled self-adjusted range* of $X^*(t)$ (Mandelbrot, 1983).

161

R/S ANALYSIS OF FRACTIONAL BROWNIAN MOTION

The range $R(\tau)$ with lag τ is a random function with the scaling property

$$R(\tau) \sim \tau^H \quad .$$

Since the true variance $S = 1$ and the sample variance is ~ 1 for the normalized fractal Brownian function, it follows that the rescaled range R/S is given by

$$R(\tau)/S \sim \tau^H$$

in distribution. The Hurst exponent H can be *estimated* by a fit of this equation to experimental or simulated results (Feder, 1989).

LITERATURE CITED

Albano, E.V. (1990) *Surface Sci.* 235, 351.

Alexander, S. and Orbach, R. (1982) *J. Phys. Lett.* 43, L625.

Allen, J.P., Colvin, J.T., Stinson, D.G., Flynn, C.P. and Stapleton, H.J. (1982) *Biophys. J.* 38, 299.

Alstorm, P. (1990) *Phys. Rev. A* 41, 7049.

Anacker, L.W. and Kopelman, R. (1984) *J. Chem. Phys.* 81, 6402.

Anacker, L.W. and Kopelman, R. (1987) *Phys. Rev. Lett.* 58, 289.

Anderson, C.M., Stenkamp, R.E., McDonald, R.C. and Steitz, T.A. (1978) *J. Mol. Biol.* 123, 15.

Anderson, C.M., Zucker, F.H. and Steitz, T.A. (1979) *Science* 204, 375.

Argos, P., Rao, J.K.M. and Hargrave, P. (1982) *Eur. J. Biochem.* 128, 565.

Argos, P. (1988) *Prot. Engg.* 2, 101.

Argyrakis, P. and Kopelman, R. (1984) *Phys. Rev. B* 29, 511.

Argyrakis, P. and Kopelman, R. (1989) *J. Phys. Chem.* 93, 225.

Argyrakis, P. and Kopelman, R. (1990a) *Phys. Rev. A* 41, 2114.

Argyrakis, P. and Kopelman, R. (1990b) *Phys. Rev. A* 41, 2121.

Auer, D.P.F. and Seviour, R.J. (1990) *Appl. Microbiol. Biotechnol.* 32, 637.

Avnir, D., Citri, O., Farin, D., Ottolenghi, M., Samuel, J. and SeriLevy, A. (1989) in *Optimal Structures in Heterogeneous Reaction Systems* Plath, P.J. ed., Springer-Verlag.

Avnir, D., Farin, D. and Pfeifer, P. (1983) *J. Chem. Phys.* 79, 3566.

Avnir, D. and Farin, D. (1990) *New J. Chem.* 14, 197.

Barlow, D.J. and Thornton, J.M. (1986a) *J. Mol. Graphics* 4, 97.

Barlow, D.J. and Thornton, J.M. (1986b) *Biopolymers* 25, 1717.

Barnsley, M. (1988) *Fractals Everywhere* Academic Press Inc.

Belisle, J.T. and Brennan, P.J. (1989) *J. Bac.* 171, 3465.

Ben-Avraham, D. (1987) *Phil. Mag. B* 56, 1015.

Ben-Avraham, D. and Havlin, S. (1982) *J. Phys. A* 15, L691.

Ben-Jacob, E. and Garik, P. (1990) *Nature* 343, 523.

Bennet, W. and Steitz, T.A. (1978) *Proc. Natl. Acad. Sci. USA* 75, 4848.

Berg, O.G., Winter, R.B. and von Hippel, P.H. (1981) *Biochemistry* 20, 6926.

Bernstein, F.C., Koetzle, T.F., William, G.J.B., Meyer, E.F., Brice, M.D., Rodgers, J.R., Kennard, O., Shimanouchi, T. and Tasumi, M. (1977) *J. Mol. Biol.* 112, 532.

Binnig, G. and Rohrer, H. (1985) *Sci. Am.* August, 40.

Block, A., von Bloh, W. and Schellnhuber, H.J. (1990) *Phys. Rev. A* 42, 1869.

Blumen, A. and Kohler, G.H. (1989) *Proc. R. Soc. Lond. A* 423, 189.

Boyer, H.W., Carton, B.C. (1968) *Arch. Biochem. Biophys.* 128, 442.

Bryan, P., Pantoliano, M.W., Ouill, S.G., Hsiao, H.Y. and Poulos, T.L. (1986a) *Proc. Natl. Acad. Sci., USA*, 83, 3743-3745.

Bryan, P.N, Rollence, M.L., Pantoliano, M.W., Wood, J., Finzel, B.C., Gilland, G.L., Howard, A.J. and Poulos, T.L. (1986b) *Protein: Struct. Funct. Genet.* 1, 326.

Carter, P. and Wells, J.A. (1987) *Science* 237, 394.

Cates, M.E. (1985) *Phys. Rev. Lett.* 54, 1733.

Chen, S-H. and Teixeira, J. (1986) *Phys. Rev. Lett.* 57, 2583.

Chibata, I. ed. (1978) *Immobilized Enzymes: Research and Development* John Wiley and Sons.

Chirgadze, Y., Kurochkina, N. and Nikonov, S. (1989) *Prot. Engg.* 3, 105.

Chothia, C. (1974) *Nature* 248, 338.

Clement, E., Kopelman, R. and Sander, L.M. (1990a) *Chem. Phys.* 146, 343.

Clement, E., Kopelman, R. and Sander, L.M. (1990b) *Europhys. Lett.* 11, 707.

Clement, E., Sander, L.M. and Kopelman, R. (1989) *Phys. Rev. A* 39, 6472.

Codner, R.C. (1969) *Methods In Microbiol.* 1, 427.

Colvin, J.T. and Stapleton, H.J. (1985) *J. Chem. Phys.* 82, 4699.

Connolly, M.L. (1983) *J. Appl. Cryst.* 16, 548.

Cooper, A.L., Dean, A.C.R. and Hinshelwood, C. (1968) *Proc. R. Soc. Lon. Ser. B* 171, 175.

Crippen, G.M. (1978) *J. Mol. Biol.* 126, 315.

Ding, J.R. and Liu, B.X. (1990) *J. Phys. C* 2, 1971.

Drenth, J. Hol, W.G.J., Jasonius, J. and Koekoek, R. (1972) *Eur. J. Biochem, 26, 177.*

Drucker, D.B. and Whittaker, D.K. (1971) *J. Bac.* 108, 515.

Dubuc, B., Quiniou, J.F., Roques-Carmes, C., Tricot, C. and Zucker, S.W. (1989b) *Phys. Rev. A* 39, 1500.

Dubuc, B., Zucker, S.W., Tricot, C., Quiniou, J.F. and Wehbi, D. (1989a) *Proc. R. Soc. Lon. A* 425, 113.

Duprez, D. Ferhat-Hamida, Z. and Bettahar, M.M. (1990) *J. Catal.* 124, 1.

Duran, J., Pelle, F. and Portella, M.T. (1986) *J. Phys. C* 19, 6185.

Edelman, G.M., Cunningham, B.A., Gall, W.E., Gottlieb, P.D., Rutishauser, U. and Waxdal, M.J. (1969) *Proc. Natl. Acad. Sci. USA.* 63, 78.

Edsall, J.T. (1968) in *Structural Chemistry and Molecular Biology* Rich, A. and Davidson, N. eds. San Francisco, Freeman.

Elber, R. and Karplus, M. (1986) *Phys. Rev. Lett.* 56, 394.

Estell, D. A., Graycar, T. P., Millers, J.P., Powers, D.B., Brunier, J.P., Ng, J.A. and Wells, J.A. (1986) *Science* 233, 659.

Estell, D. A., Graycar, T. P., Wells, J.A. (1985) *J. Biol. Chem.* 260, 6518.

Falconer, K.J. (1989) *The Geometry of Fractal Sets* Cambridge Univ. Press.

Farin, D., Peleg, S., Yavin, D. and Avnir, D. (1985) *Langmuir* 1, 399.

Farin, D. and Avnir, D. (1987) *J. Phys. Chem.* 91, 5517.

Farin, D. and Avnir, D. (1988a) *J. Am. Chem. Soc.* 110, 2039.

Farin, D. and Avnir, D. (1988b) *Proc. 9 Int. Cong. Catal.* 3, 998.

Feder, J., Jossang, T. and Rosenqvist, E. (1984) *Phys. Rev. Lett.* 53, 1403.

Feder, J. (1989) *Fractals* Plenum Press, New York.

Fujikawa, H. and Matsushita, M. (1989) *J. Phys. Soc. Jpn.* 58, 3875.

Gefen, Y., Aharony, A. and Alexander, S. (1983) *Phys. Rev. Lett.* 50, 77.

Gefen, Y., Mandelbrot, B.B. and Aharony, A. (1980) *Phys. Rev. Lett.* 45, 855.

Golberger, A.L., Rigney, D.R. and West, B.J. (1990) *Sci. Am.* 262, 34.

Goldberger, A.L., Rigney, D.R., Mietus, J., Antman, E.M. and Greenwald, S. (1988) *Experientia* 44, 983.

Goldberger, A.L. and West, B.J. (1987) *Yale J. Biol. Med.* 60, 421.

Grassberger, P. (1990) *Phys. Rev. A* 148, 63.

Guan, J.L. and Rose, J.K. (1984) *Cell* 37, 779.

Harrison, A.K. and Zwanzig, R. (1985) *Phys. Rev. A* 32, 1072.

Havlin, S., Ben-Avraham, D. and Sompolinsky, H. (1983) *Phys. Rev. A* 27, 1730.

Hebert, E. and Uhler, M. (1982) *Cell*, 30, 1.

Helman, J.S., Coniglio, A. and Tsallis, C. (1984a) *Phys. Rev. Lett.* 53, 1195.

Helman, J.S., Coniglio, A. and Tsallis, C. (1984b) *Phys. Rev. Lett.* 54, 1735.

Hermann, R.B. (1972) *J. Phys. Chem.* 76, 2754.

Hofmann, H. and Frank, M.E. (1961) *J. Gen. Microbiol.* 25, 353.

Holbrook, S.R., Muskal, S.M. and Kim, S-H. (1990) *Prot. Engg.* 3, 659.

Hopkins, C.R., Gibson, A., Shipman, M. and Miller, K. (1990) *Nature* 346, 335.

Hoshen, J. and Kopelman, R. (1976) *Phys. Rev. B* 14, 3438.

Ikemura, H., Takagi, H. and Inouye, M. (1987) *J. Biol. Chem.* 262, 7859.

Ikemura, H. and Inouye, M. (1988) *J. Biol. Chem.*, 263, 12959.

Isogai, Y. and Itoh, T. (1984) *J. Phys. Soc. Jpn.* 53, 2162.

Jacobs, M., Elisson, M., Uhlen, M. and Flock, J.I. (1985) *Nucleic Acid Res.* 13, 8913.

James, M.N.G. and Sielecki, A. (1983) *J. Mol. Biol.* 163, 299.

Janin, J. (1976) *J. Mol. Biol.* 105, 13.

Jansons, V.K. and Nickerson, W.J. (1970) *J. Bacteriol.* 104, 910.

Jorgensen, M.J., Cantor, A.B., Furie, B.C., Brown, C.L., Shoemaker, C.B. and Furie, B. (1987) *Cell* 48, 185.

Jurgens, H., Peitgen, H-O. and Saupe, D. (1990) *Sci. Am.* August, 40.

Kauzmann, W. (1959) *Adv. Prot. Chem.* 14, 1.

Kaye, B.H. (1981) in *Direct Characterization of Fine Particles* Wiley, New York.

Keyes, T. and Ohtsuki, T. (1985) *Physica A* 133, 531.

Khare, S.K. and Gupta, M.N. (1990) *Biotech. Bioengg.* 35, 94.

Klafter, J., Blumen, A., Zumofen, G. and Shlesinger, M.F. (1990) *Physica A* 168, 637.

Klafter, J., Blumen, A. and Zumofen, G. (1984) *J. Stat. Phys.* 36, 561.

Klymko, P. and Kopelman, R. (1982) *J. Phys. Chem.* 86, 3866.

Klymko, P. and Kopelman, R. (1983) *J. Phys. Chem.* 87, 4565.

Kopelman, R., Klymko, P.W., Newhouse, J.S. and Anacker, L.W. (1984) *Phys. Rev. B* 29, 3747.

Kopelman, R., Parus, S. and Prasad, J. (1986) *Phys. Rev. Lett.* 56, 1742.

Kopelman, R. (1986) *J. Stat. Phys.* 42, 185.

Kopelman, R. (1988) *Science* 241, 1620.

Koshland, D.E. (1963) *Cold Spring Harbour Symposia on Quantitative Biology* 28, 473.

Kucerova, Z., Pohl, J. and Korbova, L. (1986) *J. Chromatogr.* 376, 409.

Lee, B. and Richard, F.M. (1971) *J. Mol. Biol.* 55, 379.

Lehninger, A.L. (1984) *Principles of Biochemistry* CBS Publishers and Distributors.

Lewis, M. and Rees, D.C. (1985) *Science* 230, 1163.

Lewis, M. and Rees, D.C. (1987) in *Environmental Influences and Recognition in Enzyme Chemistry* Ed. Lrebman, J. F. and Greenberg, A.

Li, H., Li, Y. and Zhao, H. (1990) *Int. J. Biol. Macromol.* 12, 6.

Lindenberg, K., West, B.J. and Kopelman, R. (1990) *Phys. Rev. A* 42, 890.

Linderstrom-Lang, K.U. and Schellman. J.A. (1959) in *The Enzymes* 1, 443, Boyer, P.D., Lardy, H. and Myrback, K. eds., New York, Academic.

Lopez-Quintella, M.A., Perez-Moure, J.C. and Bujan-Nunez, M.C. (1987) *Chem. Phys. Lett.* 138, 476.

Obert, M., Pfeifer, P. and Sernetz, M. (1990) *J. Bacteriol.* 172, 1180.

Ohta, Y. and Inouye, M. (1990) *Molecular Microbiol.* 4, 295.

Orbach, R. (1984) *J. Stat. Phys.* 36, 735.

Orbach, R. (1986) *Science* 231, 814.

Pantoliano, M.W., Landner, R.C., Bryan, P.N., Rollence, M.L., Wood, J.F., and Poulous, T.L. (1987) *Biochemistry*, 26, 2077.

Pfeifer, P., Welz, U. and Wippermann, H. (1985) *Chem. Phys. Lett.* 113, 535.

Pfeifer, P. and Avnir, D. (1983) *J. Chem. Phys.* 79, 3558.

Pietronero, L. (1990) *Physica A* 163, 316.

Pietronero, L. and Tosatti, E. (1986) eds. *Fractals in Physics* North-Holland, Amsterdam.

Regnier, F.E. (1987) *Science* 238, 319.

Richards, F.M. (1977) *Ann. Rev. Biophys. Bioengg.* 6, 151.

Riggs, A.D., Bourgeois, S. and Cohn, M. (1970) *J. Mol. Biol.* 53, 401.

Robillard, S. and Tremblay, A-M. S. (1986) *J. Phys. A* 19, 2171.

Rose, G.D., Geselowitz, A.R., Lesser, G.J., Lee, R.H. and Zehfus, M.H. (1985) *Science* 229, 834.

Rose, G.D. (1979) *J. Mol. Biol.* 134, 447.

Rossmann, M.G. and Liljas, A. (1974) *J. Mol. Biol.* 85, 177.

Russel, A.J. Thomas, P.G. and Fersht, A.R. (1987) *J. Mol. Biol.* 193, 803.

Sadana, A., Kulkarni, B.D. and Ramachandran, P.A. (1981) *J. Appl. Chem. Biotech.* 31, 546.

Sander, L.M. (1986) *Nature* 322, 789.

Sander, L.M. (1987) *Sci. Am.* 256, 82.

Shakked, Z., Guerstein-Guzikevich, G., Eisenstein, N., Frolow, F. and Rabinovich, D. (1989) *Nature* 342, 456.

Shapiro, J.A. (1987) *J. Bacteriol.* 169, 142.

Sharma, A., Shinde, U.P. and Kulkarni, B.D. (1990a) *Biotech. Lett.* 12, 737.

Sharma, A., Shinde, U.P. and Kulkarni, B.D. (1990b) Communicated to *Phys. Rev. A.*

Sheintuch, M. and Brandon, S. (1989) *Chem. Eng. Sci.* 44, 69.

Shinde, U.P., Sharma, A. and Kulkarni, B.D. (1990) *Chaos, Solitons and Fractals* (in press).

Smirnov, B.M. (1990) *Phys. Rep.* 188, 1.

Springer, E.L. and Roth, I.L. (1972) *Can. J. Microbiol.* 18, 219.

Stahl, M.L. and Ferrari, E.J. (1984) *J. Bact.* 158, 411.

Stanley, H.E., Bunde, A., Havlin, S., Lee, J. Roman, E. and Schwarzer, S. (1990) *Physica A* 168, 23.

Stapleton, H.J., Allen, J.P., Flynn, C.P., Stinson, D.G. and Kurtz, S.R. (1980) *Phys. Rev. Lett.* 45, 1456.

Stapleton, H.J. (1985) *Phys. Rev. Lett.* 54, 1734.

Stauffer, D. (1985) *Introduction to Percolation Theory* Taylor and Francis.

Steiner, D.L. and Clark, J.L. (1968) *Proc. Natl. Acad. Sci. USA* 60, 622.

Stryer, L. (1988) in *Biochemistry* (Third edition), pp. 664 (W.H. Freeman and Company, New York).

Tambe, S.S., Badola, P. and Kulkarni, B.D. (1990) *Chem. Phys. Lett.* 173, 67.

Tanford, C. (1980) *The Hydrophobic Effect* 2nd ed., Wiley, New York.

Teller, D.C. (1976) *Nature* 260, 729.

Thomas, P.G., Russel, A.J., and Fersht, A.R. (1985) *Nature*, 318, 375.

Tocanne, J. and Teissie, J. (1990) *Biochim. Biophys. Acta* 1031, 111.

Toussaint, D. and Wilczek, F. (1983) *J. Chem. Phys.* 78, 2642.

Usami, Y. and Nagatani, T. (1990) *J. Phys. Soc. Jpn.* 59, 474.

Vasantha, N., Thompson, L.D., Rhodes, C., Banner, G., Nagle, J. and Filpula, D. (1984) *J. Bacteriol.* 159, 811.

Vayenas, C.G., Bebelis, S. and Ladas, S. (1990) *Nature* 343, 625.

Vicsek, T., Cserzo, M. and Horvath, V.K. (1990) *Physica A* 167, 315.

von Hippel, P.H. and Berg, O.G. (1989) *J. Biol. Chem.!* 264, 675.

Voss, R.F. (1988) in *The Science of Fractal Images* Peitgen, H. & Saupe, D. eds., Springer-Verlag.

Wagner, G.C., Colvin, J.T., Allen, J.P. and Stapleton, H.J. (1985) *J. Am. Chem. Soc.* 107, 5589.

Wako, H. (1989) *J. Phys. Soc. Jpn.* 58, 1926.

Wang, C.X., Shi, Y.Y. and Huang, F.H. (1990) *Phys. Rev. A* 41, 7043.

Weaver, J.C. and Astumain, D.R. (1990) *Science* 247, 459.

Wells, J.A., Ferrari, E.J., Henner, D.J., Estell, D.A. and Chen, E.Y. (1983) *Nucleic Acids Res.*, 11, 7911.

Wells, J.A. and Powers, D.B. (1986) *J. Biol. Chem.* 261, 6564.

Wells, J.A., Powers, D.B., Bott, R.R., Graycar, T.P. and Estell, D.A. (1987) *Proc. Natl. Acad. Sci. USA* 84, 1219.

Wetlaufer, D.B. (1973) *Proc. Natl. Acad. Sci. USA* 70, 697.

Whittaker, D.K. and Drucker, D.B. (1970) *J. Bac.* 104, 902.

Wiren, K.M., Potts, J.T. Jr., Kronenberg, H.M. (1988) *J. Biol. Chem.* 263, 19771.

Witten, T.A. and Sander, L.M. (1981) *Phys. Rev. Lett.* 47, 1400.

Witten, T.A. and Sander, L.M. (1983) *Phys. Rev. B* 27, 5686.

Wodak, S.J. and Janin, J. (1981) *Biochemistry*, 20, 6544.

Wong, S.L. and Doi, R.H. (1986) *J. Biol. Chem.* 261, 10176.

Wright, C.S., Alden, R.A. and Kraut, J. (1969) *Nature*, 221, 235.

Yang, M. Y., Ferrari, E and Henner, D. (1984) *J. Bacteriol.* 160, 15.

Young, D.A. and Corey, E.M. (1990) *Phys. Rev. A* 41, 7024.

Zehfus, M.H. and Rose, G.D. (1986) *Biochemistry* 25, 5759.

Zhu, X., Ohta, Y., Jordon, F. and Inouye, M. (1989) *Nature*, 339, 6224.

Zumofen, G., Blumen, A. and Klafter, J. (1989) in *Optimal Structures in Heterogeneous Reaction Systems* Plath, P.J. ed., Springer-Verlag.

Zvelebil, M.J.J.M. and Sternberg, M.J.E. (1988) *Prot. Engg.* 2, 127.

LIST OF PUBLICATIONS

PAPERS PUBLISHED / ACCEPTED

1) EFFECT OF FRACTAL NATURE ON ENZYMATIC REACTIONS
   A. Sharma, U.P. Shinde and B.D. Kulkarni
   Biotechnology Letters (1990) **12**, 737.

2) CAN MOBILE SHAPES OF FRACTALS CAUSE RATE ENHANCEMENT?
   U.P. Shinde, A. Sharma and B.D. Kulkarni
   Chaos, Solitons and Fractals (1991) (in press).

3) MOBILE SHAPES OF FRACTALS AND RATE ENHANCEMENTS
   U.P. Shinde, A. Sharma and B.D. Kulkarni
   Eighth International Conference on Mathematical and Computer Modelling held from April 1 to April 4, 1991, at Maryland, USA.

PAPERS COMMUNICATED

1) PATTERN FORMATION IN BACTERIAL COLONIES
   A. Sharma, U.P. Shinde and B.D. Kulkarni
   Physical Review A.

2) IS THE TOPOLOGY OF MEMBRANE SPANNING ALPHA HELICES OF SIGNAL PEPTIDES RESPONSIBLE FOR THEIR RECOGNITION BY SIGNAL PEPTIDE PEPTIDASES?
   U.P. Shinde, A. Sharma and Y.R. Mawal
   Journal of Theoretical Biology.

MANUSCRIPTS UNDER PREPARATION

1) AN ALGORITHM TO DESCRIBE THE ENTIRE PROTEIN SURFACE IN TWO DIMENSIONS
   U.P. Shinde, A. Sharma and B.D. Kulkarni.

2) THREE NEW GLOBAL INDICES CHARACTERIZING PROTEINS
   A.Sharma, U.P. Shinde, Krishnan, S. and B.D. Kulkarni.

3) STUDIES ON THE SURFACE PROPERTIES OF SUBTILISINS: IMPLICATIONS ON PROTEIN FOLDING
   A. Sharma, U.P. Shinde, Krishnan, S. and B.D. Kulkarni.

4) GENERATING A PERCOLATION CLUSTER ON A 200×200 LATTICE ON A PC-XT
   U.P. Shinde and A. Sharma.